WIDEBAND PHASE SHIFTER FOR 6-18 GHZ APPLICATIONS

A THESIS SUBMITTED TO
THE GRADUATE SCHOOL OF NATURAL AND APPLIED SCIENCES
OF
MIDDLE EAST TECHNICAL UNIVERSITY

BY

GÖKHAN BOYACIOĞLU

IN PARTIAL FULFILLMENT OF THE REQUIREMENTS
FOR
THE DEGREE OF MASTER OF SCIENCE
IN
ELECTRICAL AND ELECTRONICS ENGINEERING

JUNE 2010

Approval of the thesis:

WIDEBAND PHASE SHIFTER FOR 6-18 GHZ APPLICATIONS

submitted by **GÖKHAN BOYACIOĞLU** in partial fulfillment of the requirements for the degree of **Master of Science in Electrical and Electronics Engineering Department, Middle East Technical University** by,

Prof. Dr. Canan Özgen _____
Dean, Graduate School of **Natural and Applied Sciences**

Prof. Dr. İsmet Erkmen _____
Head of Department, **Electrical and Electronics Engineering**

Assoc. Prof. Dr. Şimşek Demir _____
Supervisor, **Electrical and Electronics Engineering Dept., METU**

Examining Committee Members:

Prof. Dr. Canan Toker _____
Electrical and Electronics Engineering Dept., METU

Assoc. Prof. Dr. Şimşek Demir _____
Electrical and Electronics Engineering Dept., METU

Prof. Dr. Nevzat Yıldırım _____
Electrical and Electronics Engineering Dept., METU

Assoc. Prof. Dr. Sencer Koç _____
Electrical and Electronics Engineering Dept., METU

Dr. Mustafa Akkul _____
ASELSAN Inc.

Date: 18.06.2010

I hereby declare that all information in this document has been obtained and presented in accordance with academic rules and ethical conduct. I also declare that, as required by these rules and conduct, I have fully cited and referenced all material and results that are not original to this work.

Name, Last name : Gökhan BOYACIOĞLU

Signature :

ABSTRACT

WIDEBAND PHASE SHIFTER FOR 6-18 GHZ APPLICATIONS

Boyacıoğlu, Gökhan
M.Sc., Department of Electrical and Electronics Engineering
Supervisor: Assoc. Prof. Dr. Şimşek Demir

June 2010, 159 pages

Phase shifters are common microwave circuit devices, which are widely used in telecommunication and radar applications, microwave measurement systems, and many other industrial applications. They are key circuits of T/R modules and are used to form the main beam of the electronically scanned phase array antennas. Wideband operating range is an important criterion for EW applications. Hence, wideband performance of the phase shifter is also important.

In this study, four wideband phase shifter circuits are designed, fabricated and measured for 6-18 GHz frequency range. Phase shifters are separately designed in order to get 11.25, 22.5, 45 and 90º phase shifts with minimum phase error and low return losses. Phase shifter circuits are designed and fabricated in microstrip structure onto two different substrates as Rogers TMM10i and Alumina using printed circuit board and thin film production techniques, respectively. Also phase shifter circuits that include microstrip spiral inductors for DC biasing are designed and fabricated using thin film production technique. For each design the fabricated circuits are measured and results are compared with simulation results in the content of this

thesis. Circuit designs and EM simulations are performed by using ADS2008®, Sonnet®, and CST®.

Keywords: Wideband Phase Shifter, Hybrid Coupled Phase Shifter Circuits, Lange Coupler, Radial Stub, PIN Diode.

ÖZ

6-18 GHZ UYGULAMALARI İÇİN GENİŞ BANT FAZ KAYDIRICI

Boyacıoğlu, Gökhan
Yüksek Lisans, Elektrik ve Elektronik Mühendisliği Bölümü
Tez Yöneticisi: Doç. Dr. Şimşek Demir

Haziran 2010, 159 sayfa

Faz kaydırıcılar, iletişim ve radar uygulamalarında, mikrodalga ölçüm sistemlerinde, ve bir çok farklı endüstriyel uygulamada sıklıkla kullanılan mikrodalga devre elemanlarından bir tanesidir. Faz kaydırıcılar T/R modüllerin en önemli devreleridir ve elektronik taramalı faz dizili antenlerin ana huzmesinin oluşturulmasında kullanılırlar. Geniş bant çalışma aralığı elektronik harp uygulamalarında önemli bir ölçüttür. Bu yüzden faz kaydırıcıların geniş bant performansı da önemlidir.

Bu çalışmada, 6-18 GHz frekans aralığı için dört geniş bant faz kaydırıcı devresi tasarlanmış, üretilmiş ve ölçülmüştür. Faz kaydırıcılar; 11.25, 22.5, 45 ve 90º faz kaydırma değerlerini minimum faz hatası ve düşük geriye dönüş kaybı ile elde etmek için ayrı ayrı tasarlanmıştır. Mikroşerit yapıdaki faz kaydırıcı devreler iki farklı dielektrik taban malzemesi Rogers TMM10i ve Alumina üzerine baskı devre kartı ve ince film üretim teknikleri kullanılarak tasarlanmış ve üretilmiştir. Ayrıca, DC besleme için gereken irgiteçler mikroşerit yapıda sarmal irgiteç olarak tasarlanmış ve bu irgiteçlerin kullanıldığı faz kaydırıcı devreler ince film tekniği kullanılarak üretilmiştir. Bu tez kapsamında tasarlanan faz kaydırıcı devreler üretilmiş ve ölçüm

sonuçları benzetim sonuçları ile karşılaştırılmıştır. Devre tasarımları ve elektromanyetik benzetimlerde ADS2008® , Sonnet® and CST® programları kullanılmıştır.

Anahtar Kelimeler: Geniş Bant Faz Kaydırıcı, Hibrit Bağlı Faz Kaydırıcı Devreler, Lange Bağlaç, Radyal Saplama, PIN Diyot.

To my lovely family

ACKNOWLEDGMENTS

I would like to acknowledge the invaluable help and encouragement of my supervisor Assoc. Prof. Dr. Şimşek Demir. I thank him for his patience, guidance and knowledgeable advice throughout the development of this study.

I would like to thank Dr. Mustafa Akkul, Şebnem Saygıner, Bülent Alıcıoğlu, and Tuncay Erdöl for their precious suggestions and technical advices during the improvement of this thesis. My thanks also go to all clean room staff especially Tülay Can and Sedat Pehlivan for their great help in assembling and measurement processes. I need to acknowledge to Ömer Öçal for his efforts in producing the PCB designs. I would also like to thank to ASELSAN Inc. that provides me facilities and resources to complete the fabrication and measurement processes.

I need to acknowledge to TÜBİTAK for financial support during my master education.

I want to thank all my friends who encourage me to finish this study. I owe special thanks to Ahmet Aktuğ, Halit Öğün, Nilüfer Öğün, and Fatih Yıldız for their great help and moral support.

Finally, I would like to thank my dear Mum, Dad and Brother for their absolute support and encouragement. Their understanding and loving support was helpful when I needed it the most and I will always be grateful to them.

TABLE OF CONTENTS

LIST OF TABLES

TABLES

LIST OF FIGURES

FIGURES

LIST OF ABBREVIATIONS

ADS	: Advanced Design System
ATC	: American Technical Ceramics
CST	: Computer Simulation Technology
BW	: Bandwidth
CPW	: Coplanar Waveguide
DC	: Direct Current
EW	: Electronic Warfare
EM	: Electromagnetic
ESA	: Electronically Scanned Array
FET	: Field Effect Transistor
LSB	: Least Significant Bit
MEMS	: Micro Electro Mechanical System
MESFET	: Metal Semiconductor FET
MIC	: Microwave Integrated Circuit
MMIC	: Monolithic Microwave Integrated Circuit
MSB	: Most Significant Bit
PIN	: Positive-Intrinsic-Negative
PCB	: Printed Circuit Board
RF	: Radio Frequency
RMS	: Root Mean Square
RTPS	: Reflection Type Phase Shifter
RX	: Receiver
SNR	: Signal-to-Noise Ratio
SPDT	: Single Pole Double Throw
TL	: Transmission Line
T/R	: Transmit/Receive
TX	: Transmitter
VSWR	: Voltage Standing Wave Ratio

CHAPTER 1

INTRODUCTION

Microwave and millimeter phase shifters are being used widely in a variety of radar and communication systems, microwave instrumentation and measurement systems, and industrial applications. While the applications of microwave phase shifters are numerous as mentioned above, one of the most important application is within a phased array antenna system.

Phased array antennas consist of a group of radiators. They are usually arranged in a symmetric pattern and are excited coherently through the use of phase shifters embedded in a feed network. The direction of the radiated beam is steered at a given angle in space, θ, by adjusting the phase of the signals fed to the various elements of the array. Conversely, an incident plane wave at an angle θ with respect to the array axis will induce a current in each of the array elements. Each of the signals can be all in phase by changing their phases. Then, they can be summed and the new formed signal will have an amplitude N times of the signal which is induced by one antenna element. A typical linear phased array consists of four radiating element is shown in Figure 1.1 [1]. As the two-port key element of a phased array antenna system, the phase shifter gives the role to change the phase of the input signal ideally without the insertion loss.

In this thesis, four phase shifter circuits which provide 11.25º, 22.5º, 45º and 90º phase differences, are designed, fabricated and measured for 6-18 GHz applications using PIN diodes as the switching elements. Each phase shifter circuit is designed and fabricated onto two different substrates individually. Finally, simulation and measurement results are compared each other.

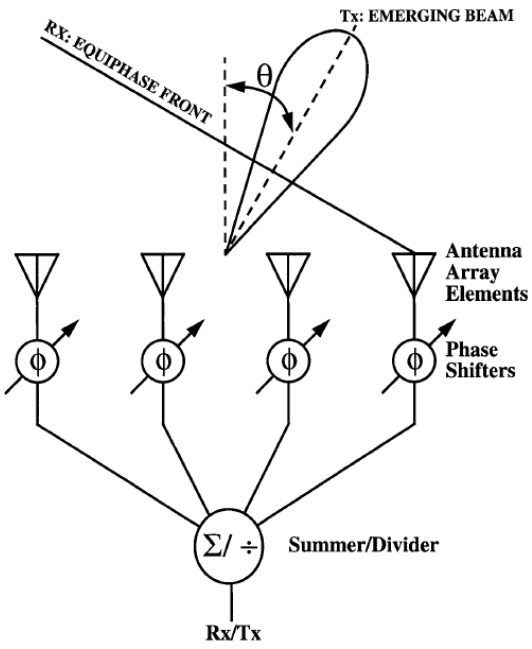

Figure 1.1 A Four-Element Linear Phased Array.

1.1 Some Phase Shifter Studies in Literature

The first examples of variable phase shifters came into existence in the 1940's. Fox proposed the rotary vane adjustable waveguide phase changer in 1947 [2]. Although these mechanical phase changers were simple to fabricate and had very low loss, they were rugged and not suitable for the phased array antenna systems.

The earliest form of electronically variable phase shifter was proposed by Reggia and Spencer [3] in 1957. They introduced an analog phase-shifting device which consists of magnetized ferrite rod that is placed at the center of a rectangular waveguide. With this study a new period began for ferrite phase shifter technology. Ferrites have the advantages in high power handling capacity, low insertion loss and low VSWR. On the other hand, ferrite phase shifters are large, have low switching speed and complex driver circuits. Moreover, ferrite's magnetic permeability and corresponding insertion phase and phase shift, are dependent on both temperature and mechanical stress on the ferrite.

In 1958 B. M. Schiffman [4] pointed out that the design of broadband 90º differential phase shift networks for the microwave region is possible by using coupled transmission lines. Schiffman phase shifter is constructed from two separated transmission lines, one of which folded (parallel-coupled) to be dispersive. The phase difference between them can be made almost constant at 90º over a broadband by choosing suitable lengths of the transmission lines. Quirarte [5] has described the general synthesis procedure of the basic Schiffman phase shifter. The original design of Schiffman phase shifter was based on stripline structure which has a homogeneous medium and supports TEM wave. The odd and even modes propagating along the coupled lines have equal phase velocities. If this circuit is designed on microstrip structure, the performance of the phase shifter will decrease. Because, the odd and even mode phase velocities of the coupled lines will be unequal. Over the years several different versions of Schiffman phase shifter have been proposed to improve its performance. However, narrow gap between the coupled lines is being a problem particularly at high frequencies. It is difficult to obtain tight coupling using PCB technology.

Abbosh [6] proposed a method for ultra-wideband phase shifters. Broadside coupling between top and bottom elliptical microstrip patches via an elliptical slot is provided in this method. The proposed structure has been used to design 30º and 45º phase shifters that have compact size. ±3º phase error has been obtained in measurements for 3.1-10.6 GHz bandwidth while better than 10 dB return loss and less than 1 dB insertion loss achieved.

Electronically controlled digital phase shifters using PIN diode as switches have become popular in 1960's. In modern phased array antennas, there are many radiating elements, so this requires many phase shifters. Hence, a design that is small, electronically controlled, and can be economically produced in large quantities is desirable. The PIN diode phase shifters meet these requirements. In hybrid MIC, all passive components are deposited on the surface of a low-loss dielectric substrate, and discrete semiconductor devices such as PIN diodes are mounted onto the passive circuit by bonding, soldering or epoxy attachment.

J.F. White [7] showed that the transmission phase shifter using PIN diode control elements is quite suitable to L- and S-Band implementation. With the advantages of semiconductor control with PIN diodes, the approach that he proposed will prove useful for array antenna beam steering.

Hybrid MIC technique has been applied to digitally controlled phase shift networks using PIN diodes as the switching elements in [8]. The phase shifters for L- and S-Band have been designed. This development showed that the feasibility of the microstrip technique on alumina ceramic for phase sensitive circuitry and provided a complete microwave phase shifter in a miniature size.

Garver [9] presented four types of phase shifters; switched line, loaded line, reflection and lumped element high-pass and low-pass circuits for broadband applications. Diodes were used as the switching elements. The diodes were connected to the circulator or 3 dB coupler in order in order to form reflection type phase shifter. Wideband phase shifting for 11.25º, 22.5º, 45º and 90º have been obtained ±2º phase error. The bandwidth is limited by the 3 dB coupler or circulator. Garver proposed that all four types of phase shifters could give octave bandwidth for low values of phase shift.

Wideband hybrid coupled phase shifter has been proposed in reference [10]. Phase shifter consists of Lange coupler as the 3 dB coupler and radial stubs as the reflective loads at the end of the direct and coupled port of Lange coupler. Other ports of the Lange coupler are used as the input and output ports of the circuit. PIN diodes have been used in order to switch between the reflective loads. Using this method four wideband phase shifters were fabricated. For 6-18 GHz frequency band, maximum phase errors were ±2.2, 2.2, 3.6, and 5.5º for the 11.25, 22.5, 45, and 90º phase shifters, respectively.

Adler and Popovich [11] have reported that all-pass networks can be used to design a broadband phase shifter. This method is based on the switching between the all-pass networks which are consist of inductors and capacitors that are calculated for the desired bandwidth. In order to increase the bandwidth, more than one stage is

cascaded. In [11], a four bit phase shifter, operating in the 4-8 GHz has been manufactured. However, as the frequency increases inductor and capacitor values become very low. This situation limits the design if cots components are used for capacitor and inductors.

Modern phase shifters are mainly based on PIN diodes, FET and ferromagnetic materials. However, as the applications move up in frequency (GHz), the insertion loss in the current systems becomes more significant [12]. In recent years, MEMS solutions have been developed and presented. In reference [13], Rebeiz discussed many different MEMS-based phase shifter designs and their corresponding advantages and disadvantages. These phase shifters are usually based on FET designs. However, instead of utilizing FETs for the switches, researchers have used MEMS switches. Although MEMS phase shifters provide low insertion loss, they suffer from the modulation speed due to their mechanical characteristics.

A low loss and ultra wideband RTPS using digitally operated capacitive MEMS switches has been reported in [14]. The fabricated phase shifter shows an average insertion loss of 3.48 dB, and maximum rms phase error ±1.80º for the relative phase shift from 0º to 90º over 5-17 GHz.

In reference [15], RF MEMS phase shifter with constant phase shift has been presented. 11.25, 22.5, and 45º phase shifter circuits comprised of open-ended stubs, short-ended stubs, and MEMS capacitive shunt switches have been fabricated for the operating frequency range 10.7 – 12.75 GHz.

With the development of MMIC technology, MMIC phase shifters come into existence in 1980's. Its small size and weight, improved reliability and reproducibility are the main advantages of the MMIC over the hybrid MIC. Since, the wire bonds are eliminated and active devices are embedded within the semiconducting substrate, the undesired parasitic effects are minimized in MMIC. Although MMIC technology provides all the advantages of integration, the flexibility of circuit tuning is lost which is available in hybrid MIC [16]. So, in order to minimize the circuit adjustment after the production, the accurate circuit design

becomes an important consideration. Various types of MMIC phase shifters using different topologies have been proposed in the literature.

A five bit MMIC phase shifter which covers over two octaves of bandwidth has been demonstrated in [17]. Phase shifter was composed of four separately optimized phase shifter sections consisting of a 180 degree bit, a 90 degree bit, a 45 degree bit, and a combined 22.5/11.25 degree section. The topologies of the 90, 45, and 22.5/11.25 degree sections utilized interdigitated quadrature couplers terminated with FET switched reflective loads.

In [18] another broadband MMIC phase shifter that operates between 6-18 GHz has been presented. The phase shift circuits design of the 5-bit phase shifter is based on the reflection type topology consisting of a 3 dB Lange coupler and a pair of reflective terminating circuits with switching FETs. The fabricated phase shifter has a typical insertion loss of 9.4 dB +/- 1.4 dB, a maximum RMS amplitude error of 0.33 dB, and a maximum RMS phase error of 70 over the operating frequency band.

MMIC 6-bit PIN diode phase shifter has been proposed in [19]. It has been designed onto the SiGe substrate and its operating frequency has been 7-11 GHz. Highpass / lowpass phase shift networks have been used for the 180º, 90º, 45º, and 22.5º phase bits. Simplified combination of capacitive and inductive elements was used in order to achieve 11.25º and 5.625º phase bits. The switching between these networks was provided by using PIN diodes.

A MMIC phase shifter which consists of microstrip radial stubs has been presented in [20]. Highpass / lowpass topologies have been used for the phase shifter that operates between 1 to 22 GHz. Four identical 22.5º phase shift units were designed and cascaded to form 90º phase shifter. MESFETs were used as the switching elements.

In recent years, there has been an important development in the area of artificial dielectric media that has negative permittivity ε and permeability μ. Such materials are usually called as metamaterials. The phase and group velocities are in the same direction in a conventional TL and they are defined as right-handed TL. On the other,

a TL that has negative dispersion with the opposite directions of the phase and group velocities is called as left-handed TL. A digital phase shifter that is based on right-handed and left-handed TLs has been demonstrated in [21]. The 180º phase shifter has been designed as switching between the right-handed TL and left-handed TL. PIN diodes were used for the switching between the TLs.

1.2 Organization of the Thesis

This thesis consists of seven chapters. The phase shifter background is explained in Chapter 2. The basic definitions, applications and requirements of a phase shifter are given in this chapter. Chapter 3 presents the classification of the phase shifters. This chapter also provides an outline of existing phase shifters with their theories and applications. Moreover, a sample design of a hybrid coupled type phase shifter is briefly explained in this chapter. Chapter 4 presents the design, fabrication, and measurement results of Lange coupler which is produced using PCB technologies. The details of modeling of PIN diode are also given in this chapter. The design, fabrication and measurement results of 11.25, 22.5, 45, and 90º phase shifter circuits that are produced onto Rogers TMM10i substrate are given in Chapter 5. Also, the simulation and the fabricated results of the phase shifter circuits are compared in this chapter. Chapter 6 includes unfolded Lange coupler and the phase shifter circuits that are designed onto Alumina substrate using thin film production techniques. The simulation and fabricated results of these circuits are compared in this chapter. , Phase shifter circuits that include microstrip spiral inductors for DC biasing are given in Chapter 7. The measurement results of these circuits are also given here. Finally, the summary and conclusions are taken part in Chapter 8.

CHAPTER 2

PHASE SHIFTER BACKGROUND

2.1 Phase Shifter and Basic Definitions

A phase shifter is a two-port microwave network providing that the phase difference between the input and the output signals may be controlled by a control signal, usually DC biasing.

An ideal phase shifter changes the transmission phase angle of the incoming signal without affecting its amplitude response. However, in practice, phase shifter has some amount of insertion loss to be minimized.

Some of the terminology and basic definitions used describing phase shifters are explained below.

2.1.1 Insertion Phase

The difference in phase between the input and output ports of the phase shifting device is called as insertion phase. If the two-port network is represented by its equivalent S-parameters, the transmission through the network is defined by the S_{21} term. In this case insertion phase can be written as:

$$\phi_{21} = \tan^{-1}\left(-\frac{\mathrm{Im}(S_{21})}{\mathrm{Re}\ S_{21}}\right) \qquad \textbf{(2-1)}$$

The general schematic of a two-port phase shifter is shown in Figure 2.1. If the phase shifter is assumed to be lossless as in ideal case, the insertion phase of the device is given as ϕ, where V_1 is the input signal and V_2 that is equal to $V_1 e^{-j\phi}$, is the output signal of the two port network.

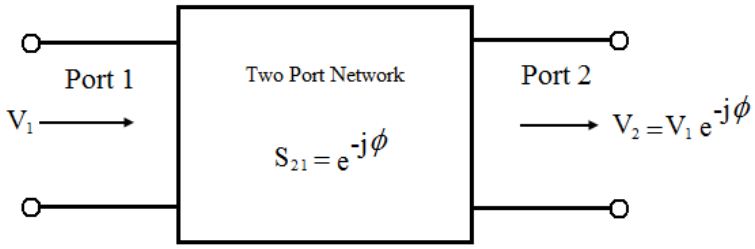

Figure 2.1 General Schematic of a Two Port Phase Shifter.

2.1.2 Differential Phase Shift

In order to obtain the given phase shift for a signal propagating through the network, phase shifters usually use the principle of switching between two different fixed insertion phases, ϕ_{21a} and ϕ_{21b}. Then the differential phase shift provided by the device can be written as:

$$\Delta\phi = \phi_{21a} - \phi_{21b} \tag{2-2}$$

Depending on the sign of $\Delta\phi$, Equation 2.2 shows that both phase delay or phase advance can be obtained.

2.1.3 Return Loss

The return loss of a phase shifter is an important criterion as in any other microwave devices. It is a measure of the loss caused by the device because of the mismatch between the source impedance and the input impedance of the phase shifter. If the source and the phase shifter are well matched, then the return loss of the device is high. The return loss of a phase shifter is given in dB as:

$$RL(dB) = -20\log_{10}|S_{11}| \tag{2-3}$$

2.1.4 Insertion Loss

The insertion loss of a phase shifter is the transmission loss of the signal resulting from the insertion of the device. It is a measure of the attenuation. So, if the insertion loss is high, signal will be attenuated more as it flows through the device. Insertion loss includes conductor losses, impedance mismatches, component losses etc. The insertion loss of a device is given by:

$$IL(dB) = -20\log_{10}|S_{21}| \quad \textbf{(2-4)}$$

2.1.5 Reciprocal and Nonreciprocal Phase Shifters

For an ideal reciprocal phase shifter, the insertion phase of the signal propagating in one direction is equal to the signal propagating in opposite direction. Hence, for the reciprocal phase shifter below equation can be written.

$$\phi_{21} = \phi_{12} \quad \textbf{(2-5)}$$

If two reciprocal phase shifter networks are used and switching is applied between these two networks, the differential phase shift will also be reciprocal, i.e.

$$\Delta\phi_{21} = \Delta\phi_{12} \quad \textbf{(2-6)}$$

$$\phi_{21a} - \phi_{21b} = \phi_{12a} - \phi_{12b} \quad \textbf{(2-7)}$$

For a nonreciprocal phase shifter, the insertion phase of the signal traveling from port 1 to port 2 is not same as the signal traveling from port 2 to port 1, i.e.

$$\phi_{21} \neq \phi_{12} \quad \textbf{(2-8)}$$

Similarly, differential phase shifts between two nonreciprocal phase shifter networks will not be the same.

$$\Delta\phi_{21} \neq \Delta\phi_{12} \quad \textbf{(2-9)}$$

$$\phi_{21a} - \phi_{21b} \neq \phi_{12a} - \phi_{12b} \quad \textbf{(2-10)}$$

2.1.6 Phase Shifter Bandwidth

The bandwidth of a phase shifter can be defined for the frequency range within a desired phase shift for the given tolerance. For instance if the tolerance given for certain phase shift ϕ is ±3º, the ±3º bandwidth of the phase shifter can be written as:

$$BW_{\pm 3^o} = f_{(\phi+3^o)} - f_{(\phi-3^o)} \quad \textbf{(2-11)}$$

A reference to the shape of phase shifter's phase versus frequency characteristic has to be considered while discussing the bandwidth of a phase shifter.

2.1.7 True Phase Shifter and True Delay Line

The true phase shifter and the true delay line which are the fundamental types of phase shifter must first be defined in order to understand the difference between them [22].

In a true phase shifter, the frequency response of the group delay is flat in the defined bandwidth of operation and its level does not change when the insertion phase is varied. The true phase shifter has a flat differential phase shift frequency response at all levels of differential phase shift. The frequency characteristics of a true phase shifter are given in Figure 2.2. True phase shifters can be used in multiple space diversity receiver-combiners in order to align RF signals within a pulse envelope.

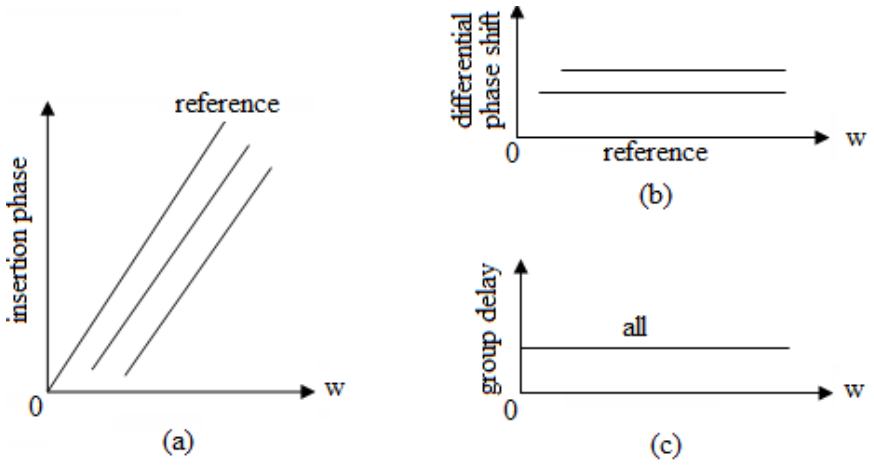

Figure 2.2 Frequency Characteristics of a True Phase Shifter.
(a) insertion phase, (b) differential phase shift and (c) group delay

In a true delay line, the frequency response of the group delay is also flat in the defined bandwidth of operation, however, its level changes when the insertion phase is varied. The true delay line has a linear differential phase shift frequency response and it changes as the value of differential phase shift varies. The frequency characteristics of a true delay line are illustrated in Figure 2.3. True delay lines are frequently used in wideband microwave signal processing, especially in beam-forming networks in phased array antennas.

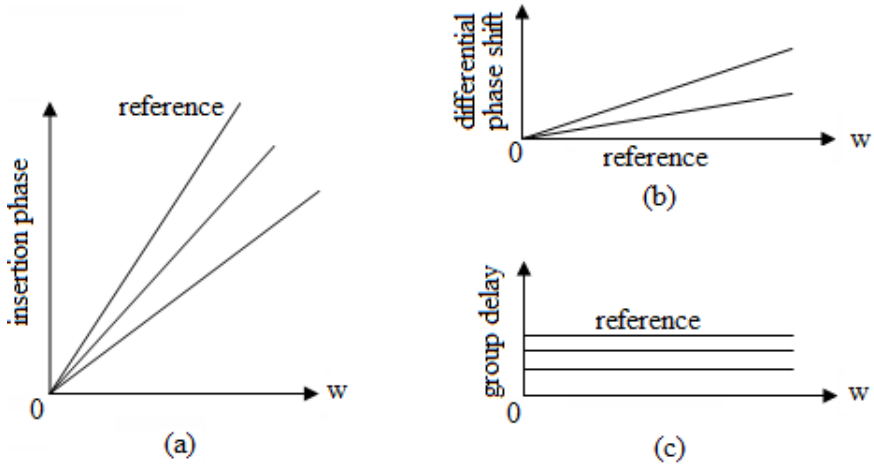

Figure 2.3 Frequency Characteristics of a True Delay Line.
(a) insertion phase, (b) differential phase shift and (c) group delay

2.1.8 Phase Shifter Requirements

There are many performance criteria such as insertion loss, operating bandwidth, phase flatness, size etc. that specify the electrical performance of a phase shifter. The importance of the each criterion varies as the application area of the phase shifter changes. For instance, in mobile and airborne systems, the physical size and weight of the phase shifter should be minimized, however this requirement can be relaxed for ground based systems. On the other hand, ground based systems need higher power handling capabilities than the mobile and airborne systems. Hence, when designing a phase shifter there are some requirements to be satisfied often resulting in some trade-offs. Some of the requirements for a phase shifter are explained below.

The insertion loss of a phase shifter should be kept as low as possible as in any other microwave component. Its effect changes according to where the phase shifter is used. If the phase shifter is used in a transmitter, the insertion loss of the phase shifter will cause a loss in the transmitter power and the heat of the transmitter will increase because of the power dissipation. If the phase shifter is used in a receiver, the insertion loss will decrease the SNR of the device. There is a trade-off between the insertion loss and the number of bits in a digital phase shifter. As the number of bits is increased, the insertion loss of the phase shifter will also increase. Also, the bandwidth of operation imposes the insertion loss. If a broadband response is needed, high insertion loss can be accepted.

The return loss is another important property for a phase shifter and it should be kept as small as possible. There are two major reasons of return loss: discontinuities and impedance mismatches. Since phase shifters are used in complex systems and cascaded with other microwave components, the return loss will directly affects the performance of the system.

Although phase shift in an ideal phase shifter is constant in the bandwidth of operation, there is always a phase shift error because of variations with frequency, phase state, temperature, and power in practice. When designing a phase shifter, the phase shift error has to be as small as possible. If a broadband operation is required,

the phase shift error can be tolerated up to acceptable values. Phase errors cause some negative effects on phased array radars. For instance, it decreases the antenna gain in a transmitting array and increases sidelobes in a receiving array. For a phase shifter in a phased array, typically up to about 6º rms phase error is reasonable.

Power handling capacity depends on the usage area of the phase shifter. For example, in a phased array radar, the phase shifter must be able to handle up to 250W peak power and 5W average power. However, for a phase shifter that is used in a T/R module can operate on the order of milliwatts.

Switching time is another important property of electronic phase shifters which have different phase states to be switched each other. While switching from one particular phase state to another, there is a time duration that is called as switching time. In a phased array radar, the minimum detectable radar range will raise as the switching time increases. It is on the order of microseconds in practice for these systems. The technologies used in designing a phase shifter changes the switching time. For example, switching time is much longer in mechanical phase shifters when they are compared with integrated circuit phase shifters.

Driver circuit is used to control switches, transistors or another electronic component which exist in phase shifter circuits. Driver circuits are important for phase shifters because complex driver circuits can affect the whole circuit. So, the driver circuit should be as simple as possible. Also, drive power is critical for the phase shifter. Low drive power should be preferred. A large drive power will cause more heat and the driver circuit may become more complex.

Number of bits in a digital phase shifter designates the phase shift resolution which is an important property for applications that require very low sidelobe levels. As the number of bits increases, the resolution of the phase shifter increases. However, insertion loss, size and cost of the phase shifter circuit will rise when the number of bits is stepped up. So, there is a trade-off between these parameters as in the other phase shifter requirements.

Bandwidth of operation is another requirement for the phase shifters which are used in the systems that need wideband applications. As explained previously, bandwidth of a phase shifter depends on the tolerance of phase shift values. If a broadband phase shifter is required, the design specifications of some parameters such as phase shift error, insertion loss, return loss etc. should have to be changed. For example, the phase shift tolerance of a phase shifter which has 0.5 octave bandwidth is ±2º. On the other hand, if an octave bandwidth is required for the same phase shifter, the phase shift tolerance may become ±5º.

In an ideal phase shifter, the magnitude of the RF signal is not disturbed while performing the phase shift operation. However, there is some amount of distortion in the amplitude of RF signal in practical applications. This situation may also introduce an undesired interfering tone signal component. Hence, in a phase shifter, amplitude variation with phase shift should be as small as possible.

Size and weight are the other parameters of a phase shifter. Of course, as in the other electronic components smaller circuits are always preferred. Generally there is a limited space for these circuits in the whole system. Weight is a significant phase shifter requirement especially in mobile and airborne systems and it should be minimized.

Cost and producibility are also important requirements for manufacturing process. Like in all productions, expense of the fabrication is significant parameter and it should be as low as possible. Also producibility is critical in manufacturing. There are many different phase shifter design topologies in the literature. While choosing a topology, the designer should consider the producibility of the design and it should be suitable for the mass production.

As explained before the importance of each criterion depends on the application of phase shifter. Unfortunately, desirable properties for all of these criteria may not be satisfied with one type of phase shifter [23].

2.1.9 Phase Shifter Applications

Phase shifters are widely used in radar and communication systems, microwave instrumentation and measurement systems, and civilian sectors. Phase shifter technology has been rapidly improved after phased arrays started to come into existence. Thousands of radiating elements appear in a typical phased array and each radiating element is connected to an electronically variable phase shifter.

Phase shifters are the key essential component of an ESA. Differential phase shift is required to scan to an angle off broadside. They are used to form the main beam of an electronically scanned phase array antennas.

They are used in radar system applications such as finding target height, detection of multiple targets, surveillance, tracking, etc.

Wireless communication systems, such as satellite communication, broadcasting, mobile communication and terrestrial communication, require various phased array antennas to be operated properly in a mobile environment. Hence, phase shifters are important components for these systems.

There are also some circuits that use phase shifters. Variable power dividers which are controlled by phase shifters, adjustable-phase 3 dB power dividers and microwave frequency translators are some examples of these circuits. Butler matrices that are beam-forming networks for arrays are formed by a combination of hybrids and fixed phase shifters.

2.2 Classification of Phase Shifters

Phase shifters can be classified into many distinct types depending on its different features. For example, they can be grouped depending on whether the phase shift control is performed through mechanical or electronic. They can be categorized as analog or digital according to the type of operation. Digital or analog phase shifters can be divided into two sub categories as ferrite phase shifters or semiconductor device phase shifters with respect to their electronic control or mechanism. Other

classifications can be done with reference to the technology used for production as waveguide, hybrid, or monolithic [16].

2.2.1 Mechanical Phase Shifters

In mechanical phase shifters, phase shift is obtained by changing the insertion phase of the structure by mechanical tuning. Mechanical phase shifters typically are analog according to the type of operation. They are usually designed in a rectangular or circular waveguide. They have very low loss and they are not complex structures to fabricate. They are also cheaper than the electronic phase shifters. However, they are vast and heavy structures. Moreover, when they are compared with electronic phase shifters, they require much more time in order to change or switch of phase shift. Although they are still used in many applications, the significance of mechanical phase shifters has deceived gradually because of the existence of electronically variable phase shifters. Coaxial trombone, waveguide short-slot hybrid, rotary-vane adjustable waveguide phase shifters are some examples of mechanical type phase shifters.

2.2.2 Analog Phase Shifters

In analog phase shifters, the phase shift is changed continuously as the control signal varies. Analog phase shifters can provide large amount of phase shift and high speed. Also, any phase shift value can be obtained by changing the control voltage. The phase resolution can be said as infinite. However, one of the disadvantages of analog phase shifters is that their phase shift is sensitive to slight variations on the control signal. Generally, varactor diode where the capacitance varies with the bias voltage is used as the semiconductor control element in analog phase shifters. There are also ferrite analog phase shifters as Regia-Spencer phase shifter and rotary field phase shifter.

2.2.3 Digital Phase Shifters

Phase shifters are called digital when the differential phase can be changed by only a few predetermined discrete values such as 180º, 90º, 45º, and 22.5º [25]. A digital phase shifter usually is based on RF switches such as PIN diodes or FET. The insertion phase of the network is altered by changing the states of the RF switches

applying a DC control signal. The phase shift is not affected from the small variations on the DC control signal. This makes digital phase shifters more immune than the analog phase shifters. Another advantage of a digital phase shifter is its compatibility of interfacing with the digital computer for control signals. The phase accuracy and the size of a digital phase shifter are better than the analog phase shifters. Nevertheless, the insertion loss of a digital phase shifter usually is higher than the analog phase shifters. Hence, typically digital phase shifters are preferred for active array antennas where the insertion loss is not critical as phase accuracy or size.

2.2.4 Basic Structure of a Digital Phase Shifter

The basic structure of a digital phase shifter is shown in Figure 2.4. There are two networks as network 1 and network 2 which are separated by a SPDT. The insertion phases varying with frequency are $\phi_1(f)$ and $\phi_2(f)$ for network 1 and network 2, respectively. When the input signal is transmitted to output over the network 1 with appropriate switch positions, the phase of the transmitted signal becomes $\phi_1(f)$ and it is accepted as a reference state. If the input signal is switched to pass through network 2, a differential phase shift is obtained as $\phi_1(f)-\phi_2(f)$ which is predetermined value such as 22.5º or 45º, etc.

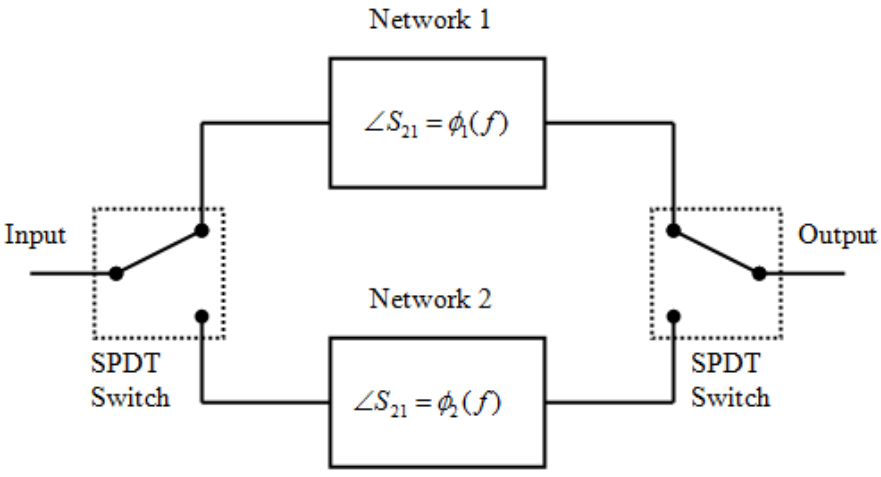

Figure 2.4 Basic Structure of One Bit Phase Shifter Structure.

Network 1 and network 2 can be designed by using different phase shifter circuit topologies according to the requirements of the phase shifter. Some of them are explained in detail in the next chapter.

PIN diodes and FETs are frequently used to realize the SPDT switches. Since, they affect the performance of the phase shifter directly; the insertion loss and the isolation of the switches are the most critical parameters.

As it can be seen easily from the Figure 2.4, this structure forms just one fixed differential phase shift value. Hence, it can be called as single-bit phase shifter. A common digital phase shifter is formed by cascading a number of bit structures that is determined by the design requirement of the application. Hence, digital phase shifters provide a discrete set of phase shift values which are controlled by two-state phase bits. If n represents the number of the bits, the digital phase shifter provides

$$M = 2^n \tag{2-12}$$

phase states. As the number of bits in a phase shifter is increased, 360º is divided into smaller steps. So, the resolution of the phase shifter is raised. However, increasing the number of bits is not very practicable especially for the wideband phase shifters. Since there is always a phase error changing with frequency, as the number of bits is increased, the phase error will become in a comparable with the minimum phase resolution.

The smallest phase shift value which is also known as least significant bit, LSB, is obtained by the following equation:

$$LSB^{\circ} = \frac{360^{\circ}}{M} \tag{2-13}$$

Above equation also gives the minimum phase increment of the n-bit phase shifter. For a single-bit phase shifter n is equal to 1, so according to above equation LSB and minimum phase increment will be 180º that is the highest order bit or most

significant bit, MSB. The next highest bit is 90º if n is equal to 2, then 45º etc. And each bit is designed to get the desired phase shift value and cascaded each other. General diagram of an n-bit digital phase shifter is illustrated in Figure 2.5.

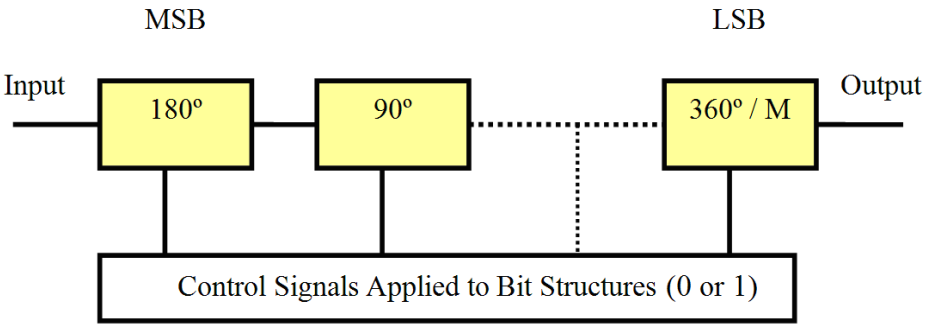

Figure 2.5 Cascaded Bits of a Digital Phase Shifter.

As explained previously, there are M phase steps in an n-bit digital phase shifters where one of the states is accepted as a reference state. The user can obtain any phase state with an increment of $360º/M$ by changing the control signals applied to the bit structures. A truth table for an n-bit digital phase shifter can be formed as shown in Table 2.1 according to the control signals of each bit.

Table 2.1Truth Table of an n-bit Phase Shifter According to Control Signals

Differential Phase Shift (º)	Control Signals Applied To Bit Structures (0 or 1)				
	Bit1 (MSB)	Bit 2	…	Bit n-1	Bit n (LSB)
0 (reference state)	0	0	…	0	0
$360/M$	0	0	…	0	1
…	…	…	…	…	…
…	…	…	…	…	…
$(360/M)(M-2)$	1	1	…	1	0
$(360/M)(M-1)$	1	1	…	1	1

If a 5-bit phase shifter is designed, there will be $2^5 = 32$ phase states with a minimum phase increment $360^o / 32 = 11.25^o$. If all the control signals are 0, then a reference state 00000 is obtained and differential phase shift becomes 0º. If the LSB is changed to 1, the differential phase shift is obtained as 11.25º. If all the bits are changed to 11111, the differential phase shift becomes 348.75º.

2.2.5 Ferrite Phase Shifters

A ferrite phase shifter operates based on the principle that the permeability of a ferrite material varies with the intensity of a DC magnetic field bias. So, as the bias field intensity changes, the phase shift of an RF signal through the material varies [24]. Ferrite phase shifters use differential bulk propagation as technical approach. Ferrite phase shifter can be a good candidate for a high power application because of its low insertion loss and high power handling capacity. They have been used in many applications because of their smaller size and lightweight. However, they are not preferred in military applications due to production complexity, high cost and frequency limitations. Also, magnetic permeability of ferrite material is very sensitive to temperature and mechanical stresses. Ferrite phase shifters operating either in analog or digital can be designed as waveguides, striplines, microstriplines and coaxial lines. Twin-toroid phase shifters, dual-mode phase shifters and Faraday rotation are some known ferrite phase shifters.

2.2.6 Semiconductor Device Phase Shifters

One of the most popular implementation of digital or analog phase shifters is using semiconductor junction devices as electronic control elements. PIN diode, GaAs FET and the varactor diodes are some examples of semiconductor electronic switches which are widely used in different kinds of phase shifter topologies. Semiconductor phase shifters usually use the switching feature of the active devices. When they are compared with ferrite phase shifters, their switching speed is much faster. Moreover, diode phase shifters are nonsusceptible to temperature and mechanical stresses with respect to ferrite phase shifters. They also need small power levels usually in the order of miliwatts in order to perform switching. On the other hand, power handling capacity of semiconductor phase shifters usually is lower than ferrite phase shifters. Generally, semiconductor phase shifters are in reciprocal; however, if the switching

element is an active switch that has an amount of gain, they can be in nonreciprocal form.

2.2.7 PIN Diode Phase Shifters

One of the most popular implementation of semiconductor phase shifter is PIN diode phase shifters. As the name implies, PIN diodes are used to perform switching mechanism between the circuits that are designed to obtain desired phase shift. The advantages of these phase shifters are its small size and weight, broad bandwidth, low drive power, fast switching, and higher reliability and reproducibility [16]. The circuits that are generally used in PIN diode phase shifters are switched line, loaded line, high-pass low-pass, and hybrid coupled. The details of these circuits are given in the next chapter.

In this thesis, PIN diodes have been used as the switching elements between the capacitive loads that terminate the two ports of hybrid coupler.

2.2.8 Amplifier-Type Phase Shifters

Amplifier-type phase shifters also known as active phase shifters provide RF signal amplification in addition to the desired phase shift. Generally, MESFETs, especially the dual-gate MESFETs, are used in the active amplifier mode in order to obtain this type of phase shifters. Active phase shifters can be divided into three groups such as: tuned-gate dual-gate MESFET phase shifter, active phase shifter using switchable SPDT amplifiers, and active phase shifter using vector modulator circuits.

2.2.9 Phase Shifter Fabrication Technologies

Microwave phase shifter designs can be realized using different manufacturing technologies such as waveguide, hybrid MIC, MMIC, RF MEMS etc. In this section some of the phase shifter types produced according to these technologies is briefly explained.

2.2.9.1 Hybrid MIC

MIC technology introduces smaller size and weight when they are compared with waveguides. Also, they are suitable for mass production because of the improved reproducibility and low costs [12].

Planar transmission lines and thin film technology are used for hybrid MIC. Transmission lines in the design generally are in microstrip form which provides tuning applications during the measurement. Dielectric is used as the substrate material. If there is an active device such as PIN diode or a transistor in the design of the phase shifter, they are attached to the passive circuit. Bonding and soldering can be done in hybrid MIC. The size and power handling capacity of a hybrid MIC is higher than MMIC. Switched line, loaded line, high-pass low-pass, and hybrid coupled circuit topologies can be used in hybrid MIC technology. One of the most popular realizations of hybrid MIC technology is PIN diode phase shifters.

2.2.9.2 MMIC

Monolithic microwave integrated circuits came into existence in the late 1970s. All passive and active devices which are required for a given circuit can be grown into the substrate [26]. Generally, Silicon (Si) or GaAs are used as a substrate. Monolithic integrated circuits provide small circuit size and light weight. A single wafer can contain a large number of circuits, all of which can be produced simultaneously. This makes MMIC amenable for mass productions. In addition, when they are compared with hybrid MIC, the parasitics that limit the circuit performance is very low in MMIC. This makes possible to design a circuit with a broader bandwidth. Nevertheless, MMIC design requires careful considerations for design and fabrication, because debugging, tuning, and trimming after production will be difficult, or impossible. Moreover, they can be expensive if small quantities are produced. MMIC is not suitable for high power applications. Most of the phase shifter topologies can be implemented using MMIC technology.

2.2.9.3 RF MEMS

Micro-Electro-Mechanical Systems (MEMS) is the integration of mechanical elements and electronics on a common substrate through microfabrication

technology. During the last years, RF MEMS technology has developed rapidly. RF MEMS switches result in low-loss phase shifters that are operated especially 8 to 120 GHz. RF MEMS phase shifters can be used to eliminate 50-75% of the T/R modules in large phased arrays. For low loss phase shifters, it may be possible to feed two to four elements from a single T/R module, reducing the complexity of the system. The phase shifters produced by using RF MEMS, provide low-loss, high isolation and low drive power. However, switching speed and power handling capacity are the disadvantages of them.

CHAPTER 3

PHASE SHIFTER DESIGN

3.1 Introduction

Various types of phase shifters are briefly explained in Chapter 2. As explained before, there are two different methods that are frequently used for designing digital phase shifters at microwave frequencies. One of them is to use ferromagnetic materials to obtain switchable phase shift. The other design for digital phase shifters uses semiconductor devices such as PIN diode or FETs. When semiconductor device phase shifters are compared to ferrite phase shifters, it can be said that they are more compact, require lower drive power levels, and have lower switching times [25]. Hence, the semiconductor device phase shifters are discussed in this chapter.

As can be seen from Figure 3.1 semiconductor phase shifters can be divided into two groups according to their circuit configurations as transmission type and reflection type. Switched-line phase shifters, loaded-line phase shifters and switched-network phase shifters are some examples of transmission type phase shifters. Circulator coupled and hybrid coupled circuits are examples of reflection type phase shifters.

The above mentioned circuits and the design of a hybrid coupled wideband phase shifter using radial stubs which is the main circuit used in the content of this thesis are explained in this chapter.

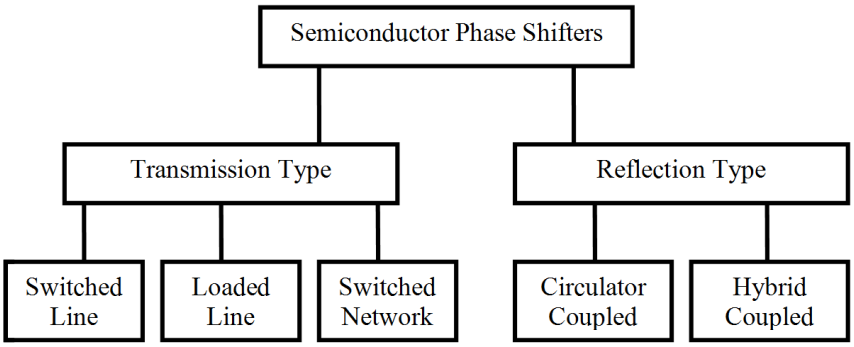

Figure 3.1 Various Types of Semiconductor Phase Shifters.

3.2 Transmission Type Circuits

3.2.1 Switched-Line Phase Shifters

The basic idea behind the switched-line phase shifter is based on switching between two transmission line sections of different lengths. The basic configuration of the circuit for a single-bit is shown in Figure 3.2.

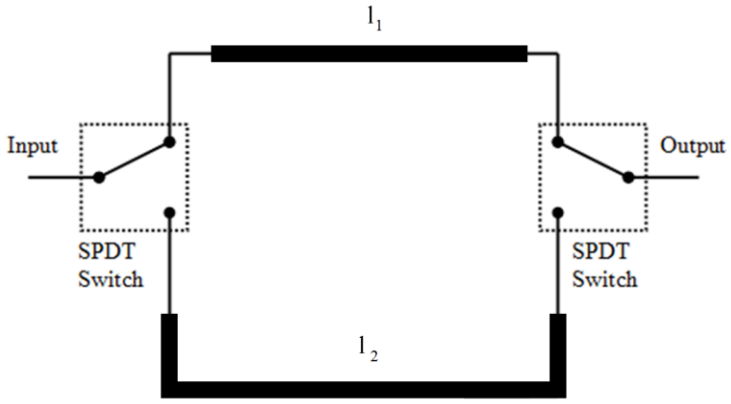

Figure 3.2 Single Bit Switched-Line Phase Shifter.

There are two ideal SPDT switches which are used to change the signal transmission path. Hence, signal passes through one of the two alternative transmission lines with the lengths of ℓ_1 or ℓ_2. All the sections of transmission line have a propagation

constant of β and a characteristic impedance, Z_0. In Figure 3.2, when signal passes through the upper branch of the phase shifter, the insertion phase becomes $\phi_1 = \beta\ell_1$. If the switches are reversed, the signal passes through the lower branch, hence the insertion phase is obtained as $\phi_2 = \beta\ell_2$. So, the differential phase between these two states can be written as:

$$\Delta\phi = \phi_1 - \phi_2 = \beta(\ell_1 - \ell_2) \quad \textbf{(3-1)}$$

Propagation constant β is given by

$$\beta = \frac{\omega}{\upsilon_p} = \frac{2\pi f}{\upsilon_p} \quad \textbf{(3-2)}$$

where υ_p is the phase velocity. As can be seen from the above equations, the differential phase shift $\Delta\phi$ is a linear function of frequency. Because of this property, switched line phase shifters are also called as a true time delay device. The time delay τ_d can be written as:

$$\tau_d = \frac{\ell_1 - \ell_2}{\upsilon_p} \quad \textbf{(3-3)}$$

The insertion loss of this type circuit is usually dependent on the SPDT switches since the transmission line losses are much lower. So, the insertion losses of the two branches are almost equal and the overall phase shifter loss will be independent of the phase shift. SPDT switches can be realized by using PIN diodes, FETs or MEMS. There is a common problem for these circuits in practice that there may be resonances in the branches due to the use of non ideal switches.

Moreover, switched-line phase shifters are not suitable for the applications required constant differential phase shift over a bandwidth. Because, the differential phase shift is directly proportional to frequency.

3.2.2 Loaded-Line Phase Shifters

Another common design for transmission type circuits is the loaded-line phase shifters where the propagation properties of the transmission line are changed. The basic configuration of the loaded-line phase shifters consists of a quarter-wavelength transmission line loaded with switchable reactive elements. These elements are usually arranged in a shunt symmetric form as shown in Figure 3.3

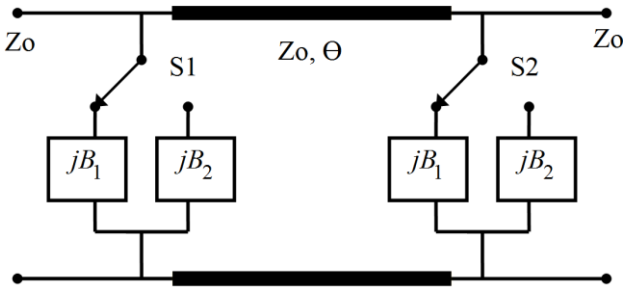

Figure 3.3 Single Bit Loaded-Line Phase Shifter.

The loaded-line phase shifter circuit can be analyzed by using the ABCD parameters of shunt susceptances and the transmission line [9]. Overall ABCD matrix of the circuit can be obtained by matrix multiplication of each element's ABCD matrix. If the circuit is connected to susceptances B_1 by the proper selection of the switches, then ABCD matrix can be given as:

$$\begin{pmatrix} A & B \\ C & D \end{pmatrix} = \begin{pmatrix} 1 & 0 \\ jB_1 & 1 \end{pmatrix} \begin{pmatrix} \cos\theta & jZ_0 \sin\theta \\ jY_0 \sin\theta & \cos\theta \end{pmatrix} \begin{pmatrix} 1 & 0 \\ jB_1 & 1 \end{pmatrix}$$
$$= \begin{pmatrix} (\cos\theta - Z_0 B_1 \sin\theta) & j(Z_0 \sin\theta) \\ j(2B_1 \cos\theta + (Y_0 - Z_0 B_1^{\,2}) \sin\theta) & (\cos\theta - Z_0 B_1 \sin\theta) \end{pmatrix} \quad \textbf{(3-4)}$$

For a reciprocal network, the transmission coefficient S_{21} and the reflection coefficient S_{11} can be obtained from the ABCD matrix by using the formulas given below:

$$S_{21} = \frac{2}{A + \frac{B}{Z_0} + CZ_0 + D} \tag{3-5}$$

$$S_{11} = \frac{\frac{B}{Z_0} - CZ_0}{A + \frac{B}{Z_0} + CZ_0 + D} \tag{3-6}$$

Z_0 is the characteristic impedance of the input and output lines. The normalized susceptance can be written as:

$$B_{N1} = B_1 Z_0 = \frac{B_1}{Y_0} \tag{3-7}$$

Transmission coefficient S_{21} of the circuit can be written using the formulas given in the equations (3-4), (3-5) and (3-7) as:

$$\begin{aligned} S_{21} &= |S_{21}| e^{j\phi_1} \\ &= \frac{2}{\left[(\cos\theta - B_{N1}\sin\theta) + j\left\{ B_{N1}\cos\theta + \left(1 - \frac{B_{N1}^2}{2}\right)\sin\theta \right\} \right]} \end{aligned} \tag{3-8}$$

The transmission phase ϕ_1 is given by:

$$\phi_1 = \tan^{-1}\left| -\frac{B_{N1} + \left(1 - \frac{B_{N1}^2}{2}\right)\tan\theta}{(1 - B_{N1}\tan\theta)} \right| \tag{3-9}$$

For a lossless structure, the magnitude of the input reflection coefficient S_{11} of the circuit can be written as:

$$\begin{aligned}|S_{11}| &= \left[1-|S_{21}|^2\right]^{1/2} \\ &= \left[1-\frac{1}{1+B_{N1}^2(\cos\theta-0.5B_{N1}\sin\theta)^2}\right]^{1/2}\end{aligned} \quad \textbf{(3-10)}$$

Setting equation (3-10) to zero results in the relation:

$$\tan\theta = \frac{2}{B_{N1}} \quad \textbf{(3-11)}$$

If the circuit is connected to susceptances B_2 by the proper selection of the switches, the equation (3-9) can be modified and the insertion phase can be found as:

$$\phi_2 = \tan^{-1}\left|-\frac{B_{N2}+\left(1-\frac{B_{N2}^2}{2}\right)\tan\theta}{(1-B_{N2}\tan\theta)}\right| \quad \textbf{(3-12)}$$

where B_{N2} is equal to

$$B_{N2} = B_2 Z_0 = \frac{B_2}{Y_0} \quad \textbf{(3-13)}$$

Using equations (3-9) and (3-12), the differential phase $\Delta\phi = \phi_1 - \phi_2$ can be found. It has also proved that [9] the widest bandwidth is obtained when $\theta = \pi/2$ and $B_{N1} = -B_{N2}$. Using also these conditions, the differential phase shift is obtained as:

$$
\begin{aligned}
\Delta\phi &= \phi_1 - \phi_2 \\
&= \tan^{-1}\left[-\frac{(1-0.5B_{N1}^2)}{B_{N1}}\right] - \tan^{-1}\left[\frac{(1-0.5B_{N1}^2)}{B_{N1}}\right] \\
&= \pi - 2\tan^{-1}\left[\frac{1-0.5B_{N1}^2}{B_{N1}}\right] \\
&= 2\tan^{-1}\left[\frac{B_{N1}}{1-0.5B_{N1}^2}\right]
\end{aligned}
\qquad \textbf{(3-14)}
$$

Thus, ±90º is the maximum insertion phase that can be obtained by using loaded-line phase shifter. This provides maximum 180º differential phase shift. However, input reflection coefficient is affected by the value of B_{N1}. Hence, it is necessary to limit the phase shift to small values in order to obtain a good input match over a large bandwidth. Therefore, the loaded-line phase shifter is often used for 45º or lower phase shift bits. Also as it can be seen from the equation (3-12), the differential phase shift is not a function of frequency; so, this circuit can be used in applications that require a constant phase shift over a large bandwidth.

3.2.3 Switched-Network Phase Shifters

Garver proposed a switched-network phase shifter in [9] as an alternative to conventional phase shifter circuits that use transmission lines. Using switched-network phase shifters with lumped elements provide physically smaller circuits than the conventional types, especially for large phase shifts. A basic diagram of this type of phase shifter is shown in Figure 2.4.

The low-pass and the high-pass filter circuit configurations shown in Figure 3.4 are the most commonly used networks in switched-network phase shifters. The low-pass and the high-pass filter circuits form the network 1 and network 2, respectively. When the low-pass filter is selected by the switches, a phase delay is occurred, and when the switches are connected to the high-pass filter a phase advance is provided by the circuit. The differential phase shift is achieved by switching between the two filters.

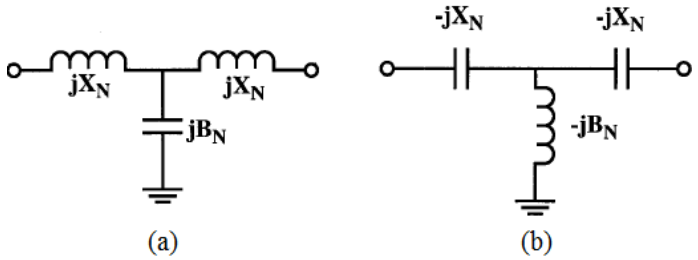

Figure 3.4 Switched Networks.
(a) Low-Pass Filter, (b) High-Pass Filter

Using ABCD matrices of the elements, the circuit can be analyzed as in the case of loaded-line phase shifter. If the circuit is switched to low-pass filter, the ABCD matrix can be written as:

$$\begin{aligned}\begin{pmatrix} A & B \\ C & D \end{pmatrix}_{LP} &= \begin{pmatrix} 1 & jX_N \\ 0 & 1 \end{pmatrix}\begin{pmatrix} 1 & 0 \\ jB_N & 1 \end{pmatrix}\begin{pmatrix} 1 & jX_N \\ 0 & 1 \end{pmatrix} \\ &= \begin{pmatrix} 1-X_N B_N & j(2X_N - B_N X_N^2) \\ jB_N & 1-X_N B_N \end{pmatrix}\end{aligned} \tag{3-15}$$

where X_N and B_N are the reactance and susceptance shown in Figure 3.4 normalized with respect to transmission line impedance Z_0 and admittance Y_0, respectively.

Then the transmission coefficient S_{21} can be written as:

$$\begin{aligned}S_{21,LP} &= \frac{2}{A+B+C+D} \\ &= \frac{2}{2(1-B_N X_N)+j(B_N+2X_N-B_N X_N^2)}\end{aligned} \tag{3-16}$$

The insertion phase of the network can be obtained from the equation (3-16) as:

$$\phi_{21,LP} = \tan^{-1}\left\{-\frac{B_N+2X_N-B_N X_N^2}{2(1-B_N X_N)}\right\} \tag{3-17}$$

When the circuit is switched to high-pass filter shown in Figure 3.4, the insertion phase of the network is obtained by replacing B_N by $-B_N$ and X_N by $-X_N$ in equation (3-12) as:

$$\begin{aligned}\phi_{21,HP} &= \tan^{-1}\left\{\frac{B_N + 2X_N - B_N X_N^2}{2(1-B_N X_N)}\right\} \\ &= -\tan^{-1}\left\{-\frac{B_N + 2X_N - B_N X_N^2}{2(1-B_N X_N)}\right\}\end{aligned} \quad \textbf{(3-18)}$$

Then differential phase of the phase shifter is given by:

$$\begin{aligned}\Delta\phi &= \phi_{21,LP} - \phi_{21,HP} \\ &= \tan^{-1}\left\{-\frac{B_N + 2X_N - B_N X_N^2}{2(1-B_N X_N)}\right\} - \left(-\tan^{-1}\left\{-\frac{B_N + 2X_N - B_N X_N^2}{2(1-B_N X_N)}\right\}\right) \\ &= 2\tan^{-1}\left\{-\frac{B_N + 2X_N - B_N X_N^2}{2(1-B_N X_N)}\right\}\end{aligned} \quad \textbf{(3-19)}$$

As it can be seen from the equation (3-19), this type of circuit does not bear true-time delay properties, since the differential phase shift is not a linear function of the frequency. Hence, this circuit configuration can be used for wideband applications that need constant phase shift.

The magnitude of transmission coefficient S_{21} should be equal to 1 in ideal case, in order to obtain perfect input and output matching. Setting the magnitude of equation (3-16) to 1 and solving B_N results in:

$$B_N = \frac{2X_N}{1+X_N^2} \quad \textbf{(3-20)}$$

Then, if B_N is replaced in equation (3-19) using the relation in equation (3-20), the differential phase shift is obtained as:

$$\Delta\phi = 2\tan^{-1}\left\{\frac{2X_N}{X_N^2 - 1}\right\} \quad \textbf{(3-21)}$$

Finally, X_N and B_N can be found in terms of $\Delta\phi$ using the equations (3-20) and (3-21) as:

$$X_N = \tan\left(\frac{\Delta\phi}{4}\right) \quad \textbf{(3-22)}$$

$$B_N = \sin\left(\frac{\Delta\phi}{2}\right) \quad \textbf{(3-23)}$$

Switching between the low-pass and the high-pass circuits provide constant phase shift over a large bandwidth without considerable disturbing the performance of input return loss.

3.3 Refection Type Circuits

Reflection type phase shifters are another significant class of phase shifters. The basic circuit configuration is shown in Figure 3.5. A uniform transmission line is terminated with a switchable reflection network. The network has two structures that have two different reflection coefficients such as, $\Gamma_1 = |\Gamma_1| \angle \phi_1$ and $\Gamma_2 = |\Gamma_2| \angle \phi_2$. The differential phase shift $\Delta\phi = \phi_1 - \phi_2$ is obtained when the reflection coefficient is switched from Γ_1 to Γ_2 [25]. The ratio of the reflected power to the incident power is given by $|\Gamma|^2$ in each state. In an ideal case, $|\Gamma|$ is equal to unity so that all the power coming to switchable network shown in Figure 3.5 is reflected back. Hence, there is no loss associated with the phase shifting operation.

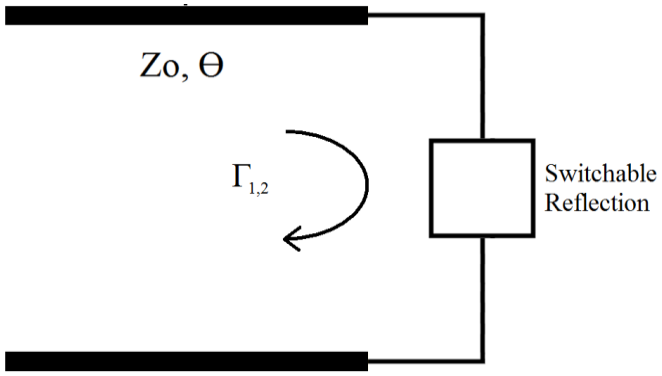

Figure 3.5 Basic Configuration of Reflection Type Phase Shifter.

The circuits provided reflection can be realized in two different ways. In the first group, an additional line length is added at the reflection plane. The concept is similar to that used in switched-line phase shifters. In the second group, the reactance terminating the line is altered and different reflection coefficient is obtained for each them.

The circuit illustrated in Figure 3.5 is a one-port device. Nevertheless, two port phase shifter circuits are usually required for the most of the systems using phase shifters. The use of a circulator or a 90º hybrid makes converting one-port network into two-port network possible. These two circuit configurations are shown in Figure 3.6 and Figure 3.7, respectively.

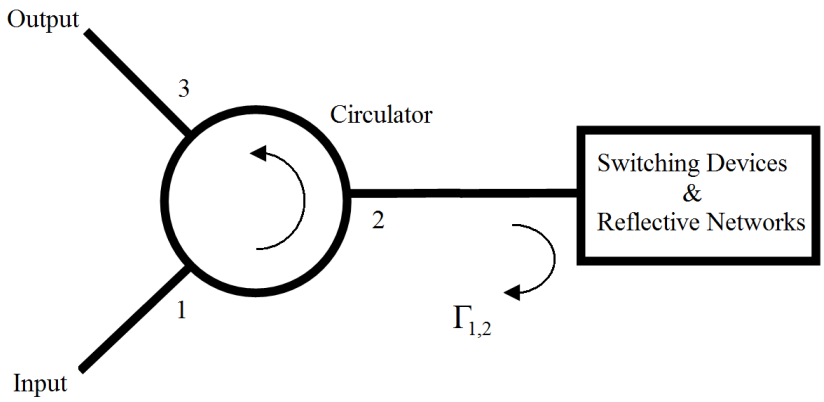

Figure 3.6 Circulator Coupled Reflection Type Phase Shifter.

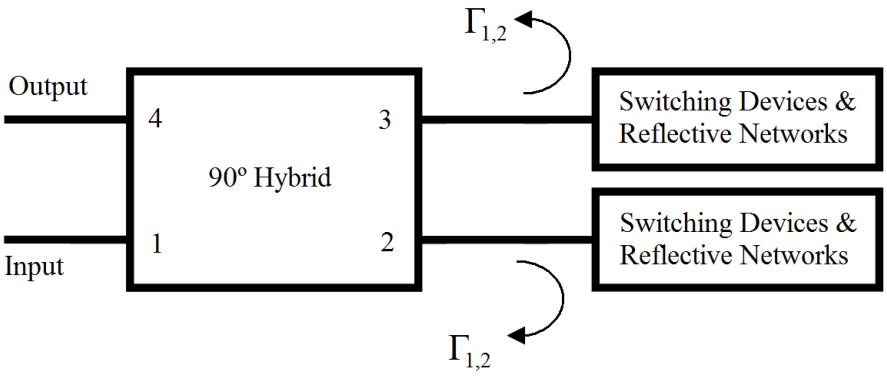

Figure 3.7 Hybrid Coupled Reflection Type Phase Shifter.

As it can be seen from Figure 3.7, the hybrid coupled phase shifter is formed by using a 90º hybrid coupler where two ports of is terminated reflective circuits. 90º hybrid coupler is a four-port device that is used to equally split an input signal coming from port 1 with a resultant 90° phase shift between output ports port 2 and port 3. The signals are reflected from the two symmetric terminations and they add up at port 4 since they are in phase. They cancel each other at port 1, so that no signal returns back to port 1. Port 2 and port 3 are terminated with two identical reflective networks. When the signal is applied to port 1, the signals are reflected from the terminations with the same reflection coefficient Γ_1 and sum up at port 4. If the terminations are switched to other two identical networks, the reflection coefficient will be Γ_2 and the differential phase shift will be obtained.

When these circuits are compared, the hybrid coupled phase shifters require two identical phase shift networks that are connected to through and coupled ports of the 90º hybrid, while the circulator coupled phase shifter uses one. Hence, the number of devices used in the circuit is doubled. However, in reflection type phase shifter design, hybrid coupled circuits are preferred to circulator coupled circuits. Primarily, 90º hybrids are more suitable for MICs and MMICs than the circulators. Also, the power handling capacity of the phase shifter is increased due to the use of two switching devices. Moreover, ease of fabrication, lower insertion loss, lower size and cost are the other advantages of the hybrid coupled phase shifters.

3.4 Wideband Hybrid Coupled Phase Shifter Design

One of the most popular implementation of a wideband phase shifter is using a 3 dB, 90º coupler whose direct port and coupled port are terminated with two identical capacitive loads, as shown in Figure 3.8 [10]. If a signal is applied from the input port of the coupler such as $a_1 = 1\angle 0^\circ$, then this signal is equally divided and sent to direct and coupled ports as $b_2 = 1/\sqrt{2}\angle -90^\circ$ and $b_3 = 1/\sqrt{2}\angle -180^\circ$, respectively. These signals are reflected by the capacitive load with a reflection coefficient of Γ. The reflected signals at the direct port and the coupled port become $a_2 = \Gamma/\sqrt{2}\angle -90^\circ$ and $a_3 = \Gamma/\sqrt{2}\angle -180^\circ$, respectively. Then these signals are sent to input port and isolated port. The signal at the input port becomes $b_1 = \Gamma/2\angle 0^\circ + \Gamma/2\angle -180^\circ$, so that reflected signals at input cancel each other since they are out of phase. The signal at isolated port becomes $b_4 = \Gamma/2\angle 90^\circ + \Gamma/2\angle 90^\circ$, so that the reflected signals are add up since they are in phase. Hence, when the reflection coefficient of the capacitor pair is Γ, then the insertion phase can be written as:

$$\phi = 90^\circ + \phi_\Gamma \qquad \textbf{(3-24)}$$

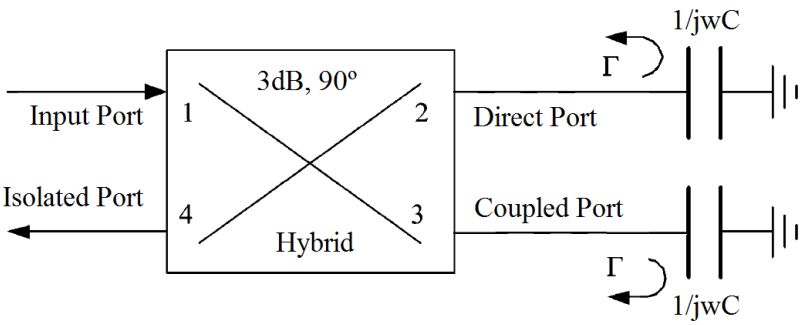

Figure 3.8 Hybrid Coupled Phase Shifter with Capacitive Reflective Loads.

The reflection coefficient of the capacitive load Γ can be written as:

$$\Gamma = 1\angle\left[-2\tan^{-1}\ \omega C Z_0 \ \right] \qquad \textbf{(3-25)}$$

where C is the capacitance of the load and Z_0 is the characteristic impedance of the hybrid coupler. A typical phase shifter consists of two different pairs of capacitors C_1 and C_2. So, there are two different states according to the selected capacitor pair. The differential phase shift is achieved by switching between C_1 and C_2 and it is given as:

$$\phi = 2\tan^{-1}\left(\frac{\omega Z_0\ C_2 - C_1}{1+\omega^2 Z_0^2 C_1 C_2} \right) \qquad \textbf{(3-26)}$$

where Z_0 is the characteristic impedance of the hybrid coupler.

In this thesis hybrid coupled reflection type phase shifter is designed where Lange coupler is used as a 3 dB, 90º hybrid and radial stubs are used as capacitive loads in order to provide reflection. It will be useful to mention the Lange coupler and the radial stub before talking about the linear design of the phase shifter.

3.4.1 Lange Coupler

A 3 dB, 90º hybrid coupler is required in order to design a hybrid coupler phase shifter. Generally, to obtain 3 dB coupling factor using conventional coupled lines is very difficult in practice, since the spacing between the lines become very narrow as the coupling factor is increased. Using several lines parallel to each other is one way to increase the coupling between the lines. Fringing fields at both edges contribute to the coupling [27]. One popular implementation of this approach is the Lange coupler developed by Dr. Julius Lange around 1969. Closely spaced transmission lines such as microstrip lines provide tight coupling. A typical geometry of a four fingers Lange coupler is illustrated in Figure 3.9. There are three important physical parameters that determine the coupling coefficient, center frequency, and bandwidth of a Lange coupler. These are the width of the conductors (w), spacing between the conductors (s) and the length of the conductors (l).

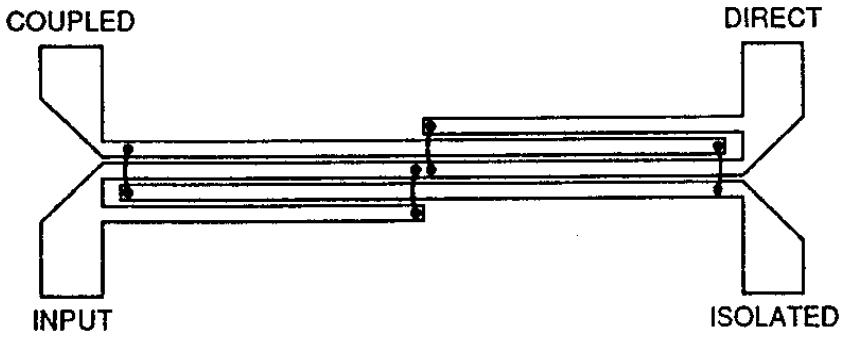

Figure 3.9 Lange Coupler Geometry.

Here, four coupled lines are used with interconnections to provide the tight coupling. Lange coupler is designed such that when a signal is applied to the input port, power is divided into two equally but 90º out of phase and sent to the direct and coupled ports but none of the power to the isolated port. Lange coupler is a type of quadrature coupler, since there is 90º phase difference between the direct and coupled ports. The scattering matrix of an ideal Lange coupler is given by:

$$S = \frac{-1}{\sqrt{2}} \begin{bmatrix} 0 & j & 1 & 0 \\ j & 0 & 0 & 1 \\ 1 & 0 & 0 & j \\ 0 & 1 & j & 0 \end{bmatrix} \quad \textbf{(3-27)}$$

With an octave or more bandwidth, 3 dB coupling ratios can be achieved using Lange coupler. There is also another configuration for Lange coupler called as unfolded Lange coupler [28] which is shown in Figure 3.10.

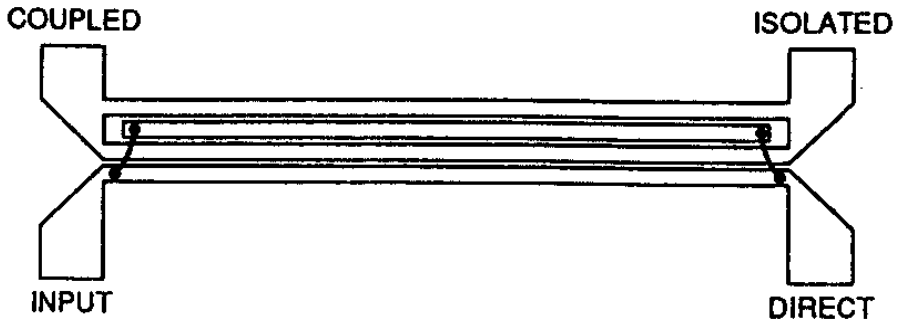

Figure 3.10 Unfolded Lange Coupler Geometry.

The unfolded Lange coupler basically has same operational properties as the typical Lange coupler. However, from the physical point of view, the isolated and direct ports positions are interchanged. Also, unfolded form requires fewer wire connections than the typical Lange coupler.

The unfolded Lange coupler is used in this thesis in order to design wideband phase shifter bits, since the direct port and the coupled port are not located on the same side of the coupler.

3.4.2 Radial Stub

Radial stubs, generally in microstrip form, are widely used in RF and microwave circuits for impedance matching, for bias lines and in filter circuits. They are usually used in both MICs and MMICs. Radial stubs are preferred to conventional line stubs in wideband applications, since their reflection coefficient is much higher. Also, radial stubs provide a low impedance levels in a wide frequency band. A typical radial stub is shown in Figure 3.11. For a radial stub, there are three important parameters as the angle, inner and outer radius.

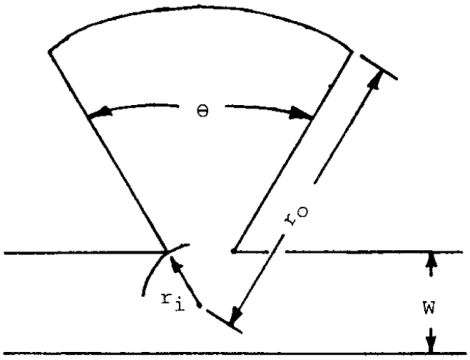

Figure 3.11 Radial Stub Connected to a Transmission Line.

For the radial stub shown above, the input impedance Z_{in} is written in the following form [29]:

$$Z_{in} = -j\frac{120\pi h}{r_i\theta\sqrt{\varepsilon_{eff}}}\frac{Y_0(\beta r_i)J_1(\beta r_o)-J_0(\beta r_i)Y_1(\beta r_o)}{J_1(\beta r_i)Y_1(\beta r_o)-Y_1(\beta r_i)J_1(\beta r_o)} \quad \textbf{(3-28)}$$

where J_m and Y_m are the m-order Bessel functions of the first and second type, respectively. $\beta = 2\pi\sqrt{\varepsilon_{eff}}/\lambda_0$ is the phase constant where ε_{eff} is the effective dielectric constant. h is the thickness of the dielectric layer [10]. Bessel functions in equation (3-28) can be extended into a series, assuming $r_0 < \lambda/8$ and $r_i \approx r_o/10$:

$$Z_{in} \cong -j\frac{120\pi h}{\theta\sqrt{\varepsilon_{eff}}}\left(\frac{2}{\beta r_0^2}-\beta\left(2.8-\frac{10r_i}{r_0}\right)\right) \quad \textbf{(3-29)}$$

Equation (3-29) can be thought as a series combination of a capacitor $C \equiv \theta r_o^2\varepsilon_{eff}/(240\pi hc)$ and an inductor $L \equiv 120\pi h(2.8-10r_i/r_o)/(c\theta)$ where c is the speed of light. Hence, the phase of the reflection coefficient ϕ_Γ is obtained as [10]:

$$\phi_\Gamma(x) = 2\tan^{-1}\left(\frac{1}{x}X_C(\omega_0)-xX_L(\omega_0)\right)-\pi \quad \textbf{(3-30)}$$

where $x \equiv \omega / \omega_0$ and $0.5 \le x \le 1.5$.

$X_C(\omega_0) \equiv 1/(\omega_0 C Z_0)$ and $X_L(\omega_0) \equiv \omega_0 L / Z_0$ are the capacitive and inductive parts of the normalized input impedance $Z_{in}(\omega_0)/Z_0$ at the center frequency ω_0. If the equation (3-29) is expanded into Taylor series for $x = 1$, the phase of the reflection can be written as:

$$\phi_\Gamma(x) \cong \phi_\Gamma(1) + \phi_\Gamma'(1)(x-1) \qquad \textbf{(3-31)}$$

where $\phi_\Gamma'(1) \equiv d\phi_\Gamma(x)/dx\big|_{x=1}$.

3.4.3 Phase Shifter Design Using Lange Coupler and Radial Stubs

As explained previously, the Lange coupler can be used as a 3 dB, 90º hybrid coupler and radial stubs for the capacitive loads. The phase shifter obtained with the use of these elements and the switches required for the selection of the stubs is shown in Figure 3.12.

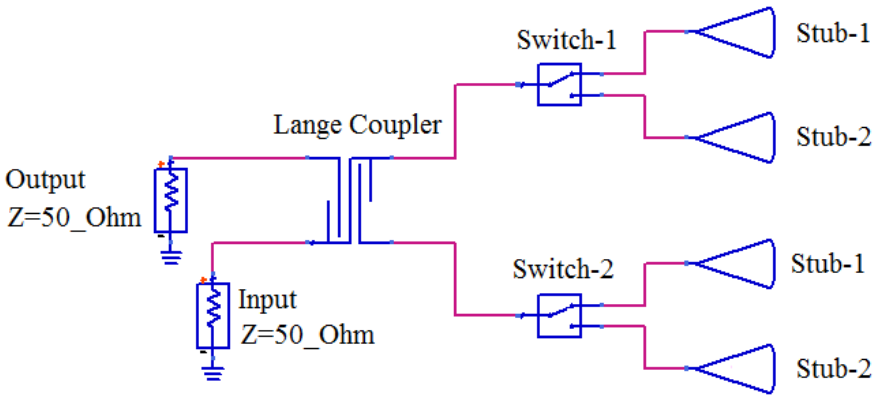

Figure 3.12 Hybrid Coupled Phase Shifter Using Lange Coupler and Radial Stubs.

In equation (3-31) the reflection coefficient has been found for the radial stub. The insertion phase of the above structure has been found in equation (3-24) for the reflection coefficient of a capacitor. Now, if the capacitors shown in Figure 3.7 are

replaced with a pair of identical radial stubs, the insertion phase at the output (isolated port of the Lange coupler) is given by:

$$\phi(x) = 90^{o} + \phi_{\Gamma}(x) \tag{3-32}$$

where $\phi_{\Gamma}(x)$ has been given in equation (3-30) and (3-31). So the differential phase shift for the phase shifter shown in Figure 3.11 can be given as:

$$\begin{aligned} \Delta\phi(x) = & \ 90^{o} + \phi_{\Gamma_1}(x) \ - \ 90^{o} + \phi_{\Gamma_2}(x) \\ = & \ \phi_{\Gamma_1}(x) - \phi_{\Gamma_2}(x) \end{aligned} \tag{3-33}$$

where $\phi_{\Gamma_1}(x)$ and $\phi_{\Gamma_2}(x)$ are the phase of the reflection coefficients of radial stubs 1 and radial stubs 2 and they can be easily written according to equation (3-30) as:

$$\begin{aligned} \phi_{\Gamma_1}(x) &= 2\tan^{-1}\left(\frac{1}{x}X_{C_1}(\omega_0) - xX_{L_1}(\omega_0)\right) - \pi \\ \phi_{\Gamma_2}(x) &= 2\tan^{-1}\left(\frac{1}{x}X_{C_2}(\omega_0) - xX_{L_2}(\omega_0)\right) - \pi \end{aligned} \tag{3-34}$$

where $X_{C_1}(\omega_0) \equiv 1/(\omega_0 C_1 Z_0)$, $X_{C_2}(\omega_0) \equiv 1/(\omega_0 C_2 Z_0)$, $X_{L_1}(\omega_0) \equiv \omega_0 L_1 / Z_0$ and $X_{L_2}(\omega_0) \equiv \omega_0 L_2 / Z_0$.

Also $C_1 \equiv \theta_1 r_{o1}^2 \varepsilon_{eff} / (240\pi hc)$ and $L_1 \equiv 120\pi h(2.8 - 10 r_{i1} / r_{o1}) / (c\theta_1)$ where θ_1 , r_{i1} and r_{o1} are the angle, inner radius and outer radius for the radial stub 1, respectively. C_2 and L_2 is written for the radial stub 2 in a similar way.

In reference [10], for a desired differential phase shift of $\Delta\phi(1)$ at the center frequency and a desired maximum phase error of $\Delta\phi_{err}$, the normalized impedances of radial stubs should satisfy the following equations:

$$X_{C_2}(\omega_0) - X_{L_2}(\omega_0) = \frac{X_{C1}(\omega_0) - X_{L_1}(\omega_0) - \tan(\phi(1)/2)}{1 + \; X_{C1}(\omega_0) - X_{L_1}(\omega_0) \; \tan(\phi(1)/2)} \tag{3-35}$$

$$\left|(\phi'_{\Gamma_1}(1) - \phi'_{\Gamma_2}(1))/2\right| \le \Delta\phi_{err} \tag{3-36}$$

where $\phi'_{\Gamma_1}(1) \equiv d\phi_{\Gamma_1}(x)/dx\big|_{x=1}$ and $\phi'_{\Gamma_2}(1) \equiv d\phi_{\Gamma_2}(x)/dx\big|_{x=1}$.

3.4.4 Sample Design

6-18 GHz wideband hybrid coupled phase shifter for 11.25º is designed as an example. Minimum phase error and return loss are aimed while designing the circuit. Advanced Design System is used for design and simulations. 15-mil thick Alumina substrate is chosen with a dielectric constant $\varepsilon_r = 9.8$. As a first step, the Lange coupler that is shown in Figure 3.13 is designed for 6-18 GHz. The center frequency of the coupler is 12 GHz. The width and the length of the conductors are 0.9 mils and 97.8 mils, respectively. The spacing between the conductors is 0.67 mils.

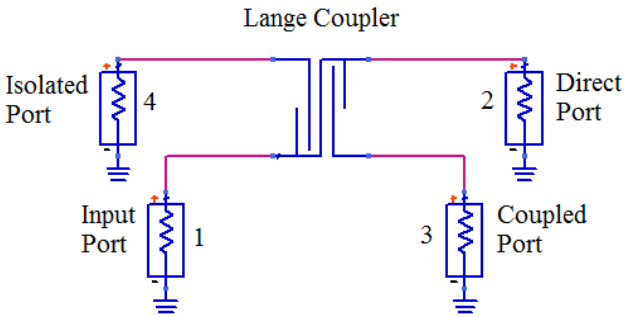

Figure 3.13 Lange Coupler Design in ADS.

The magnitude response of the Lange coupler is shown in Figure 3.14. As it can be seen from the figure, the differences between S_{21} and S_{31} values at 6, 12, and 18 GHz almost remain same and it is about 1.6 dB. This response is different than the typical Lange coupler response and it can be called as overcoupled since the transmission coefficient of the coupled port is higher than the transmission

coefficient of direct port in some frequency range. The return loss and the isolation are approximately better than -20 dB up to 18 GHz.

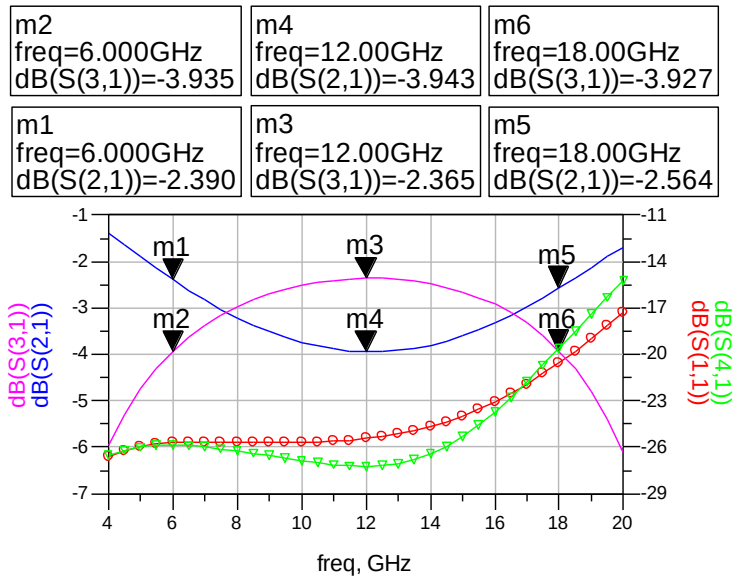

Figure 3.14 Magnitude Response of Lange Coupler.

The phase response of the Lange coupler is shown in Figure 3.15. As it is expected the phase difference between the direct port and the coupled port is almost 90º.

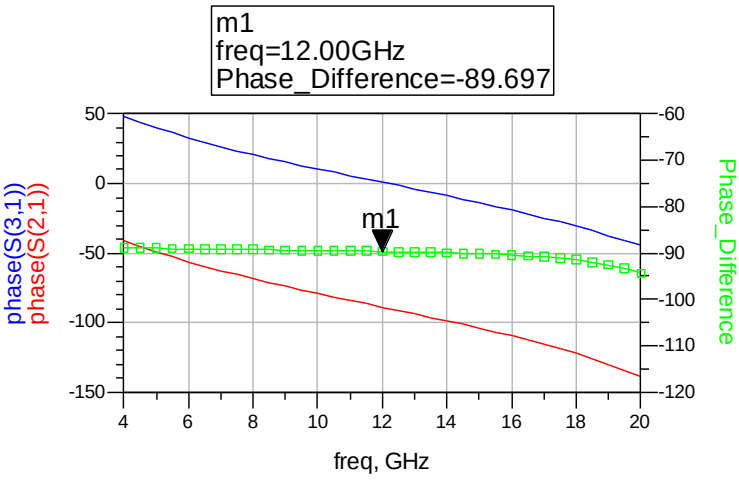

Figure 3.15 Phase Response of Lange Coupler.

In the next step, the radial stubs are determined in order to obtain 11.25º with a minimum return loss. Radial stubs are also designed into 15-mil thick Alumina substrate. In ADS, the radial stub shown in Figure 3.16 is defined by width of input line (W), length of stub (L) and angle subtented by stub (A). The radial stub size parameters that are found using ADS to achieve 11.25º±0.5º differential phase shift are given in Table 3.1.

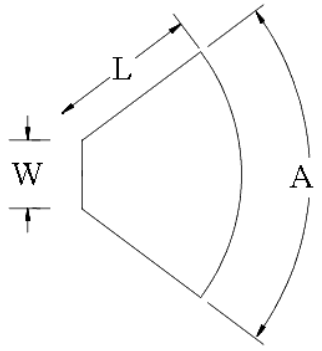

Figure 3.16 Radial Stub Parameters in ADS.

Table 3.1 Radial Stub Parameters

Stub Parameters:	Stub-1	Stub-2
W (mils)	10.5	6.2
L (mils)	39.6	35
A (º)	90	100

The overall circuit that is obtained by connecting the Lange coupler's direct and coupled ports to the radial stub pairs is shown in Figure 3.17. The ideal switches are used in this example. However, of course, in practical implementation these switches will be replaced by PIN diodes.

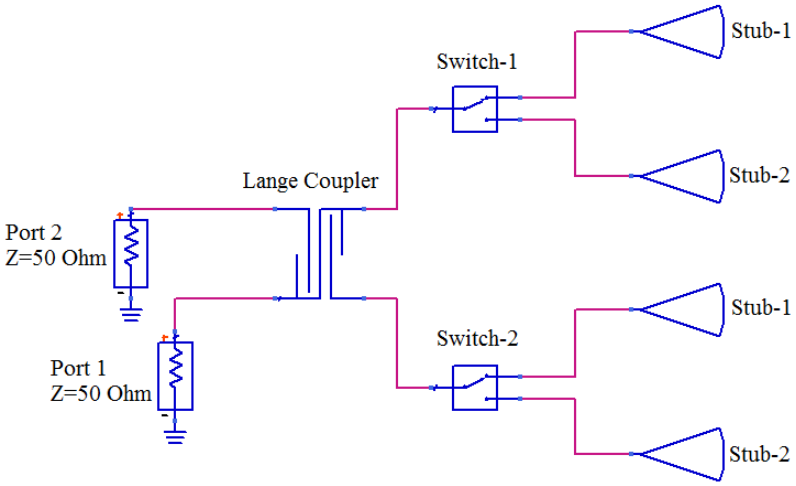

Figure 3.17 Basic Structure of the Phase Shifter.

When the lossless switches are arranged to select the Stub-1 as the capacitive reflective loads; the insertion loss, the input return loss and the output return loss of the circuit are obtained as shown in Figure 3.18. The input return loss and output return loss are lower than -14 dB for the frequency range 6-18 GHz. The insertion loss is larger than -0.3 dB for the same frequency range. The dielectric and conductor losses are calculated in this simulation. Hence, they caused some amount of loss in the transmission.

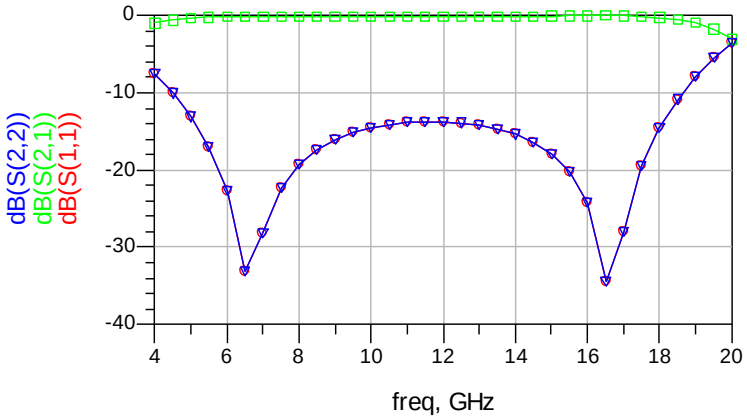

Figure 3.18 Input and Output Return Losses When The Stub-1 Is Selected.

When the switches are arranged to select the Stub-2 as the capacitive reflective loads; the insertion loss, the input return loss and the output return loss of the circuit are obtained as shown in Figure 3.19. The input return loss and output return loss are lower than -13 dB for the frequency range 6-18 GHz. The insertion loss is larger than -0.3 dB for the same frequency range.

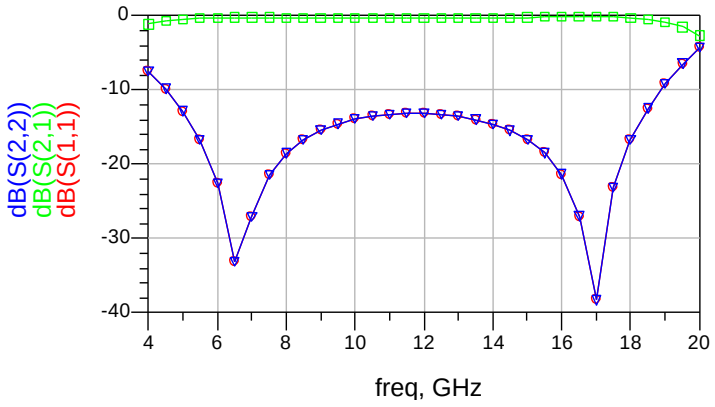

Figure 3.19 Input and Output Return Losses When The Stub-2 Is Selected.

Figure 3.20 shows the insertion phases of the circuit when the Stub-1 and the Stub-2 are selected as the reflected loads. Phase(S(2,1)) shows the phase response of the circuit when the Stub-1 is selected, while Phase(S(4,3)) shows the phase response of the circuit when the Stub-2 is selected.

Figure 3.20 The Insertion Phases of The Circuit for Stub-1 and Stub-2.

The differential phase shift is obtained by subtracting the phase responses shown in Figure 3.20. So, the differential phase shift response of the circuit presented in this example is shown in Figure 3.21.As it can be seen from the figure, the differential phase shift for 11.25º is achieved with ±0.5º phase error.

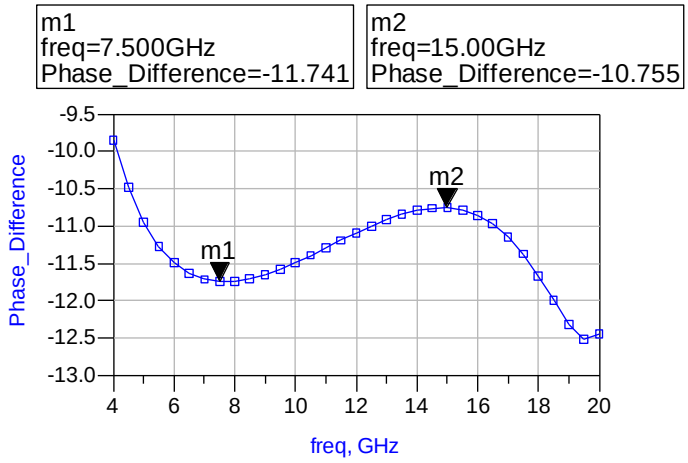

Figure 3.21 The Differential Phase Shift Between Insertion Phases.

This example can be realized using different production techniques. In this thesis MIC technology is used with PIN diodes in order to provide switching between the loads. The phase shifter bits for 11.25º, 22.5º, 45º, and 90º are designed onto two different substrates Rogers TMM10i and Alumina. The phase shifter bits designed onto TMM10i substrate have been produced in ASELSAN facilities using PCB techniques. On the other hand, the phase shifter bits designed onto Alumina have been produced by American Technical Ceramics (ATC) using thin film production techniques. In the next four chapters, the designs and the measurement results of the phase shifter bits fabricated by these two different production techniques are explained in detail.

CHAPTER 4

LANGE COUPLER DESIGN ON TMM10I SUBSTRATE AND MODELING OF PIN DIODE

At the end of Chapter 3 the linear design of a wideband phase shifter is briefly explained using ADS program. In the design, the linear responses of the Lange coupler and radial stubs are used with lossless ideal switches. However, the phase shifter designs will be more realistic if the measurement results of Lange coupler and switches are used. Two PIN diodes are used instead of each switch shown in Figure 3.17. In this chapter, the details of unfolded Lange coupler and PIN diode are explained.

The Lange coupler is the most important component in the design of the phase shifter circuits that are in the scope of this thesis. If it does not work properly, the remaining part of the circuit is meaningless. Because of this reason, firstly the Lange coupler is designed, fabricated and measured in the beginning of this study. The fabrication and measurements of Lange coupler are performed in ASELSAN Inc. facilities. Secondly, the PIN diode which is another important component of the circuit is measured. Also, its model for linear simulations is extracted in order to use it in the design of the phase shifter circuits.

4.1 The Dielectric Substrate and Metallization

The Lange couplers in the content of this and next chapter are realized on Rogers TMM10i substrate.

The dielectric constant ε_r of TMM10i substrate is 9.8 that is equal to the dielectric constant of Alumina. However, the dissipation factor $\tan\delta$ of TMM10i is given as 0.002 where the tangent loss of the Alumina is 0.0002. So, it is obvious that TMM10i

is much more lossy than the Alumina. On the other hand, the electrical and mechanical properties of TMM10i combine the benefits of both ceramic and conventional PTFE microwave circuit laminates, without requiring the thin film production technique as in the case of Alumina. So, the designs can be manufactured using PCB technique in ASELSAN facilities.

The thickness of the substrate is chosen as 25 mils. Of course, the substrate thickness should be low for high frequency applications since the substrate loss is increased. However, when the thickness of the substrate is decreased the spacing between the lines of the Lange coupler will decrease, too. Since the PCB technology is used, there are some limitations for the width of the lines and spacing between the lines. If the thickness were chosen as 15 mils, the spacing between the coupled lines would be smaller than 1 mil which is almost impossible for PCB technique. This is the reason of why the substrate thickness is selected as 25 mils. The metal conductor of the substrate is copper with a thickness of 1.42 mils.

Since TMM10i is based on thermoset resins and does not soften, wire bonding which is required for Lange coupler fabrication can be performed without concerns of pad lifting or substrate deformation.

4.2 Unfolded Lange Coupler

As explained previously, the Lange coupler is the most important component of the circuit. The design, EM simulation, fabrication and measurement results of the Lange coupler are given in this part.

4.2.1 Design and EM Simulation

Microstrip unfolded Lange coupler is designed to operate for 6-18 GHz frequency band. ADS program is used for linear simulation of the coupler. Width and length of the coupled lines and spacing between the coupled lines are obtained as 2, 95 and 1.4 mils, respectively. With these parameters, the Lange coupler designed on 25-mils thick TMM10i substrate has frequency response as shown in Figure 4.1.

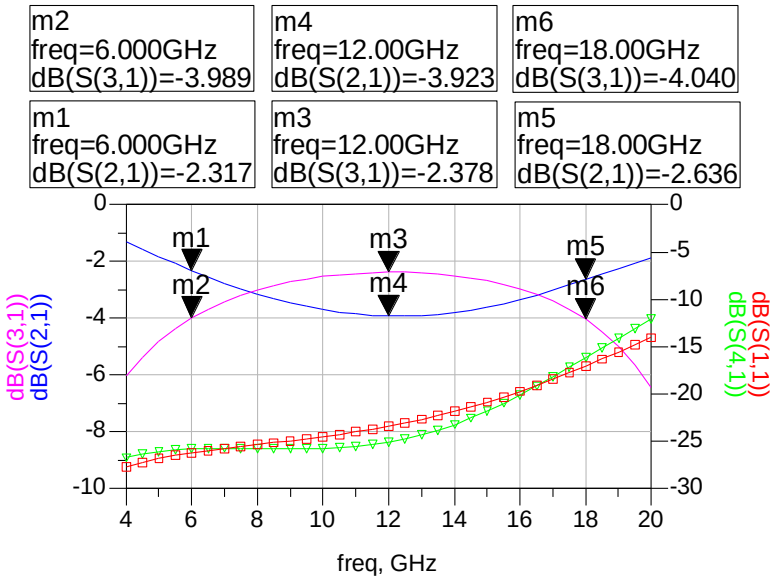

Figure 4.1 Linear Simulation Result of Unfolded Lange Coupler.

The differences between the S21 and S31 values at 6, 12 and 18 GHz are tried to be at same levels. The input return loss is lower than -17 dB while the isolation is lower than -16 dB at 18 GHz.

In the next step, the EM simulations are performed using CST software. The circuit that is simulated in this program is shown in Figure 4.2. The Lange coupler is designed to measure by using probe station which will be also explained in the measurement setup. Hence, there are some modifications on 50 Ohm transmission lines such as extending and bending on them. Also, the limitations of the laser machine to produce the design are taken into account. Hence, the spacing between the coupled lines is increased to 2.2 mils. The width of the coupled lines is increased to 3 mils in order to increase the strength of the metal conductor on the substrate. The length of the coupled lines is 112 mils.

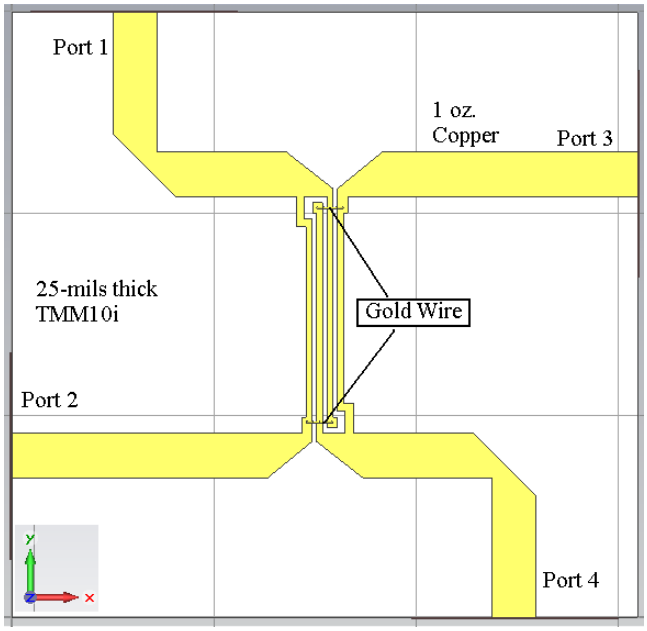

Figure 4.2 The CST Layout of Unfolded Lange Coupler.

Two gold wires are used in order to connect the coupled lines. The radius and the length of the wire are 1 and 6 mils. The pads that are placed for bonding are tried to be bigger due to the limits of the laser machine. EM simulation frequency response of the unfolded Lange coupler is shown in Figure 4.3.

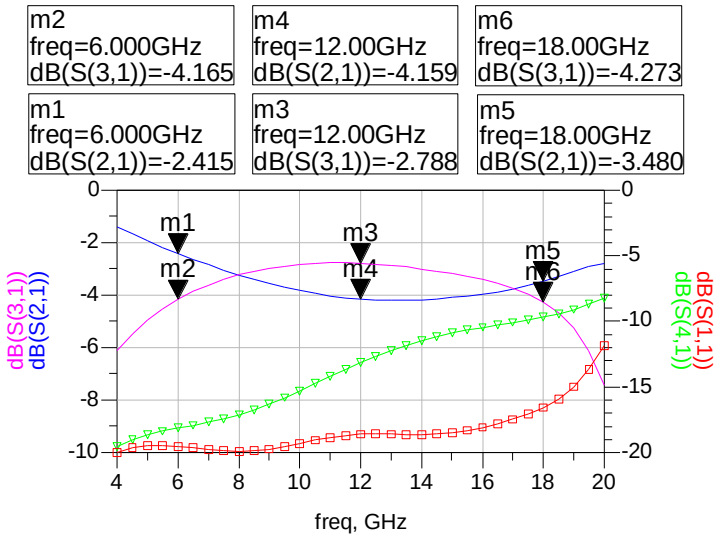

Figure 4.3 EM Simulation Result of the Unfolded Lange Coupler.

When the above response is compared with linear simulation result, it can be seen that there is a slope on S21 and S31 which are the direct port transmission coefficient and coupled port transmission coefficient, respectively. Because, as the frequency is increased, the dielectric and conductor losses are also increased. Input return loss is below -15 dB while the isolation is lower than -9 dB at 18 GHz. The response can be shifted to low frequency side increasing the length of the coupled lines, however, the transmission coefficient S21 will decrease. The unfolded Lange coupler shown in Figure 4.2 is manufactured. The fabrication details are given in next section.

4.2.2 Fabrication and Measurement

The spacing between the coupled lines is the most critical parameter in the production process, since it requires very small value in order to provide tight coupling for Lange coupler. LPKF Proto Laser 200 machine shown in Figure 4.4 is used for PCB fabrication.

Figure 4.4 LPKF Proto Laser 200.

Many trials are done changing the machine properties in order to fabricate the coupler properly. Realization of the spacing between the coupled lines which is 2.2

mils was the hardest part of the production. Finally, the coupler that is shown in Figure 4.5 is fabricated.

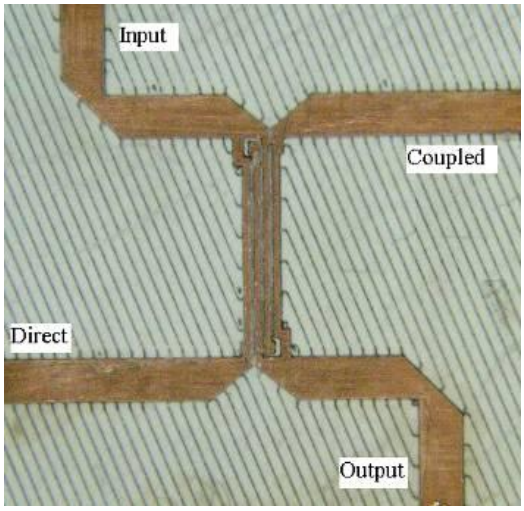

Figure 4.5 Fabricated Unfolded Lange Coupler.

Afterwards, bonding between the pads of the coupled lines is performed by using ball bonder machine Kulicke Soffa AG 4124 that is shown in Figure 4.6. Golden wire of diameter 1mil is used for bonds.

Figure 4.6 Kulicke Soffa AG 4124 Ball Bonder Machine.

After ball bond operation coupler is attached to a gold plated carrier using conductive epoxy. In order to measure the coupler using probe station, test points which are shown in Figure 4.8 are required. However, test point is 10 mils high where the height of the substrate is 25 mils. Hence, gold discs that are 10 mils high are attached to under the test points in order to decrease the height differences between the coupler and test point. Test points are attached over the gold discs using conductive epoxy. Finally, the connections between the coupler's 50 Ohm transmission lines and the test points are performed by using Unitek Peco Model UB25 welding machine shown in Figure 4.7. 10 mil width golden ribbons are used in the connections.

Figure 4.7 Unitek Peco Model UB25.

All these operations are performed in clean room facility of ASELSAN Inc. The picture of the coupler that is ready for measurement is shown in Figure 4.8. The components used in assembling are also shown in this figure.

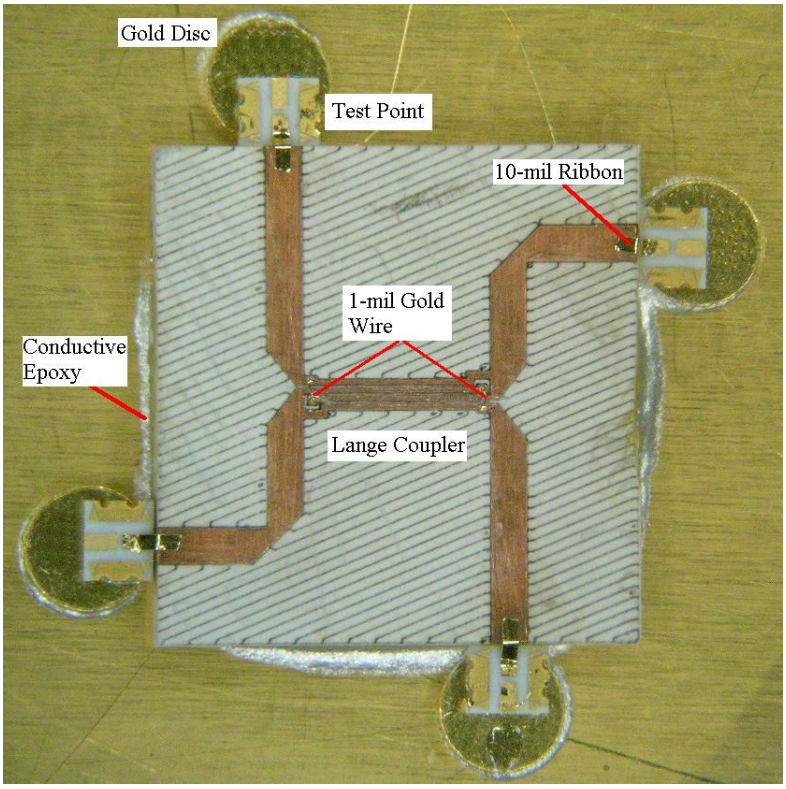

Figure 4.8 Assembled Unfolded Lange Coupler for Measurement.

The measurement of unfolded Lange coupler is performed by using Cascade Microtech Microwave Probing Station and Agilent N5242A PNA-X 4 Port Network Analyzer operating between 10 MHz and 26.5 GHz. The measurement setup and probes that are approached to the coupler test points are illustrated in Figure 4.9 and Figure 4-10, respectively. The calibration of the four port network analyzer is done from the end points of the probes. Picoprobe calibration substrate CS-9 is used for the calibration process. Calibration is the most important part of measurements, since all results are dependent on the calibration done.

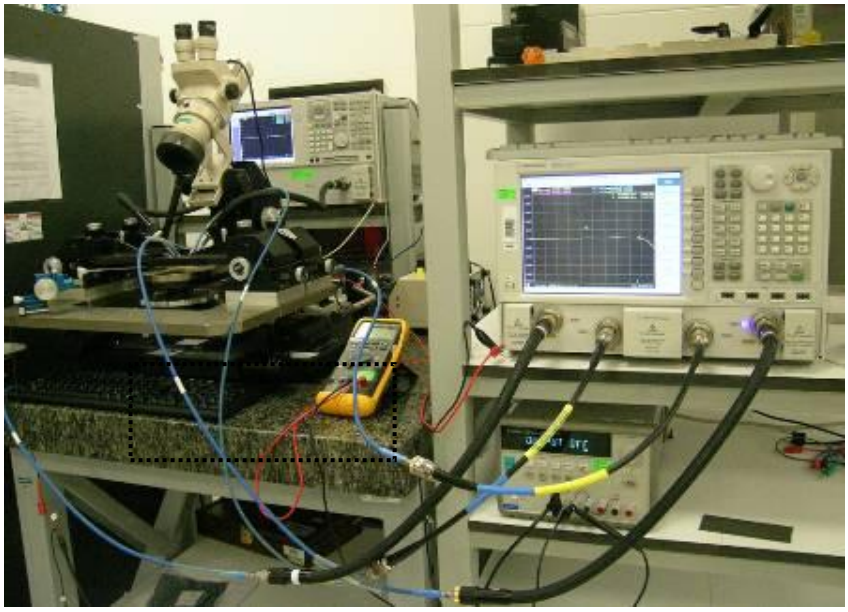

Figure 4.9 Measurement Setup of Lange Coupler.

The measurement results are shown in Figure 4.11. The losses for S21 and S31 are increased especially after 16 GHz due to the loss of the dielectric substrate. If the substrate were thinner, the loss would be lower. Also, the coupling is decreased, since the spacing between the coupled lines is increased in order to be in the limits of the laser machine in PCB process. The input return loss is lower than -10 dB up to 18 GHz where the isolation of the coupler is lower than -10 dB up to 16 GHz. This result is the optimum when the design specifications and limitations on the production are taken into account. This measurement result is used while designing the phase shifter bits.

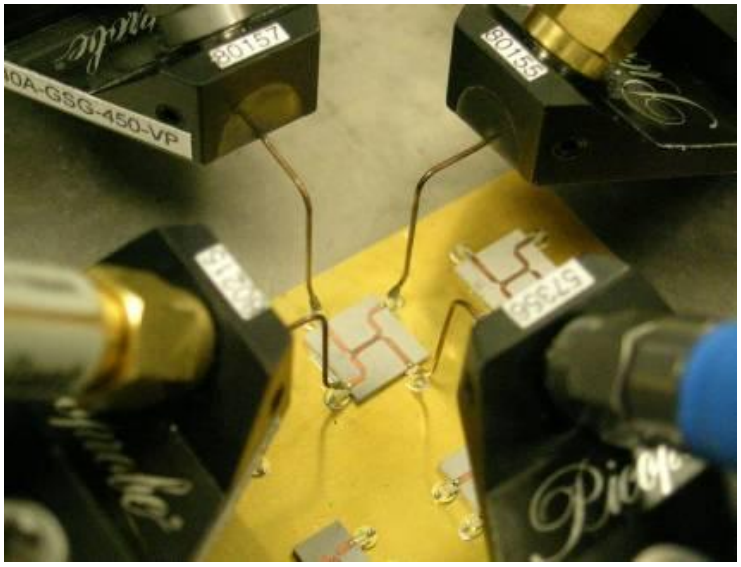

Figure 4.10 Close View of the Measurement.

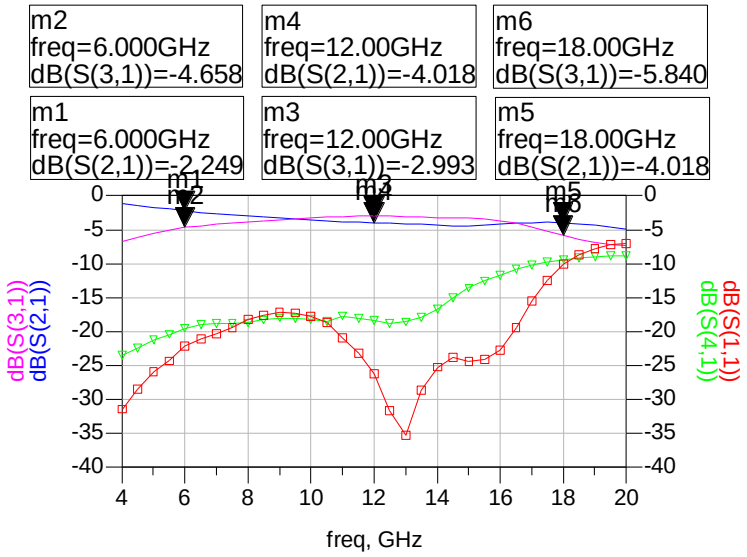

Figure 4.11 Measurement Result of Lange Coupler.

4.3 Measurement and Modeling of PIN Diode

As in the basic structure of phase shifter shown in Figure 3.16, switches are required in order to select appropriate radial stub pair in the phase shifting operation. In this thesis PIN diodes are used for switching components.

A PIN diode is a semiconductor device that operates as a variable resistor at microwave and RF frequencies. PIN diode is a current controlled component where the forward biased DC current determines the resistor value of the diode. Low insertion loss and fast switching speed make PIN diodes amenable for the microwave and RF applications. When the diode is forward biased, the switch is on. On the other hand if the diode is reversed biased, the input power is reflected back since the switch is off. Equivalent circuits of a typical PIN diode are given in Figure 4.12 when the diode is forward and reversed biased.

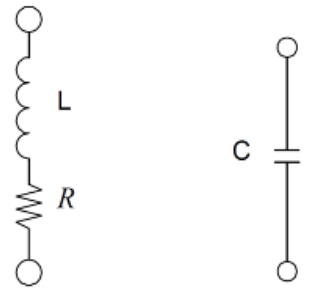

(a) Forward Biased (b) Reversed Biased

Figure 4.12 Equivalent Circuit Models of PIN Diode.

Agilent HPND-4038 Beam Lead PIN Diode shown in Figure 4.13 is used in phase shifter circuits in the content of this thesis. A beam lead diode installed using a proprietary technique reduces the series inductance and has a significant improvement in performance. The datasheet of the HPND-4038 PIN diode is given in Appendix A. The circuit model of the PIN diode for forward and reverse biasing is obtained from the measurement result of the diode. The details of the measurement are explained in the next section.

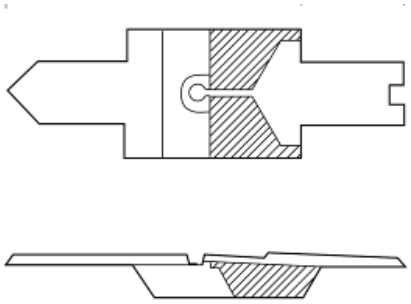

Figure 4.13 Layout of HPND-4038 PIN Diode.

The HPND-4038 PIN diode is used as a single pole, single throw switch between the ports of unfolded Lange coupler and the radial stubs. For a series configuration of the diode, the bias network is illustrated in Figure 4.14.

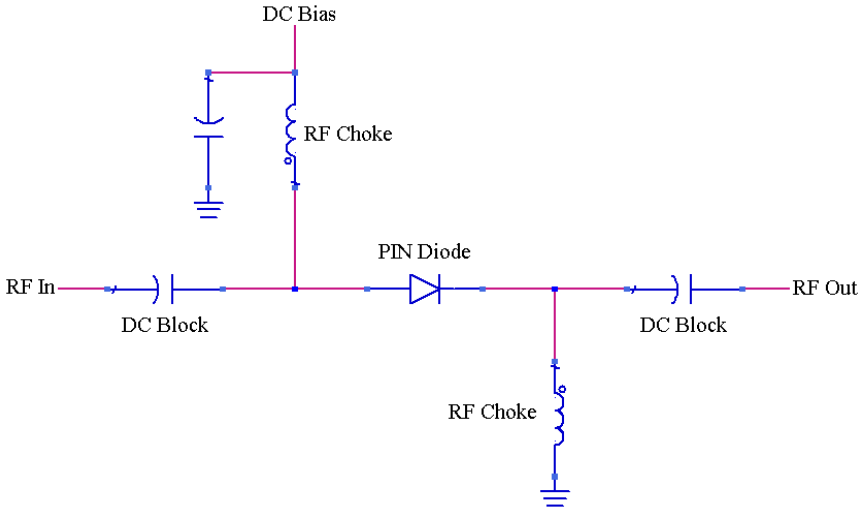

Figure 4.14 Bias Network of PIN Diode for Series Configuration.

The circuit shown in Figure 4.15 is prepared for the measurement of PIN diode. Since the phase shifter bits are designed on 25-mil thick TMM10i, the measurement of the diode is performed on the same substrate. Two 50 Ohm transmission lines are designed leaving 10 mils space between them. The width and the length of the transmission lines are 22 and 120 mils, respectively. The substrate is placed onto a gold plated carrier. The diode is assembled between these lines using conductive

epoxy. RF choke inductors are realized by gold wires. The diameter of the wire is 1 mil where its length is approximately 280 mils. This configuration of gold wire provides almost 7-8 nH. One of the gold wires is bonded between the transmission line and 10 nF thin film surface mount capacitor that is used for DC source filtering. The other wire is bonded between the transmission line and carrier for ground connection. Wire bonds are strengthened by applying epoxy to the connection points. A 50 Ohm resistor is used between 10 nF capacitor and jumper to limit the DC current. To apply the DC signal a jumper is assembled to the circuit. Connections between the components are performed by using 1 mil gold wires. Test points that are connected to the transmission lines using 10 mil ribbons are placed to the input and output of the circuit

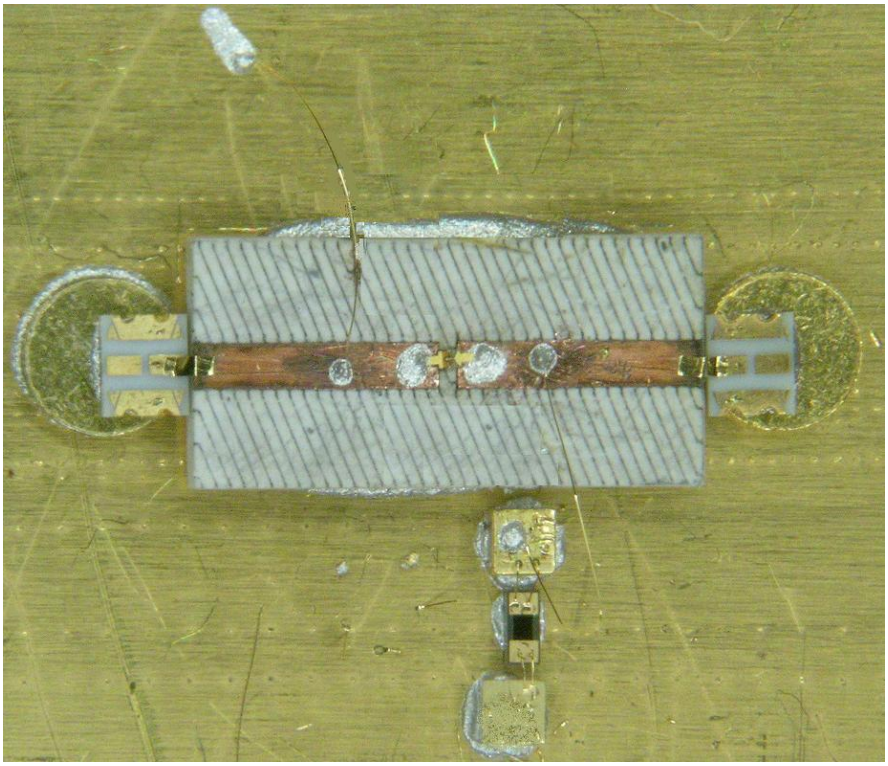

Figure 4.15 Measurement Circuit of HPND-4038 PIN Diode.

The measurement of the circuit is performed by using calibrated probing station, network analyzer and DC power supply. The DC blocking capacitors operating for DC-26.5 GHz are connected between the measurement cables and RF probes. For

forward biasing of the PIN diode 11 mA DC current is applied from the power supply and -1.5 V signal is applied for the reverse biasing of the PIN diode. The insertion loss and input and out return losses of the forward biased circuit are given in Figure 4.16 and Figure 4.17, respectively. These results contain transmission line losses, discontinuities, parasitic effects from biasing circuit and test point losses.

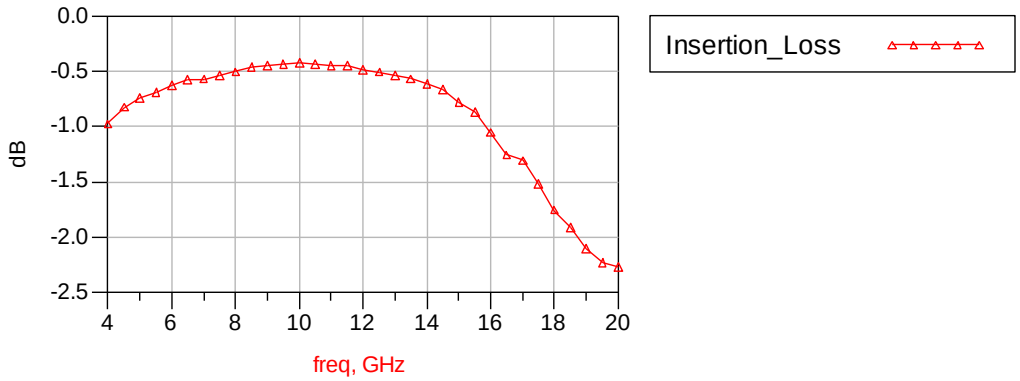

Figure 4.16 Insertion Loss of the Forward Biased Circuit.

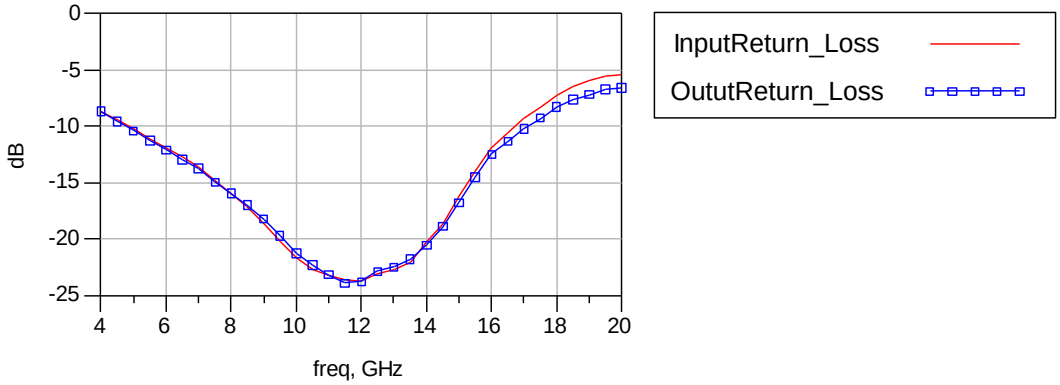

Figure 4.17 Input and Output Return Losses of the Forward Biased Circuit.

The insertion loss and input and out return losses of the reversed biased circuit are given in Figure 4.18 and Figure 4.19, respectively. Similarly, these results contain transmission line losses, discontinuities, parasitic effects from biasing circuit and test point losses.

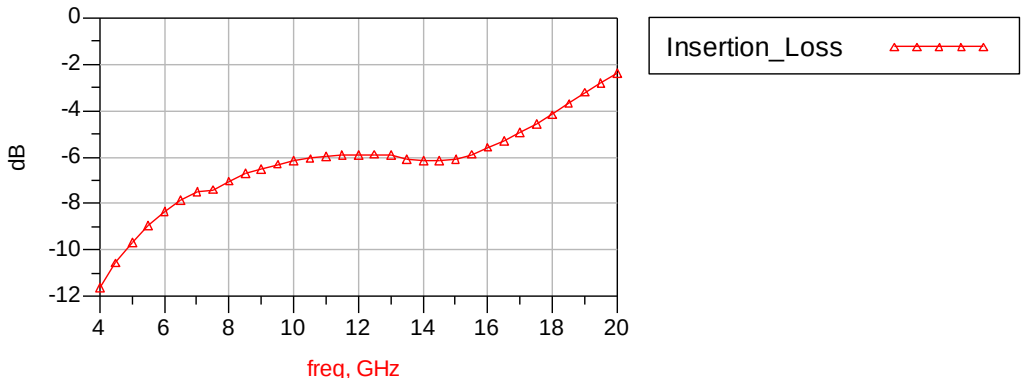

Figure 4.18 Insertion Loss of the Reversed Biased Circuit.

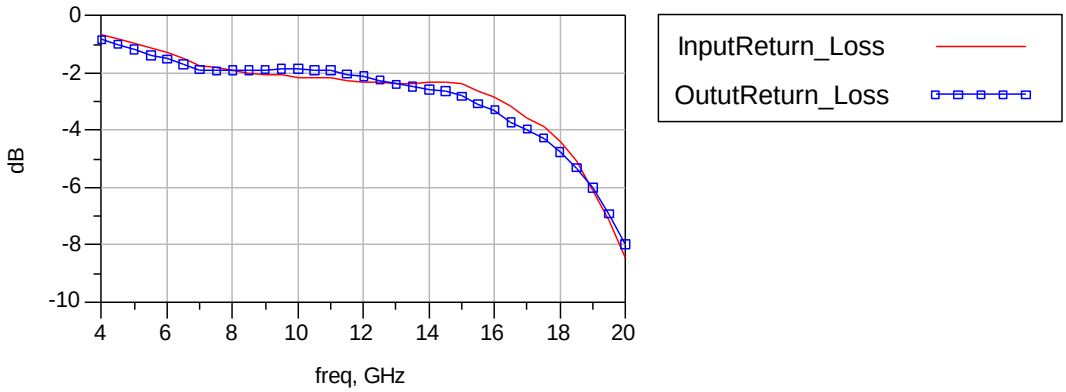

Figure 4.19 Input and Output Return Losses of the Reversed Biased Circuit.

Afterwards the same circuits for both forward biased and reversed biased are simulated in ADS. These circuits are compared with the measurement results in order to obtain the forward biased and reversed biased equivalent circuits of the PIN diode. Compared circuits for forward biasing are given in Figure 4.20. The measurement results of 50 Ohm transmission lines are used in this circuit.

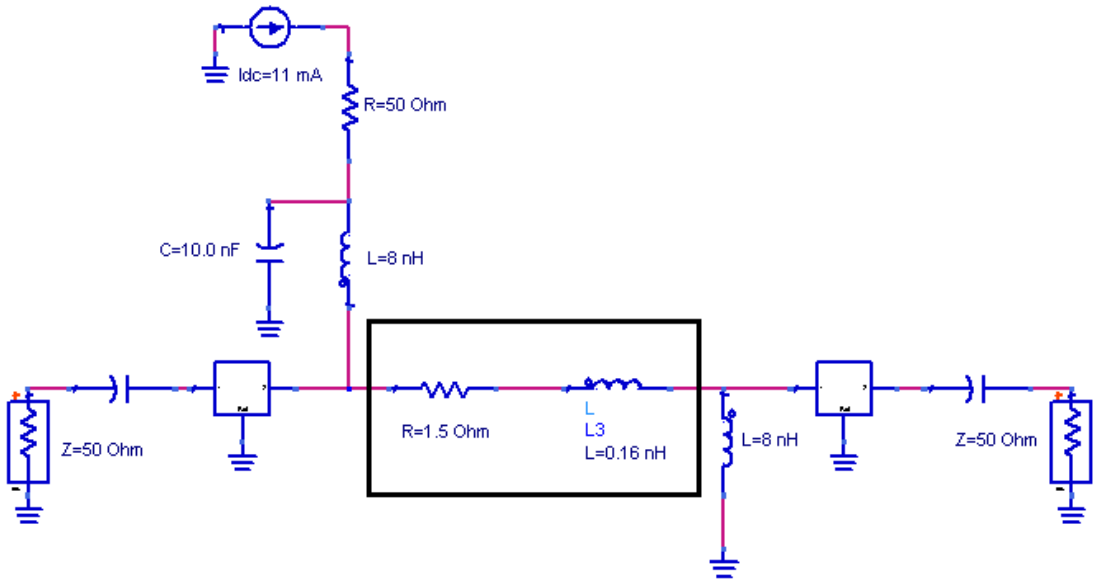

Figure 4.20 Equivalent Circuit of Figure 4.15 for Forward Biased.

The equivalent model of the PIN diode is shown in a rectangle in Figure 4.20. With the values shown in above figure, the simulation result and measurement result of the circuit shown in Figure 4.15 are compared in Figure 4.21 and Figure 4.22. The results are close each other up to 16 GHz. Hence, the equivalent model for the forward biased PIN diode is found based on Figure 4.12 as L= 0.16 nH and R=1.5 Ohm.

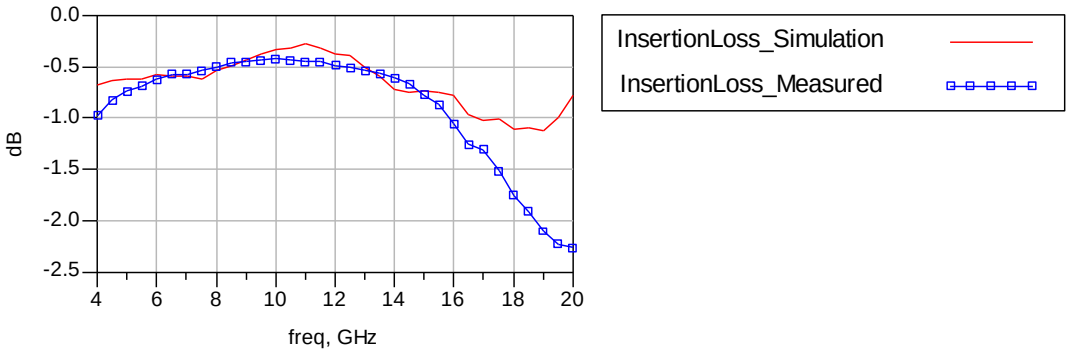

Figure 4.21 Insertion Losses of Simulation and Measurement (Forward Biased).

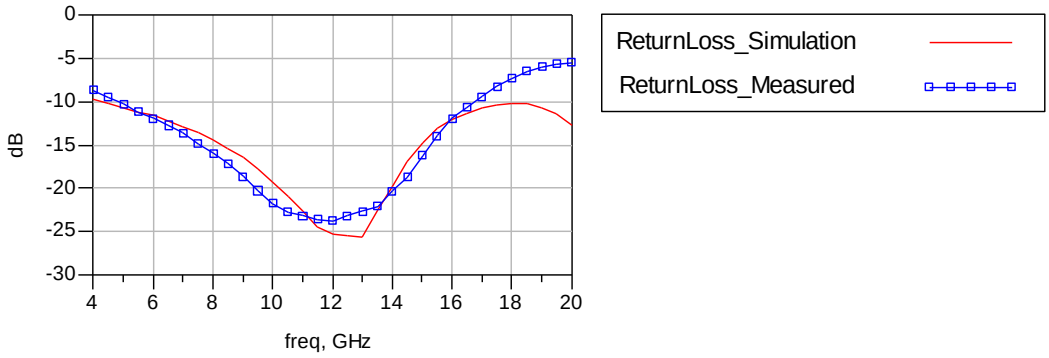

Figure 4.22 Return Losses of Simulation and Measurement (Forward Biased).

Similar simulation is performed for reverse biasing case. The equivalent ADS circuit is given in Figure 4.23. So that, the equivalent circuit model for the reverse biased PIN diode is found based on Figure 4.12 as C= 0.085 pF. The ADS simulation and measured results are compared in Figure 4.24 and Figure 4.25. The results are similar up to 16 GHz.

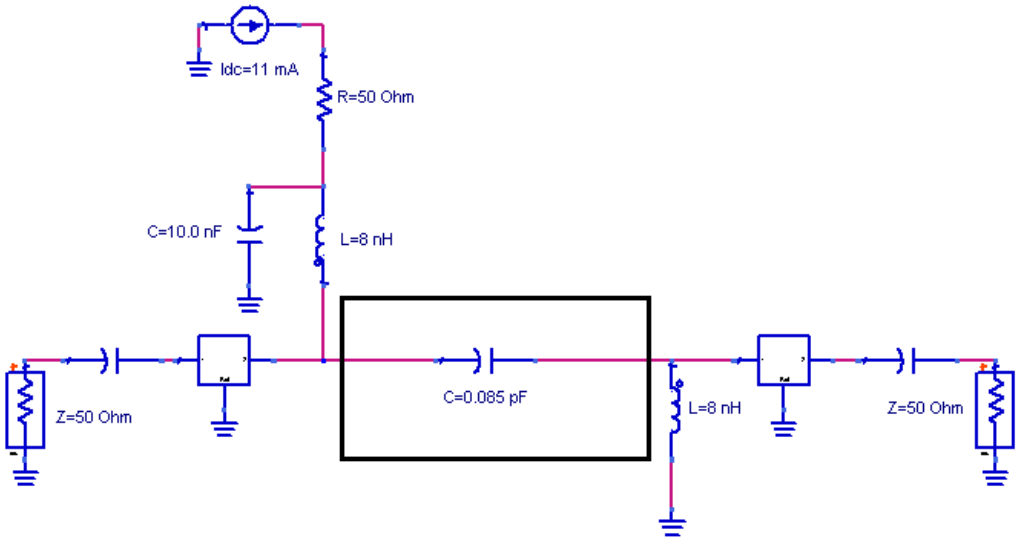

Figure 4.23 Equivalent Circuit of Figure 4.15 for Reverse Biased.

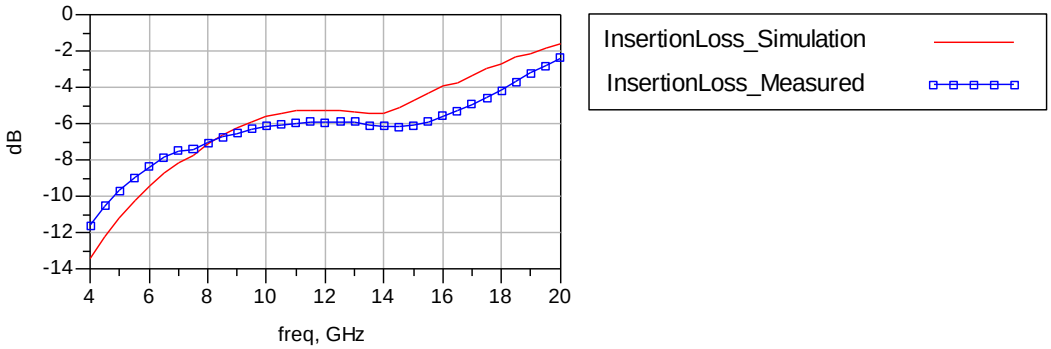

Figure 4.24 Insertion Losses of Simulation and Measurement (Reverse Biased).

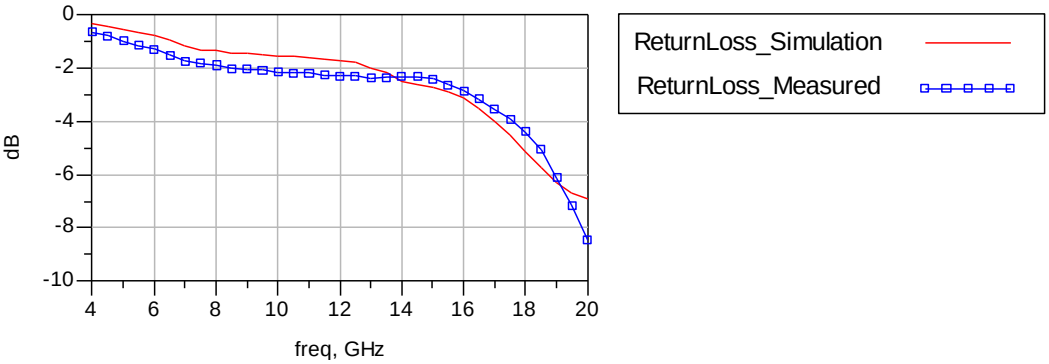

Figure 4.25 Return Losses of Simulation and Measurement (Reverse Biased).

Two important components, unfolded Lange coupler and PIN diode are measured and modeled for the design of phase shifter bits 11.25, 22.5, 45 and 90º. The design, fabrication, and measurement details of them are explained in the next chapter.

CHAPTER 5

PHASE SHIFTER DESIGNS ON TMM10I SUBSTRATE

The measurement results of unfolded Lange coupler and the model of PIN diode are obtained in Chapter 4. With the use of measured data of Lange coupler and the model of PIN diode, the phase shifter circuits for 11.25, 22.5, 45 and 90º bits are formed by adding the radial stubs to the circuit. In this chapter, the design, fabrication, and measurements of the wideband phase shifter bits for 11.25, 22.5, 45 and 90º are explained in detail. The phase shifter bits are fabricated onto Rogers TMM10i substrate using PCB production technology in ASELSAN facilities where PIN diodes are mounted to the circuits as the switching component. In the beginning of the work, the operating frequency band for the phase shifter bits is determined as 6-18 GHz. However, because of the limitations on Lange coupler, thickness of the substrate and the biasing problems of PIN diode, the operating frequency band is obtained as 7-14 GHz. Over the whole frequency band, the measured maximum phase errors were ±2.1, 3.2, 5.5, and 13º for the 11.25, 22.5, 45, and 90º phase shifters, respectively. The maximum insertion losses were 2.1, 2.0, 2.1, and 2.3 dB in the frequency band for the 11.25, 22.5, 45, and 90º phase shifters, respectively. Also, input and return losses of all phase shifter circuits in any state are lower than -10 dB. The comparison of the simulation and fabricated results are given at the end of the chapter.

5.1 Design of Phase Shifter Bits

5.1.1 11.25º Phase Shifter Bit

After obtaining the measurement result of unfolded Lange coupler shown in Figure 4.11 and model of the PIN diode in previous chapter, determining the radial stubs of the phase shifter bits forms the remaining part of the work. Figure 5.1 shows the circuit designed in ADS for a phase shifter bit where the Stub-1 pair is selected as the reflective load of the direct and coupled ports of unfolded Lange coupler.

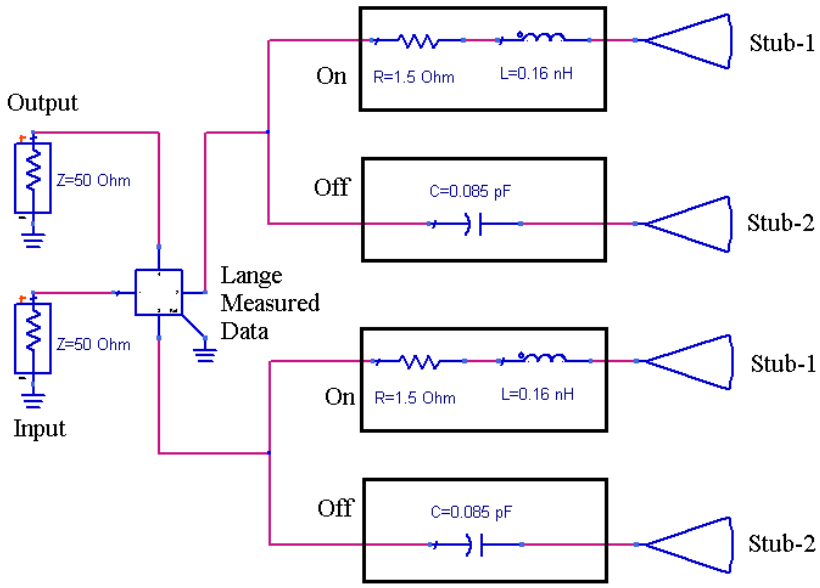

Figure 5.1 The Circuit Designed in ADS.

The measured data of unfolded Lange coupler and the model of the PIN diode for both forward biased (diode is ON) and reverse biased (diode is OFF) are used in ADS simulations. The biasing circuits are not illustrated in the above circuit.

Similarly, another circuit is designed where Stub-2 pair is selected as the reflective load. In order to get the desired differential phase shift the insertion phases of each circuit are subtracted from each other as explained previously. So Stub-1 and Stub-2 sizes are determined for the desired differential phase shift. The input and output return losses of the circuit for both state are tried to be minimized while designing the stubs. Tuning and optimization properties of ADS are used in the design stages. The differential phase shift, insertion loss, input and output return loss for both states of 11.25º phase shifter bit are shown in Figure 5.2, Figure 5.3 and Figure 5.4.

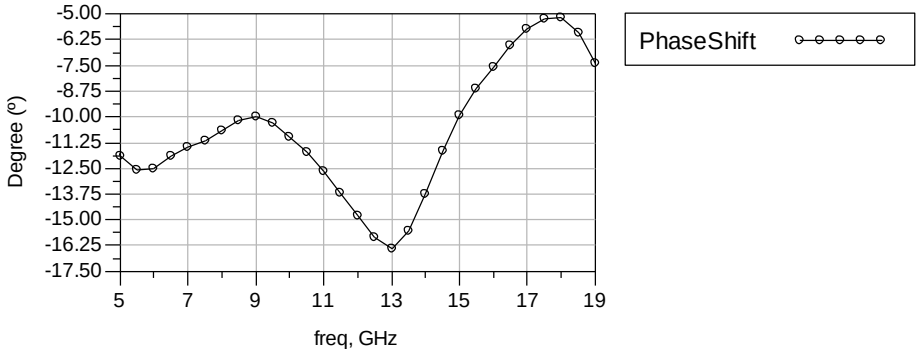

Figure 5.2 Differential Phase Shift for 11.25° Bit.

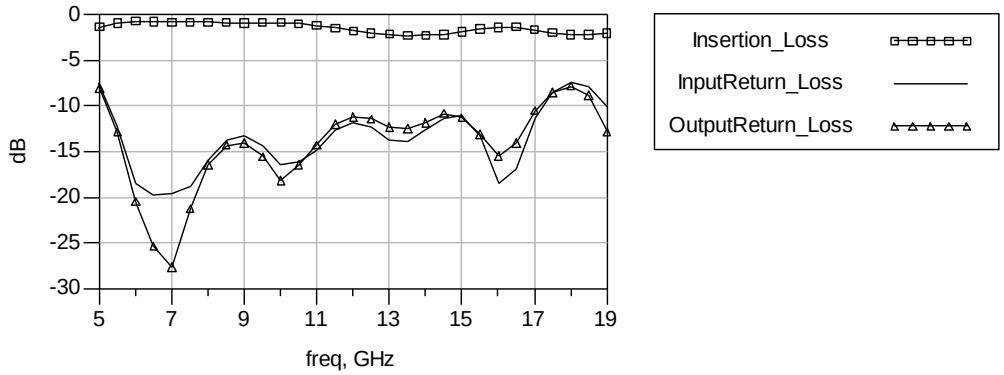

Figure 5.3 Insertion and Return Losses when Stub 1 is Selected.

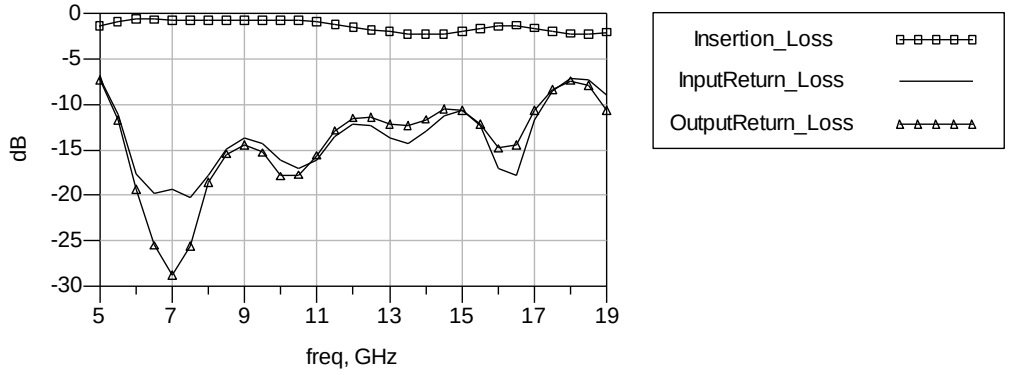

Figure 5.4 Insertion and Return Losses when Stub 2 is Selected.

When the results are examined, the phase shift for 11.25º ±1.25º is satisfied for only 6-11 GHz bandwidth. Also the insertion and return losses for both states are getting worse for the frequencies above 11 GHz.

The unfolded Lange coupler measurement is the reason of this degradation on the results. Coupler measurement is performed using circuit in Figure 4.5. In this configuration the direct and coupled port 50 Ohm transmission lines are almost 120 mils long in order to perform the measurement using probing station. This length of transmission lines do not cause a problem while measuring the coupler alone since all the ports are terminated with 50 Ohm probes. However, when direct and coupled ports are terminated by different loads instead of 50 Ohms; the length of these lines becomes important. Hence, the length of these lines should be smaller. According to this result, the circuit shown in Figure 5.5 is formed where the direct and coupled port lines are shortened using -100 mils length 50 Ohm transmission line in ADS.

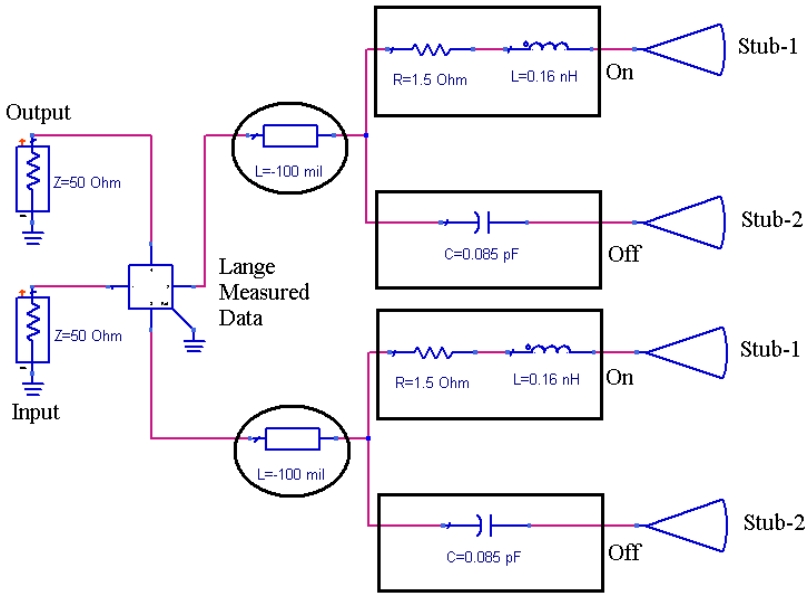

Figure 5.5 The Use of -100 mils Length of Transmission Lines.

The biasing circuits are not shown here but they are included in the simulations. Similarly, another circuit is designed where Stub-2 pair is selected as the reflective load. In order to get the desired differential phase shift the insertion phases of each

circuit are subtracted from each other as explained previously. After obtaining the stub sizes that are given in Table 5.1 using tuning and optimization, the differential phase shift, insertion loss, input and output return losses for both states of 11.25º bit are shown in Figure 5.6, Figure 5.7 and Figure 5.8.

Table 5.1 Radial Stub Sizes for 11.25º Phase Shifter Bit

Stub Parameters:	Stub-1	Stub-2
W (mils)	9	11.5
L (mils)	38	36
A (º)	100	85

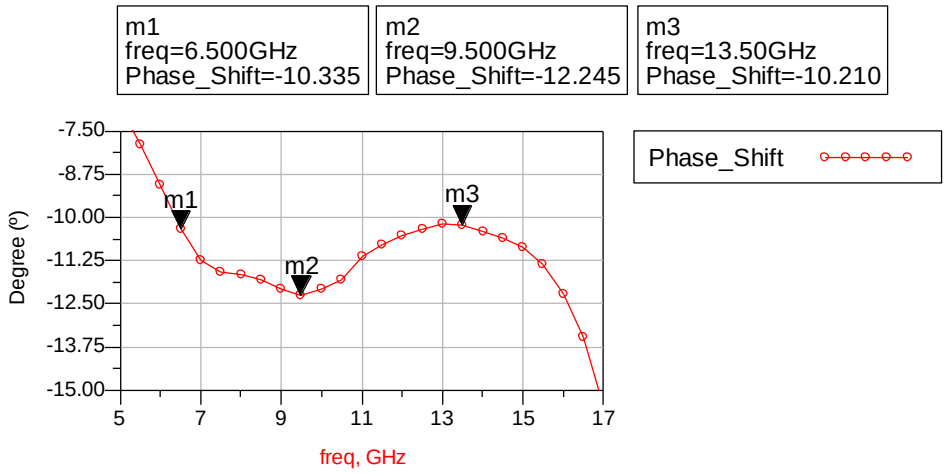

Figure 5.6 Differential Phase Shift for 11.25º Bit.

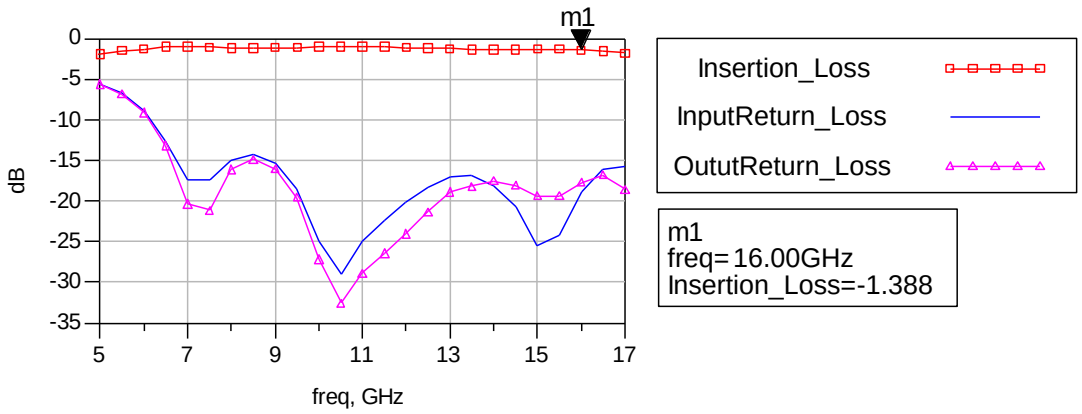

Figure 5.7 Insertion and Return Losses when Stub 1 is Selected.

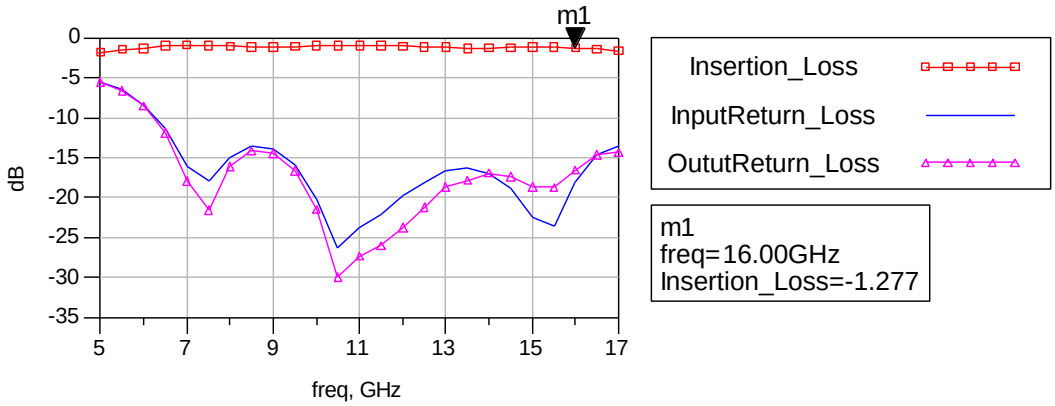

Figure 5.8 Insertion and Return Losses when Stub 2 is Selected.

As can be seen from the graphs above, 11.25º phase shift is satisfied for the frequency range 6.5-16 GHz with almost ±1º tolerance. Also the input and output return losses for both states are lower than -13 dB for 6.5-16 GHz frequency range. Insertion losses for both states are higher than -1.4 dB approximately.

5.1.2 22.5º Phase Shifter Bit

The same circuit configuration given in Figure 5.5 is used for the design of 22.5º phase shifter bit. The stub values that are obtained performing tuning and optimization are shown in Table 5.2.

Table 5.2 Radial Stub Sizes for 22.5º Phase Shifter Bit

Stub Parameters:	Stub-1	Stub-2
W (mils)	9	13
L (mils)	39	34
A (º)	105	80

The differential phase shift, insertion loss, input and output return losses for both states of 22.5º bit are shown in Figure 5.9, Figure 5.10 and Figure 5.11.

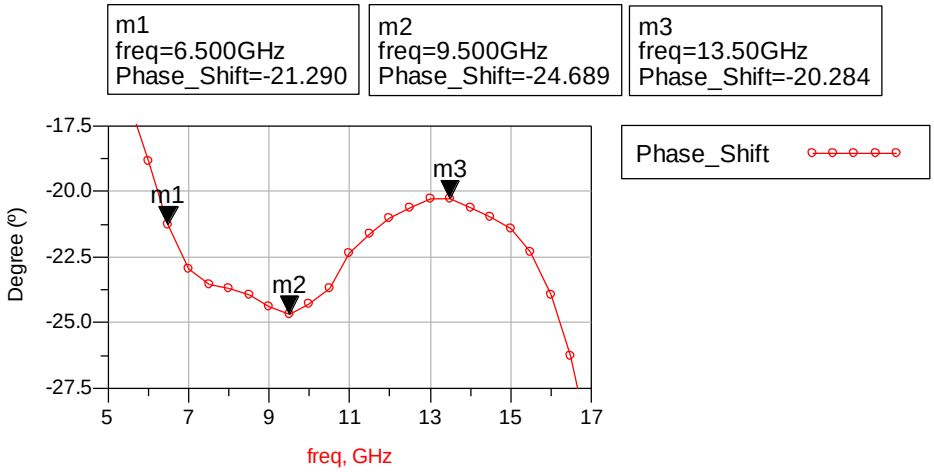

Figure 5.9 Differential Phase Shift for 22.5° Bit.

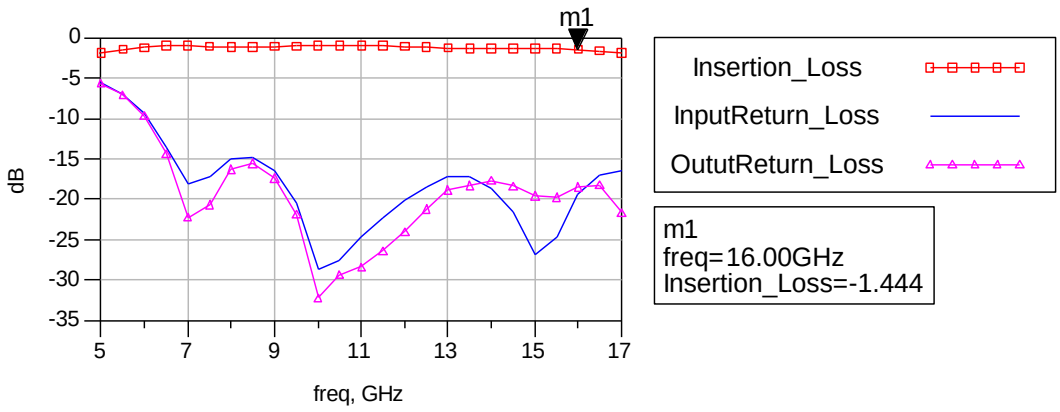

Figure 5.10 Insertion and Return Losses when Stub 1 is Selected.

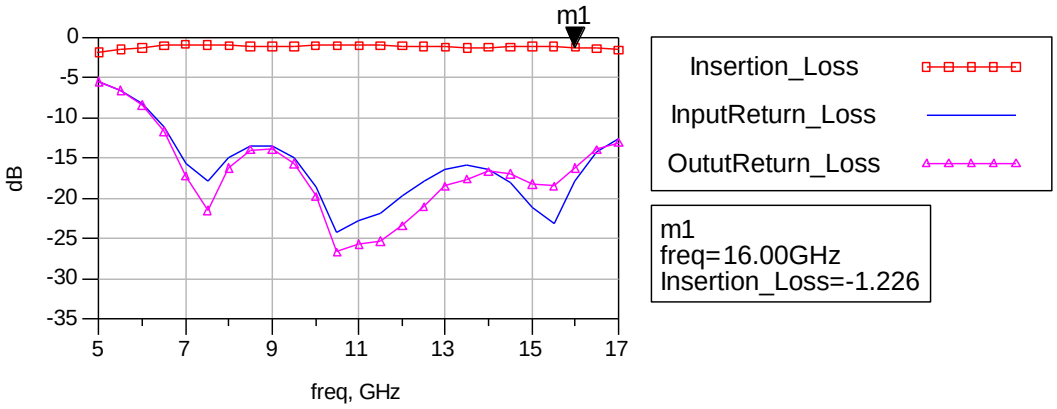

Figure 5.11 Insertion and Return Losses when Stub 2 is Selected.

As can be seen from the graphs above, 22.5º phase shift is satisfied for the frequency range 6.5-16 GHz with almost ±2.2º tolerance. Also the input and output return losses for both states are lower than -14 dB for 6.5-16 GHz frequency range. Insertion losses for both state are higher than -1.45 dB approximately.

5.1.3 45º Phase Shifter Bit

The same circuit configuration given in Figure 5.5 is used for the design of 45º phase shifter bit. The stub values that are obtained performing tuning and optimization are shown in Table 5.3.

Table 5.3 Radial Stub Sizes for 45º Phase Shifter Bit

Stub Parameters:	Stub-1	Stub-2
W (mils)	8	15
L (mils)	41	29
A (º)	115	75

The differential phase shift, insertion loss, input and output return losses for both states of 45º bit are shown in Figure 5.12, Figure 4.13 and Figure 5.14.

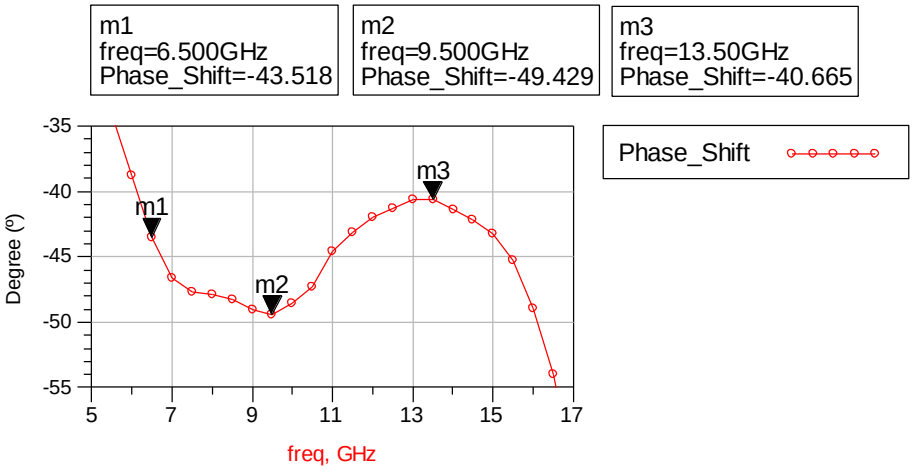

Figure 5.12 Differential Phase Shift for 45º Bit.

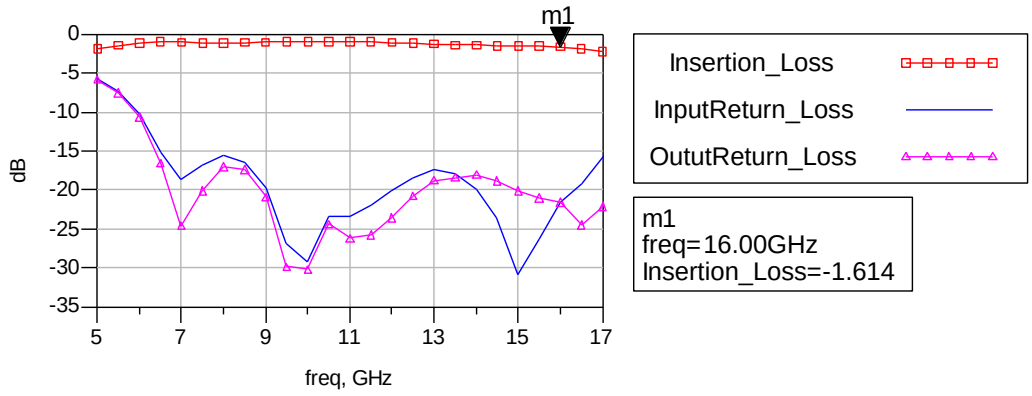

Figure 5.13 Insertion and Return Losses when Stub 1 is Selected.

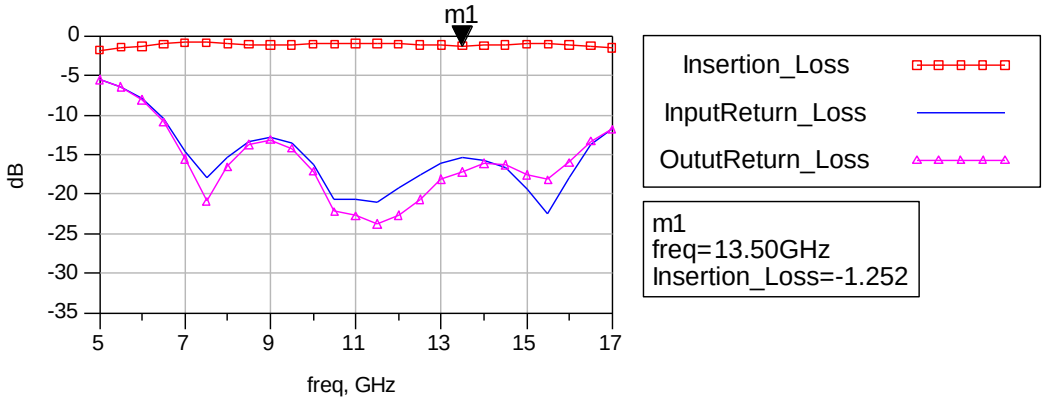

Figure 5.14 Insertion and Return Losses when Stub 2 is Selected.

As can be seen from the graphs above, 45º phase shift is satisfied for the frequency range 6.5-16 GHz with almost ±4.4º tolerance. The input and output return losses when Stub 1 is selected are lower than -15 dB for 6.5-16 GHz frequency range where insertion loss is higher than -1.6 dB approximately. The input and output return losses when Stub 2 is selected are lower than -11 dB for 6.5-16 GHz frequency range where insertion loss is higher than -1.3 dB approximately.

5.1.4 90º Phase Shifter Bit

The same circuit configuration given in Figure 5.5 is used for the design of 90º phase shifter bit. The stub values that are obtained performing tuning and optimization are shown in Table 5.4.

Table 5.4 Radial Stub Sizes for 90º Phase Shifter Bit

Stub Parameters:	Stub-1	Stub-2
W (mils)	5	16
L (mils)	51	26
A (º)	125	60

The differential phase shift, insertion loss, input and output return losses for both states of 90º bit are shown in Figure 5.15, Figure 5.16 and Figure 5.17.

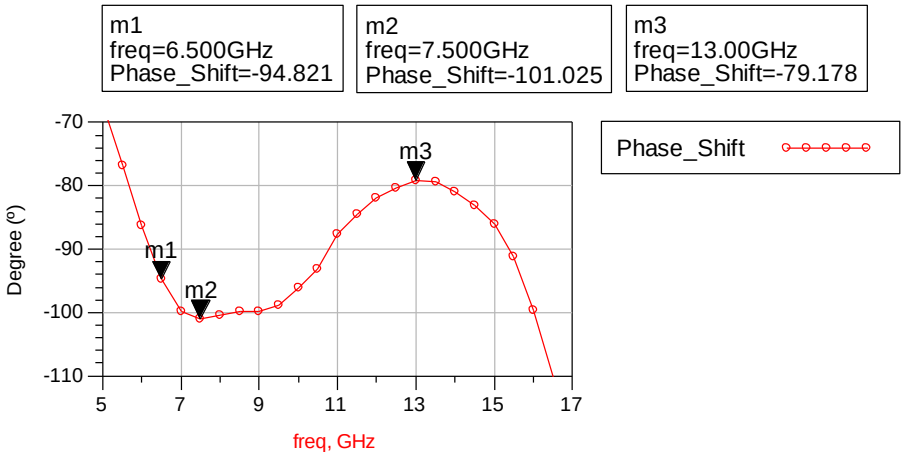

Figure 5.15 Differential Phase Shift for 90º Bit.

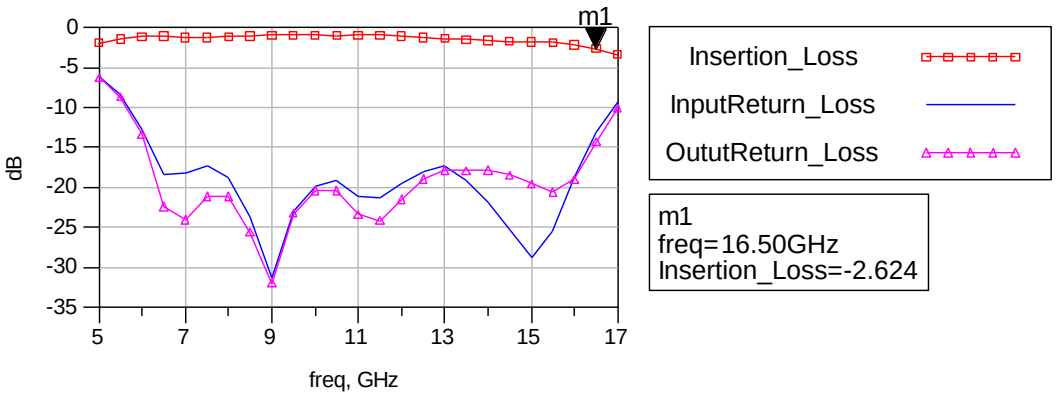

Figure 5.16 Insertion and Return Losses when Stub 1 is Selected.

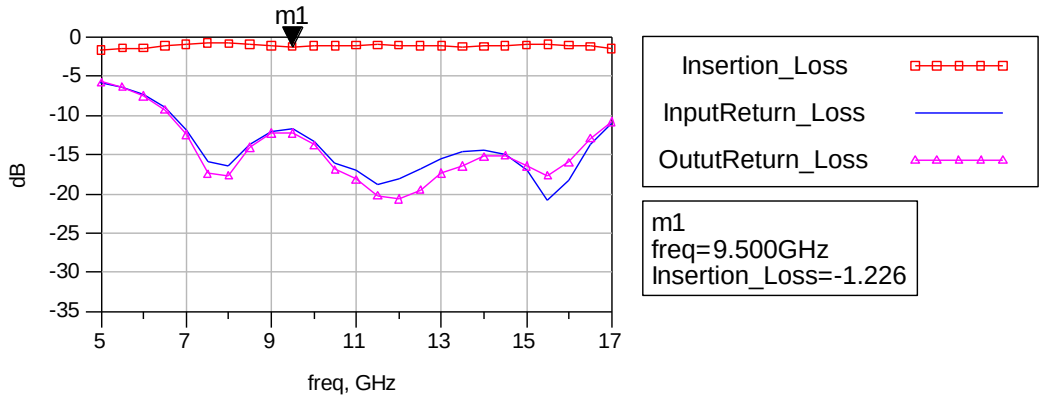

Figure 5.17 Insertion and Return Losses when Stub 2 is Selected.

As can be seen from the graphs above, 90º phase shift is satisfied for the frequency range 6.5-16 GHz with almost ±11º tolerance. The input and output return losses when Stub 1 is selected are lower than -17 dB for 6.5-16 GHz frequency range where insertion loss is higher than -2.6 dB approximately. The input and output return losses when Stub 2 is selected are lower than -10 dB for 6.5-16 GHz frequency range where insertion loss is higher than -1.3 dB approximately.

5.2 Fabrication and Measurement of Phase Shifter Bits

5.2.1 11.25º Phase Shifter Bit

The fabricated 11.25º bit is shown in Figure 5.18. LPKF Proto Laser shown in Figure 4.4 is used for PCB production. All assembling processes are performed in clean room facilities of ASELSAN Inc. The substrate is placed onto a gold plated carrier. The PIN diodes are mounted using conductive epoxy between the radial stubs and ports of unfolded Lange coupler. Since the bias voltage is applied from the direct and coupled ports of the coupler, the directions of the diodes at one port are different from each other. Hence, when a positive voltage is applied to the circuit, the current flows over one of the stubs and related diode is ON while the other is OFF. RF choke inductors are realized by gold wires. The diameter of the wire is 1 mil where its length is approximately 280 mils. This configuration of gold wire provides almost 7-8 nH. Two of the gold wires are bonded between the ports of the Lange coupler and 10 nF thin film surface mount capacitors that are used for DC source filtering. The

other four wires are bonded between the radial stubs and carrier for ground connection. Two 50 Ohm resistors are used between 10 nF capacitors and jumpers to limit the DC current. To apply the DC signal two jumpers are assembled to the circuit. Connections between the components are performed by using 1 mil gold wires. Test points are connected to the input and isolated ports of Lange coupler using 10 mil ribbons for measuring processes.

The measurement of 11.25º is performed by using Cascade Microtech Microwave Probing Station, Agilent E8346B PNA Network Analyzer operating between 10 MHz and 50 GHz, and Agilent E3631A Triple Output DC Power Supply. The DC blocking capacitors operating for DC-26.5 GHz are connected between the measurement cables and RF probes. The measurement setup is shown in Figure 5.19. The calibration of the network analyzer is done from the end points of the probes. Picoprobe calibration substrate CS-9 is used for the calibration process. The DC probes are used to apply the DC signal from power supply to the jumper.

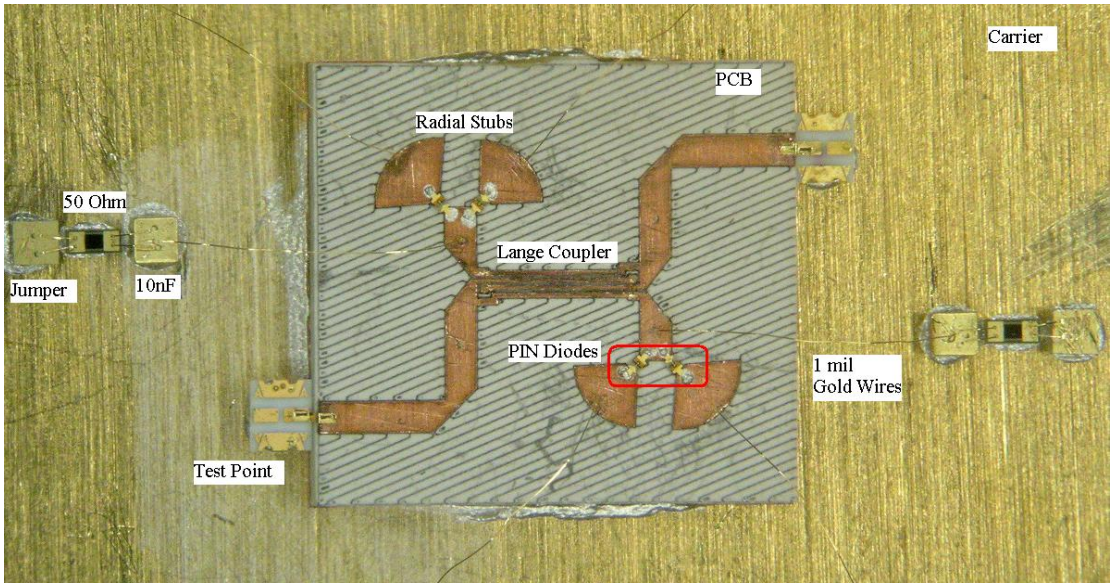

Figure 5.18 Fabricated 11.25º Phase Shifter Bit.

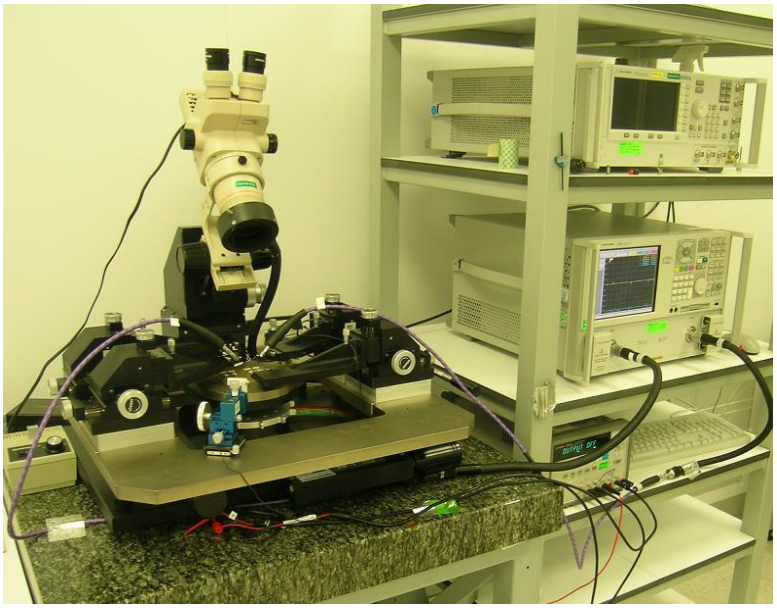

Figure 5.19 Measurement Setup.

When +1.5 V is applied from the power supply to the jumpers the PIN diodes that are connected to Stub 1 are forward biased. When -1.5 V is applied, the PIN diodes that are connected to Stub 2 are forward biased. Hence, the Stub 1 and Stub are selected by applying +1.5 V or -1.5 V. The differential phase shift occurs between these two states. The differential phase shift between these states is shown in Figure 5.20. The insertion loss and input and output return losses for both states are given in Figure 5.21 and Figure 5.22.

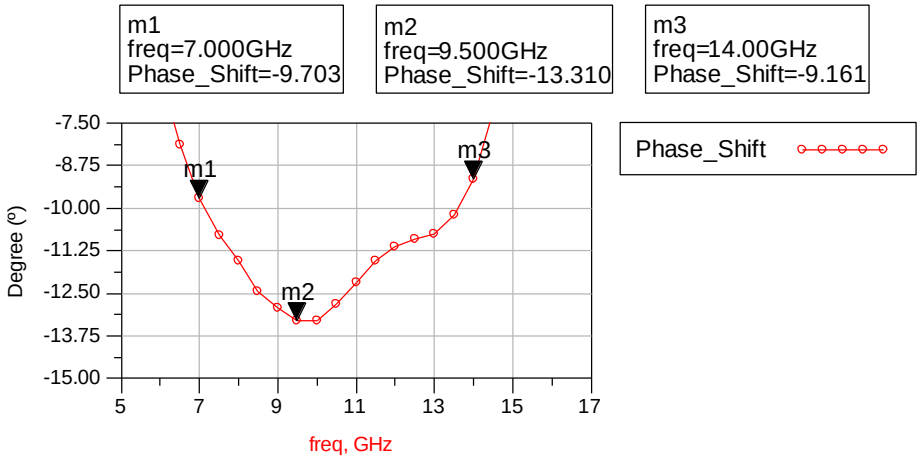

Figure 5.20 Differential Phase Shift for 11.25° Bit.

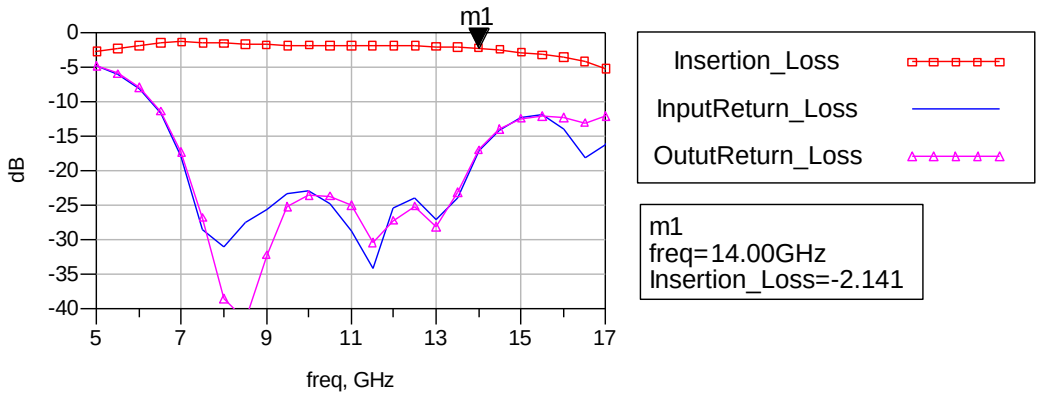

Figure 5.21 Insertion and Return Losses when Stub 1 is Selected.

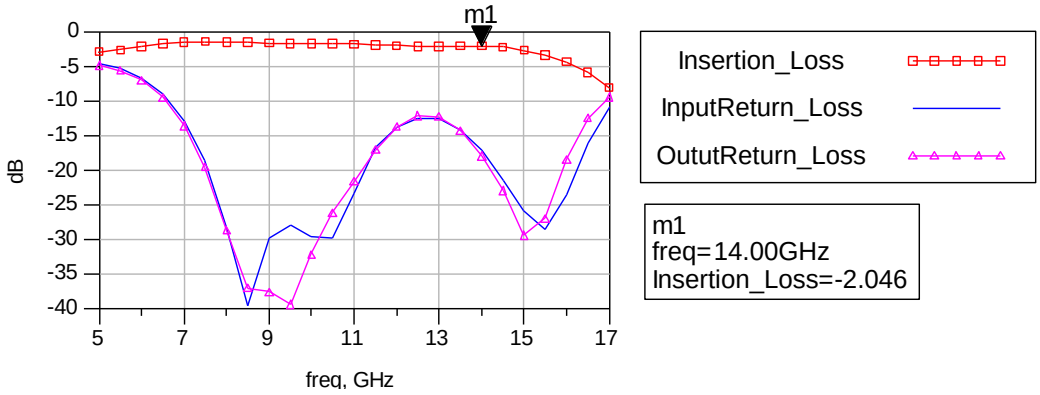

Figure 5.22 Insertion and Return Losses when Stub 2 is Selected.

When the measurement results are examined the differential phase shift for 11.25º is satisfied with phase error ±2.1º for 7-14 GHz. When the Stub 1 is selected the insertion loss for this frequency band is lower than -2.2 dB. The input and return losses are lower than -15 dB. When the Stub 2 is selected the insertion loss for this frequency band is lower than -2.1 dB. The input and return losses are lower than -11 dB.

5.2.2 22.5º Phase Shifter Bit

The fabricated 22.5º bit is shown in Figure 5.23. The fabrication and measurement processes are performed in the same way as in 11.25º bit.

The differential phase shift between the states is shown in Figure 5.24. The insertion loss and input and output return losses for both states are given in Figure 5.25 and Figure 5.26.

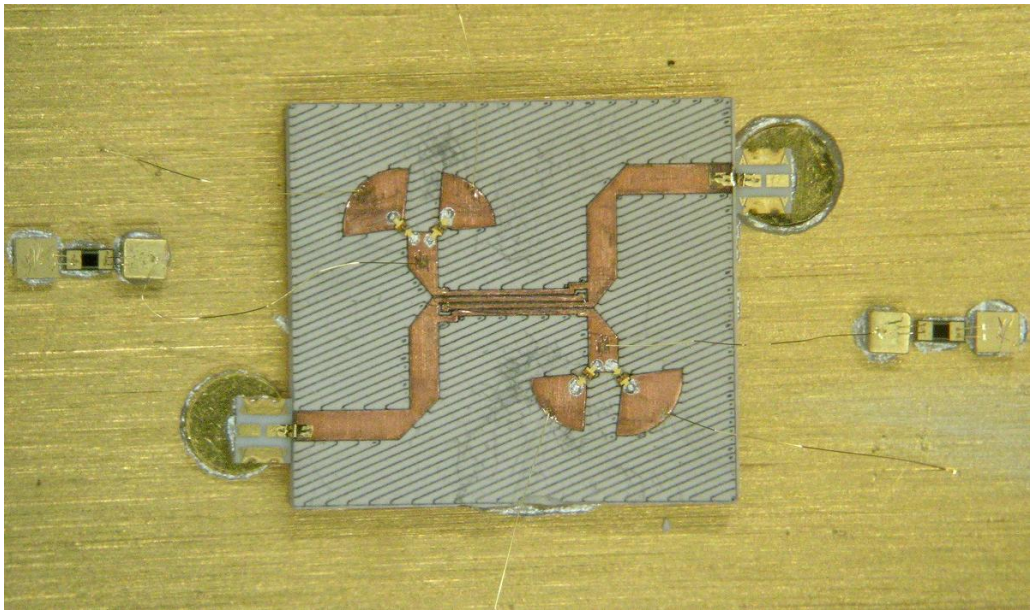

Figure 5.23 Fabricated 22.5º Phase Shifter Bit.

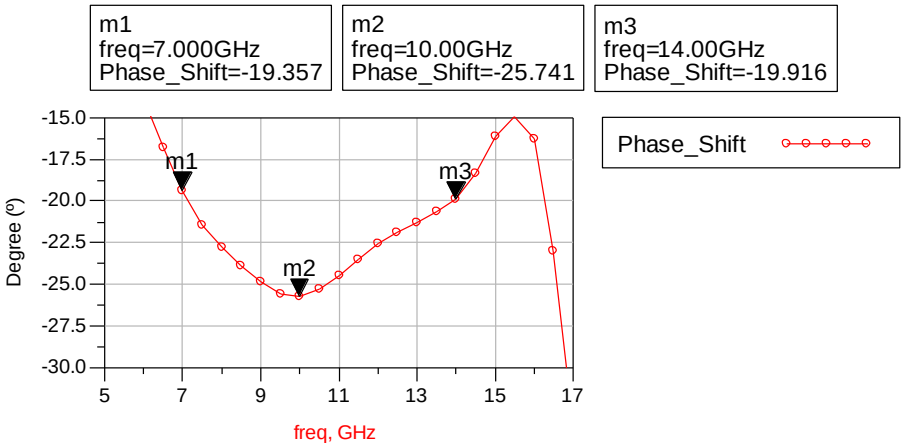

Figure 5.24 Differential Phase Shift for 22.5º Bit.

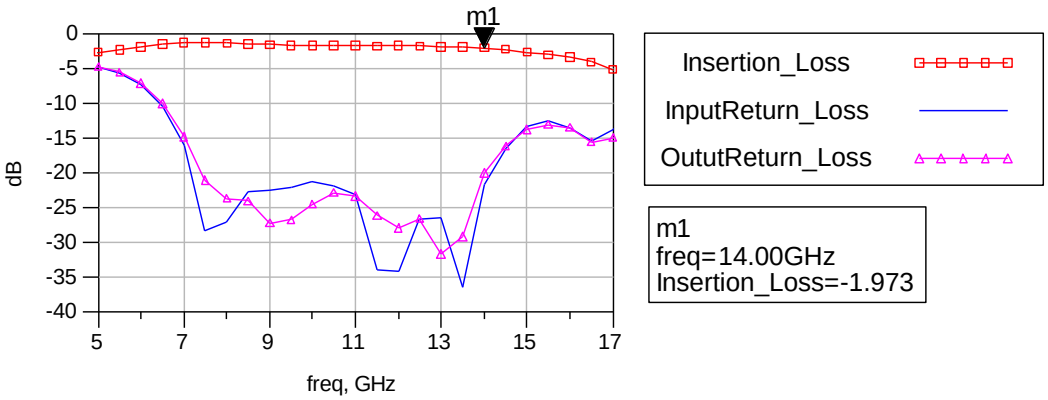

Figure 5.25 Insertion and Return Losses when Stub 1 is Selected.

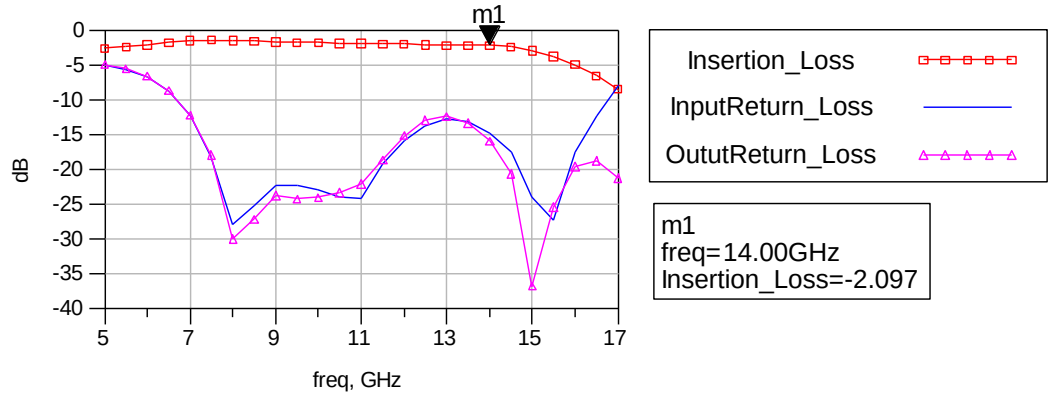

Figure 5.26 Insertion and Return Losses when Stub 2 is Selected.

When the measurement results are examined the differential phase shift for 22.5º is satisfied with phase error ±3.2º for 7-14 GHz. When the Stub 1 is selected the insertion loss for this frequency band is lower than -2.0 dB. The input and return losses are lower than -17 dB. When the Stub 2 is selected the insertion loss for this frequency band is lower than -2.1 dB. The input and return losses are lower than -12 dB.

5.2.3 45º Phase Shifter Bit

The fabricated 45º bit is shown in Figure 5.27. The fabrication and measurement processes are performed in the same way as in 11.25º bit.

The differential phase shift between the states is shown in Figure 5.28. The insertion loss and input and output return losses for both states are given in Figure 5.29 and Figure 5.30.

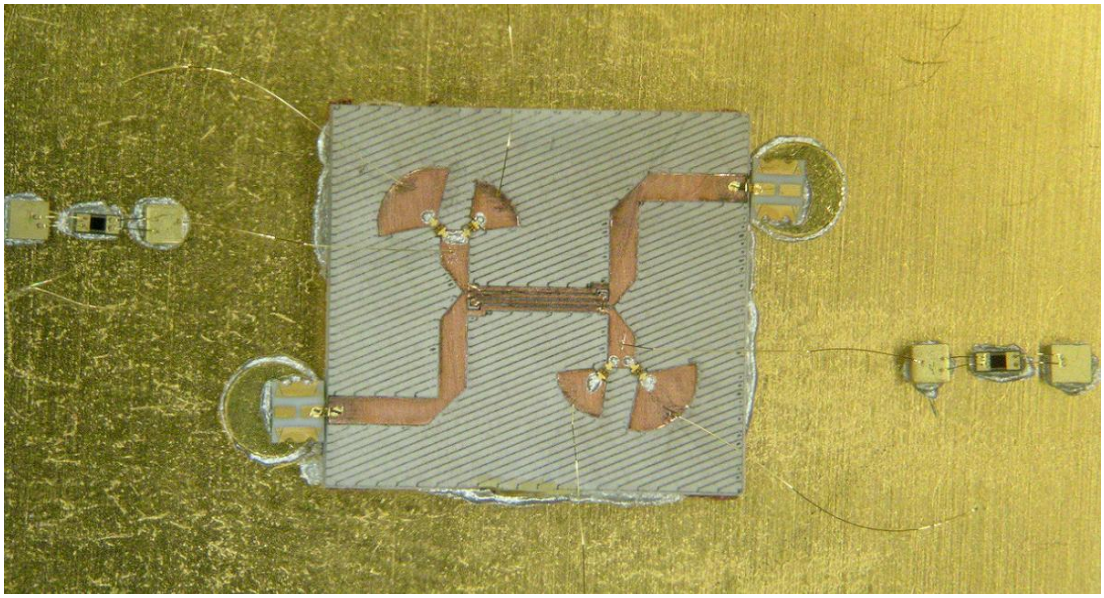

Figure 5.27 Fabricated 45º Phase Shifter Bit.

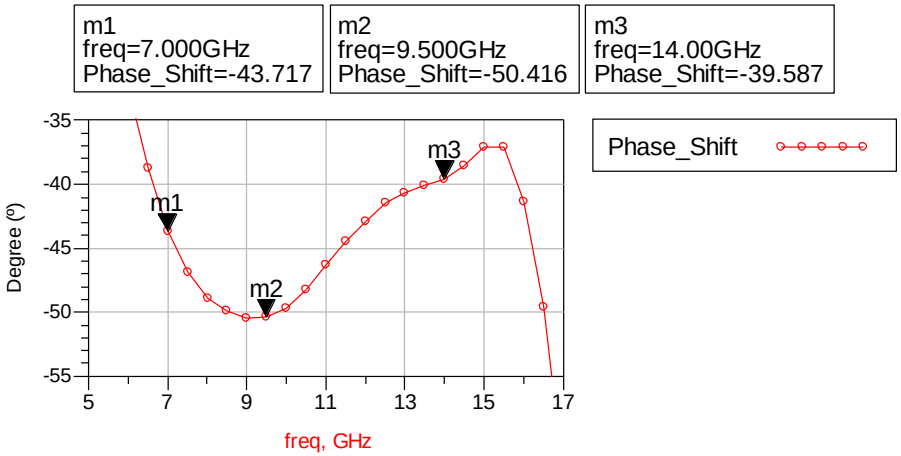

Figure 5.28 Differential Phase Shift for 45º Bit.

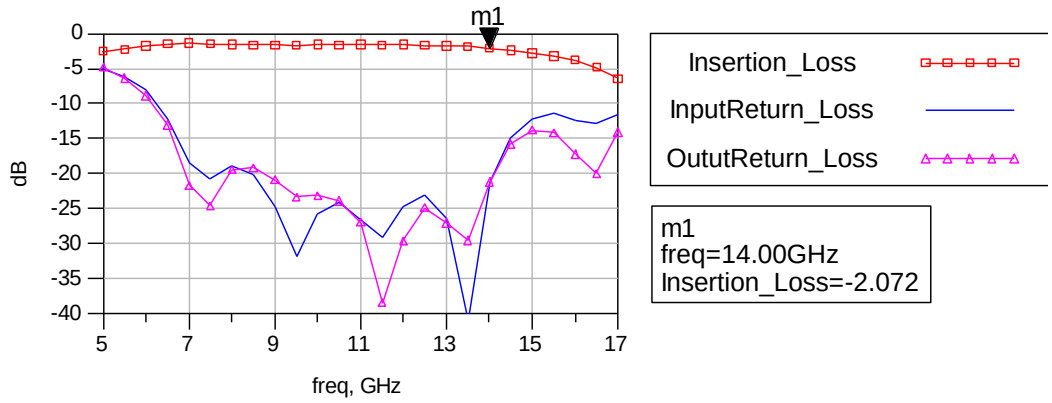

Figure 5.29 Insertion and Return Losses when Stub 1 is Selected.

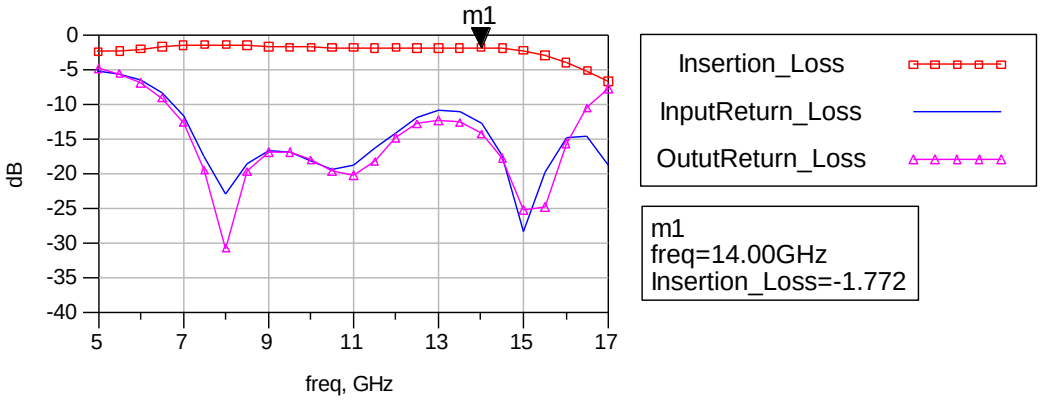

Figure 5.30 Insertion and Return Losses when Stub 2 is Selected.

When the measurement results are examined the differential phase shift for 45º is satisfied with phase error ±5.5º for 7-14 GHz. When the Stub 1 is selected the insertion loss for this frequency band is lower than -2.1 dB. The input and return losses are lower than -19 dB. When the Stub 2 is selected the insertion loss for this frequency band is lower than -1.8 dB. The input and return losses are lower than -11 dB.

5.2.4 90º Phase Shifter Bit

The fabricated 90º bit is shown in Figure 5.31. The fabrication and measurement processes are performed in the same way as in 11.25º bit.

The differential phase shift between the states is shown in Figure 5.32. The insertion loss and input and output return losses for both states are given in Figure 5.33 and Figure 5.34.

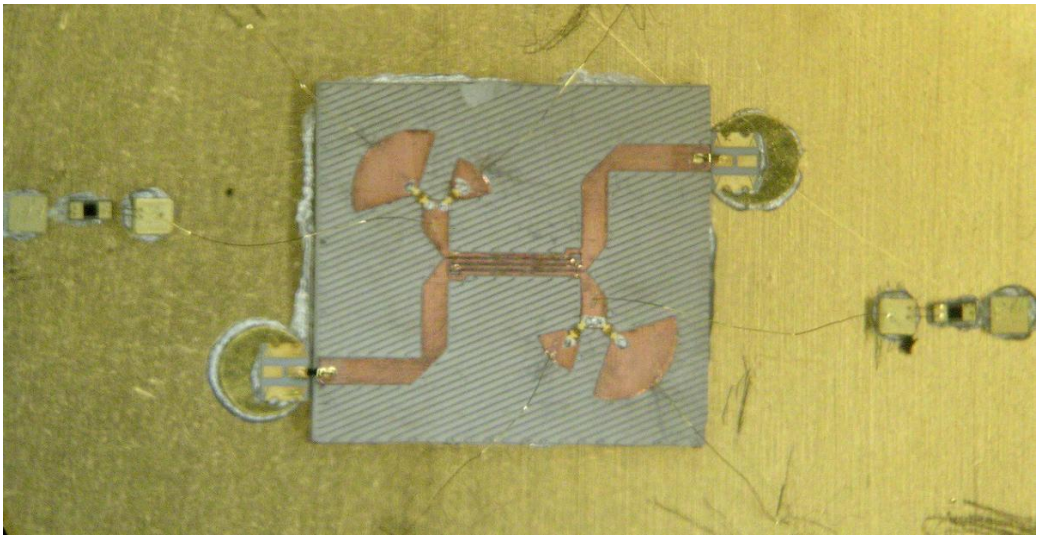

Figure 5.31 Fabricated 90º Phase Shifter Bit.

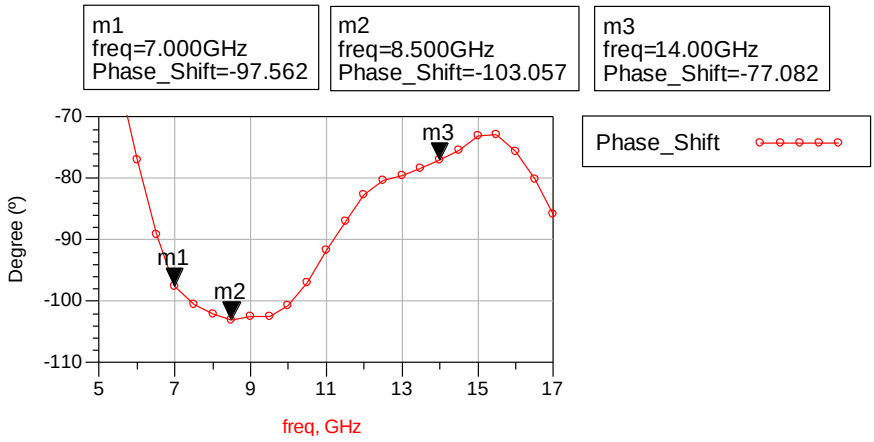

Figure 5.32 Differential Phase Shift for 90º Bit.

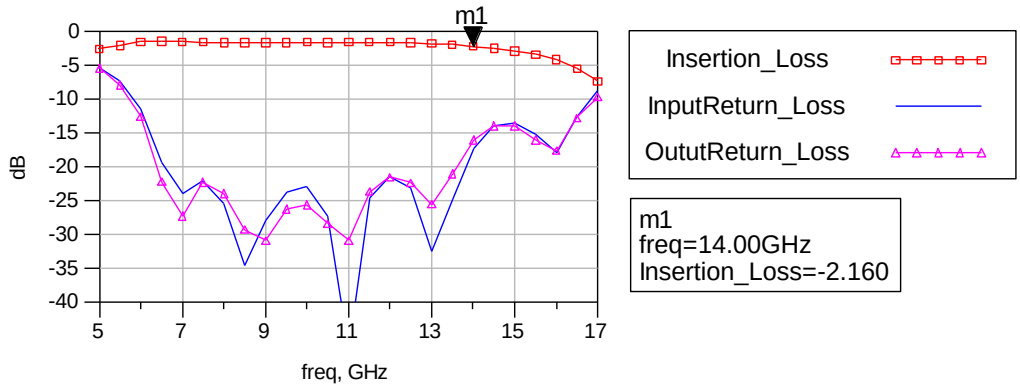

Figure 5.33 Insertion and Return Losses when Stub 1 is Selected.

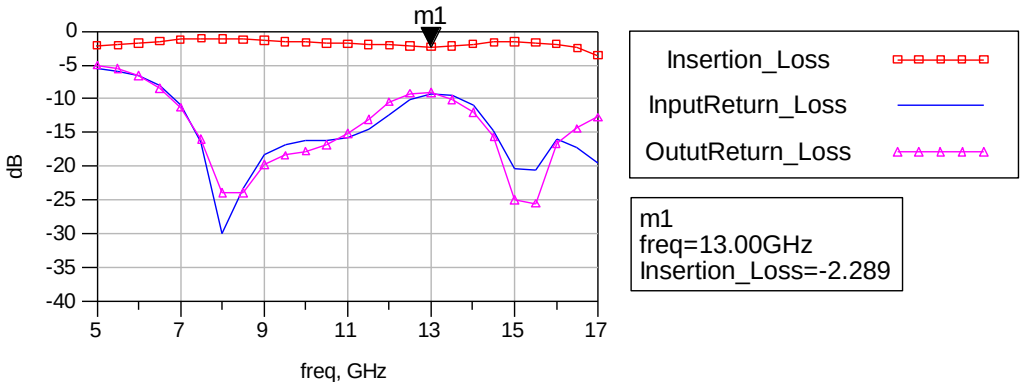

Figure 5.34 Insertion and Return Losses when Stub 2 is Selected.

When the measurement results are examined the differential phase shift for 90º is satisfied with phase error ±13º for 7-14 GHz. When the Stub 1 is selected the insertion loss for this frequency band is lower than -2.2 dB. The input and return losses are lower than -17 dB. When the Stub 2 is selected the insertion loss for this frequency band is lower than -2.3 dB. The input and return losses are lower than -9 dB.

The measurements results show that the phase shifter bits provide desired phase shift for 7-14 GHz frequency band. The comparison between the results of simulation and fabrication are given in the next section for 6-15 GHz frequency band.

5.3 Comparison of Simulation and Fabricated Results

5.3.1 Comparison of 11.25º Phase Shifter Bit

Figure 5.35 shows the comparison of differential phase shifts between the simulation and fabricated results. The insertion loss and input return losses are compared for both states in Figure 5.36 and Figure5.37.

Figure 5.35 Comparison of 11.25º Phase Shifter Bit.

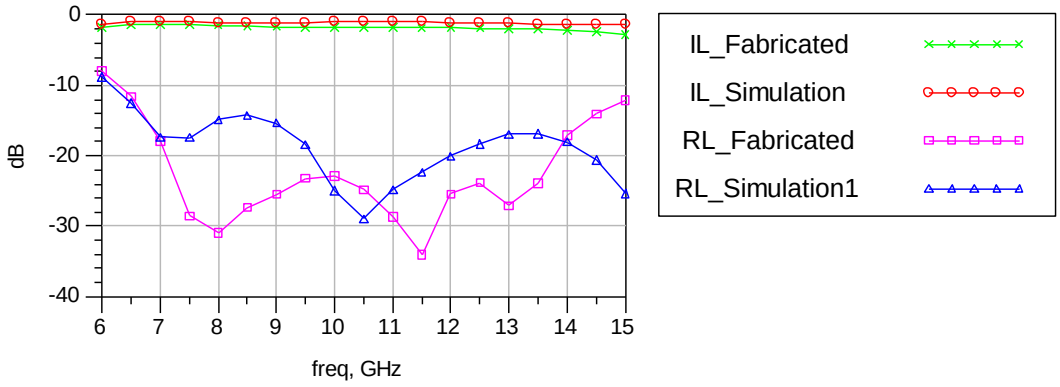

Figure 5.36 Comparison of Insertion and Input Return Losses for Stub 1.

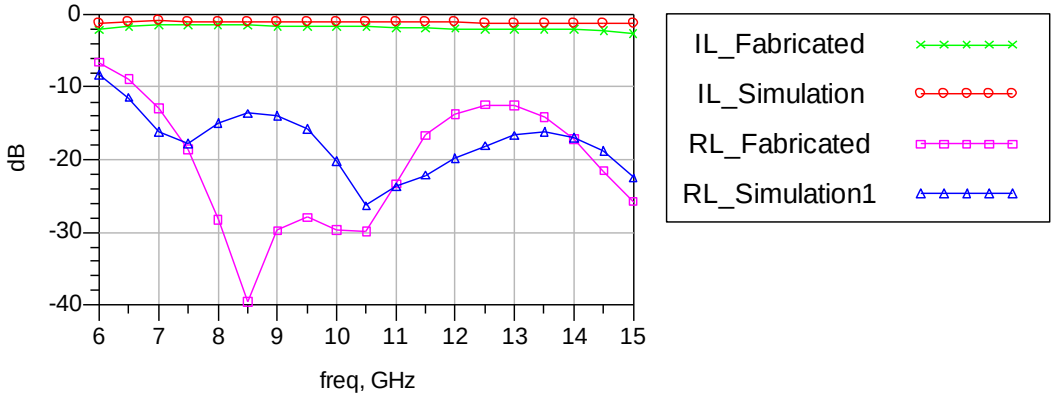

Figure 5.37 Comparison of Insertion and Input Return Losses for Stub 2.

5.3.2 Comparison of 22.5º Phase Shifter Bit

Figure 5.38 shows the comparison of differential phase shifts between the simulation and fabricated results. The insertion loss and input return losses are compared for both states in Figure 5.39 and Figure 5.40.

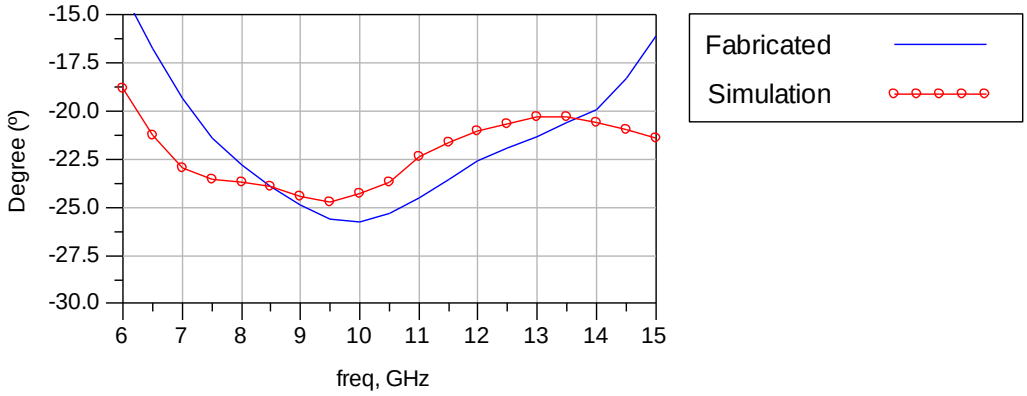

Figure 5.38 Comparison of 22.5º Phase Shifter Bit.

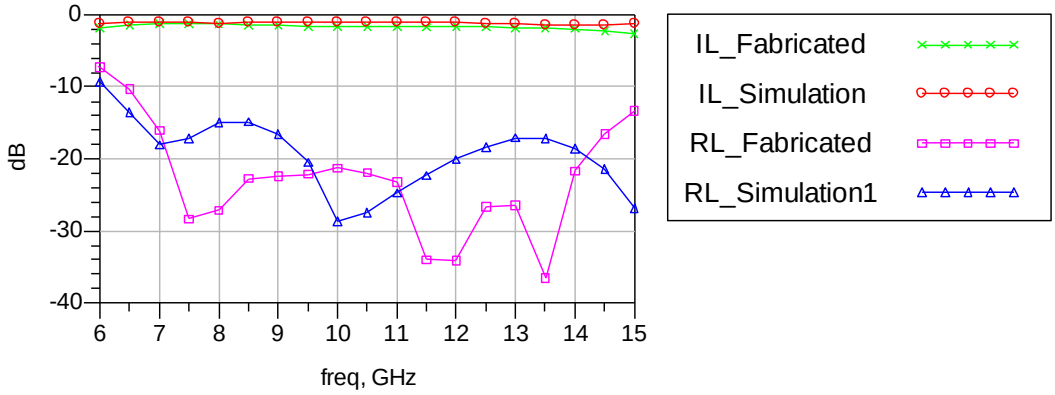

Figure 5.39 Comparison of Insertion and Input Return Losses for Stub 1.

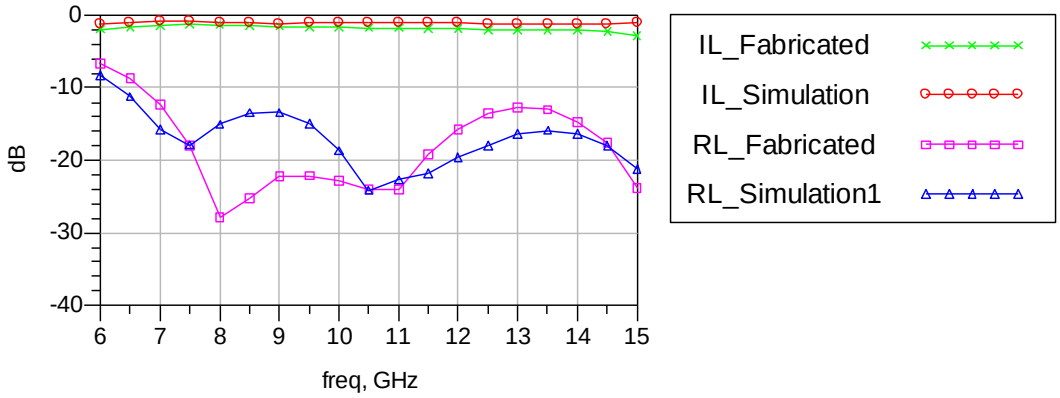

Figure 5.40 Comparison of Insertion and Input Return Losses for Stub 2.

5.3.3 Comparison of 45º Phase Shifter Bit

Figure 5.41 shows the comparison of differential phase shifts between the simulation and fabricated results. The insertion loss and input return losses are compared for both states in Figure 5.42 and Figure 5.43.

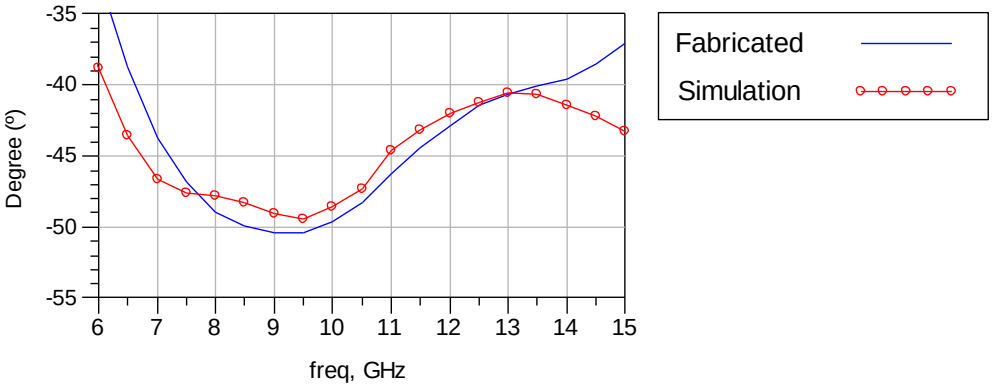

Figure 5.41 Comparison of 45° Phase Shifter Bit.

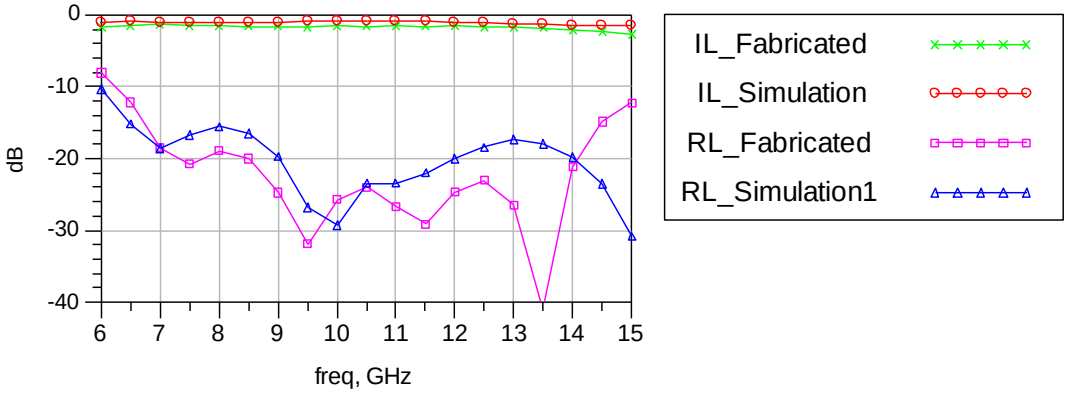

Figure 5.42 Comparison of Insertion and Input Return Losses for Stub 1.

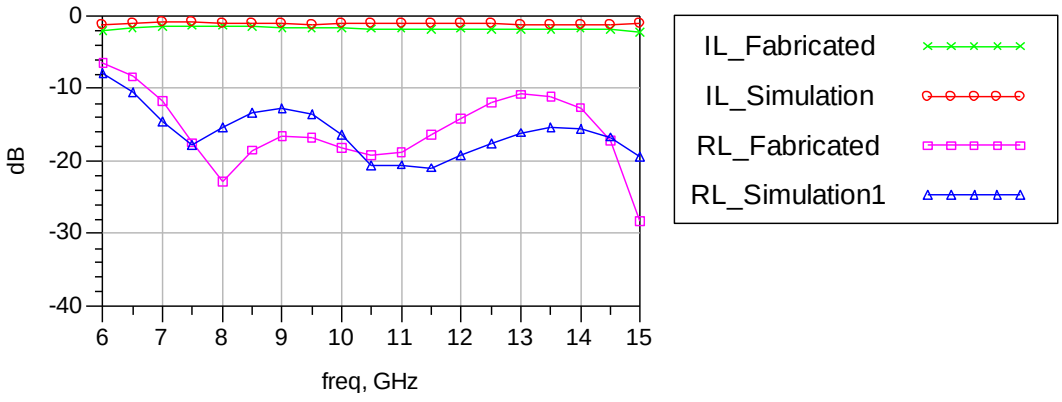

Figure 5.43 Comparison of Insertion and Input Return Losses for Stub 2.

5.3.4 Comparison of 90º Phase Shifter Bit

Figure 5.44 that the comparison of differential phase shifts between the simulation and fabricated results. The insertion loss and input return losses are compared for both states in Figure 5.45 and Figure 5.46.

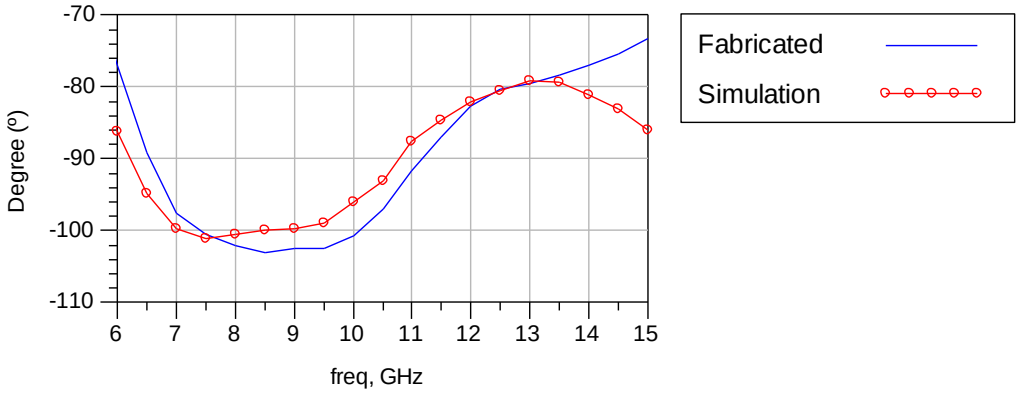

Figure 5.44 Comparison of 90º Phase Shifter Bit.

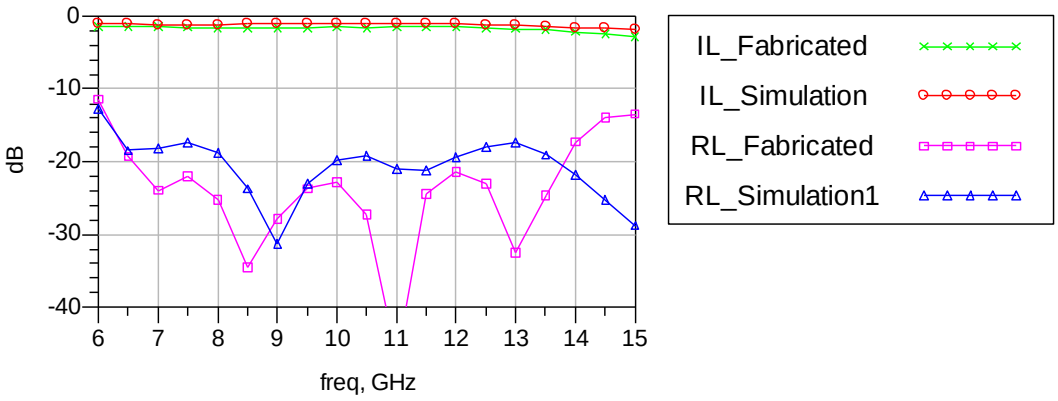

Figure 5.45 Comparison of Insertion and Input Return Losses for Stub 1.

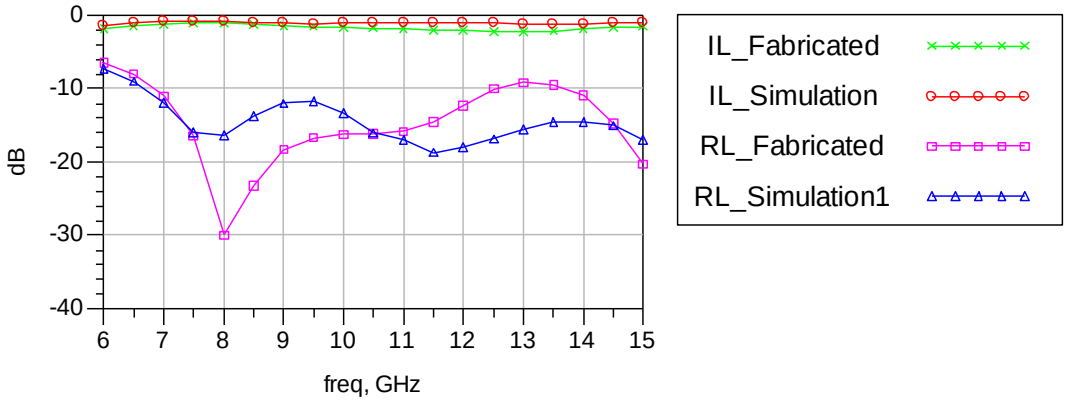

Figure 5.46 Comparison of Insertion and Input Return Losses for Stub 2.

CHAPTER 6

PHASE SHIFTER DESIGNS ON ALUMINA SUBSTRATE

Four wideband phase shifter bits are designed, simulated and fabricated onto TMM10i substrate in previous chapter. Using the same phase shifter circuit topology that includes unfolded Lange coupler, PIN diodes and radial stubs, 11.25, 22.5, 45, and 90º phase shifter circuits are designed and fabricated onto 15-mil thick Alumina substrate. In this chapter, the design, fabrication, and measurements of the wideband phase shifter bits for 11.25, 22.5, 45 and 90º are explained in detail. The phase shifter bits are fabricated onto Alumina substrate using thin film production technology in American Technical Ceramics.

In the beginning of the work unfolded Lange coupler is designed in ADS and EM simulation is performed using Sonnet Software. Afterwards, using the S-parameter file of PIN diodes between the coupler ports and radial stubs, stub sizes are determined according to the desired phase shift value in ADS. Then, the EM simulation of the whole circuit that includes unfolded Lange coupler and radial stubs is performed. Finally, the S-parameter files of PIN diodes are embedded into this circuit in ADS. The phase shifter circuits are tried to be designed with minimum phase shift errors in 6-18 GHz frequency band with minimum return losses. Assembling and measurement processes of fabricated phase shifters are performed in clean room facilities of ASELSAN Inc. Since the biasing circuits of the PIN diodes are not included in the simulations, there occurred some amount of phase offsets and tuning is performed on radial stubs sizes in order to compensate these effects. For the 6-18 GHz frequency band, maximum phase errors of the fabricated phase shifters are ±1.6, 2.8, 5.6, and 10.6º for the 11.25, 22.5,45, and 90º phase shifters, respectively. The maximum insertion losses are 3.5, 3.4, 3.9, and 4 dB at 15.5 GHz for the 11.25, 22.5,45, and 90º phase shifters, respectively. Also, the simulation and experimental results are compared in this chapter.

Also, the phase shifter bits are designed with spiral inductors that are connected behind the radial stubs. Inductors are used to bias the PIN diodes and DC signal flows to ground over these inductors where the RF signal reflects back. 11.25, 22.5, 45, and 90º phase shifters are redesigned by changing the stub sizes in order to compensate the loading of spiral inductor of radial stub. Four phase shifters are fabricated onto 15-mil thick Alumina as previous ones in American Technical Ceramics and measurement results of them are given in this chapter. Since, the inductance value of spiral inductor can be achieved maximum 4-5nH up to 18 GHz without any resonances, the bandwidth of the phase shifters starts from 7 GHz. The measurement results show that for 7-18 GHz frequency band, maximum phase errors of the fabricated phase shifters are ±1.5, 2.5, 4, and 10.3º for the 11.25, 22.5,45, and 90º phase shifters, respectively. The maximum insertion losses are 2, 2.2, 3.5, and 3.1 dB at 18 GHz for the 11.25, 22.5,45, and 90º phase shifters, respectively.

6.1 The Dielectric Substrate and Metallization

Aluminum oxide, commonly referred to as alumina, is used as the dielectric material for the realization of unfolded Lange coupler and phase shifter circuits that are explained in this chapter.

Alumina is one of the most cost effective and widely used materials in microwave and RF frequencies. The purity of the substrate ranges from 94% to 99.5% for different applications. Good dielectric properties at high frequencies, hard and wear resistant, high strength, and good thermal conductivity are some properties of alumina material. In this study, polished 99.5% pure alumina is selected where the dielectric constant ε_r is 9.8. The tangent loss of this type of alumina is 0.0002. So, it is not as lossy as Rogers TMM10i substrate told in previous chapter. Thin film production technique is required in order to fabricate the circuits that are scope of this thesis.

The thickness of the substrate is chosen as 15 mils. Of course, the substrate thickness should be low for high frequency applications since the substrate loss is increased.

However, when the thickness of the substrate is decreased the spacing between the lines of the Lange coupler will decrease, too. The thin film production used in this study allows minimum 0.5 mil line and space width with 0.1 mil tolerances. If the thickness of the substrate was selected lower than 15 mils the spacing between the conductors of Lange coupler would take critical values to fabricate.

The metallization of the substrate is formed by using 300 Å thick TiW over alumina and 150 micro inches Au over TiW.

6.2 Unfolded Lange Coupler

As explained previously, the Lange coupler is the most important component of the circuit. The details of design, EM simulation, fabrication and measurement results of the Lange coupler are given in this part.

6.2.1 Linear Design and EM Simulation

Microstrip unfolded Lange coupler is designed to operate for 6-18 GHz frequency band where 12 GHz is the center frequency. ADS program is used for linear simulation of the coupler. Width and length of the coupled lines and spacing between them are obtained as 0.9, 98 and 0.7 mils, respectively. With these parameters, when the signal is applied from the input port of the Lange coupler designed on 15-mils thick alumina substrate the frequency response is obtained as shown in Figure 6.1. The differences between the direct and coupled port values at 6, 12 and 18 GHz are tried to be at same levels. The input return loss is lower than -20 dB while the isolation is lower than -17 dB at 18 GHz.

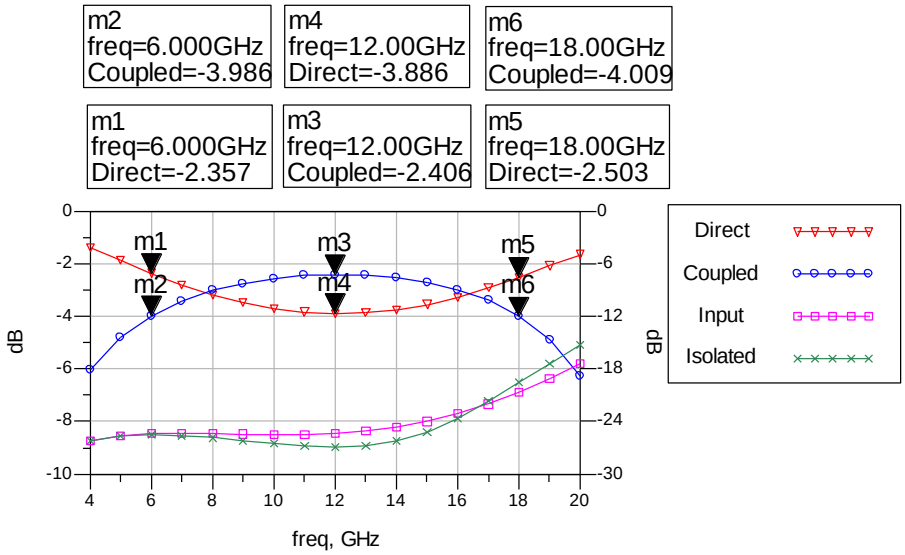

Figure 6.1 Linear Simulation Result of Unfolded Lange Coupler.

In the next step, the EM simulations are performed using Sonnet software. The circuit that is simulated in this program is shown in Figure 6.2. The Lange coupler is designed to measure by using probe station shown in Figure 6.5. Hence, some modifications on 50 Ohm transmission lines are made such as extending their length and bending them. The width of the 50 Ohm transmission lines is 14.4 mils. Also, CPW transmission lines are designed at the end of each microstrip transmission lines in order to measure the coupler directly using probes. The plated half vias with radius 5 mils are used between the top metal layer and bottom metal layer to provide grounding for CPW lines. The width of the CPW transmission line is 10.8 mils where the spacing between the lines is 7 mils.

The width, spacing, and length of the coupled lines of unfolded Lange coupler are 1, 0.6 and 102 mils, respectively. The air bridges are designed to connect the relevant coupled lines each other. The bridge height is 0.4 mils. The close view of the air bridge is also shown in Figure 6.2.

The EM simulation result of the coupler is shown in Figure 6.3.

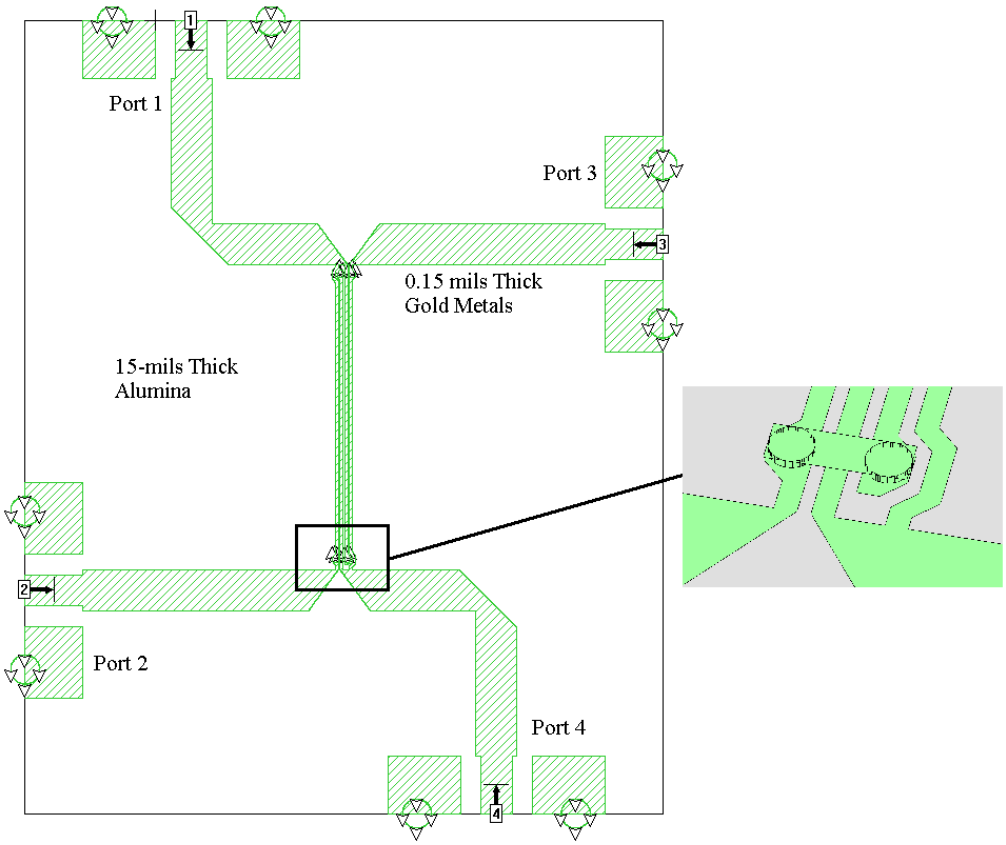

Figure 6.2 Layout of Unfolded Lange Coupler and Close View of Air Bridge.

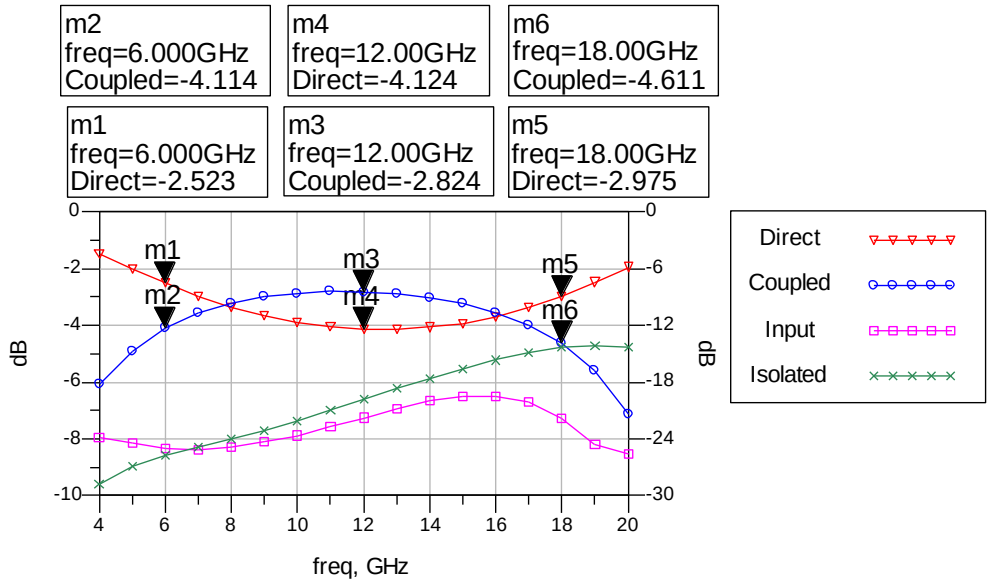

Figure 6.3 EM Simulation Result of the Unfolded Lange Coupler.

When the above response is compared with linear simulation result, it can be seen that there is a slope on S21 and S31 which are the direct port transmission coefficient and coupled port transmission coefficient, respectively. Because, as the frequency is increased, the dielectric and conductor losses are also increased. Input return loss is below -19 dB while the isolation is lower than -14 dB at 18 GHz. The unfolded Lange coupler shown in Figure 6.2 is manufactured. The fabrication details are given in next section.

6.2.2 Fabrication and Measurement

The unfolded Lange coupler shown in Figure 6.2 is fabricated using thin film technology in American Technical Ceramics. The photograph of fabricated coupler that is attached to the gold plated carrier using conductive epoxy is given in Figure 6.4. Since the air bridges are used in the production, gold wires are not used for connection of relevant coupled lines. The close view of air bridge is also shown in Figure 6.4. The coupler on the carrier is ready for the measurement, because the probes of probing station will directly go down to the CPW transmission lines that are designed for this purpose.

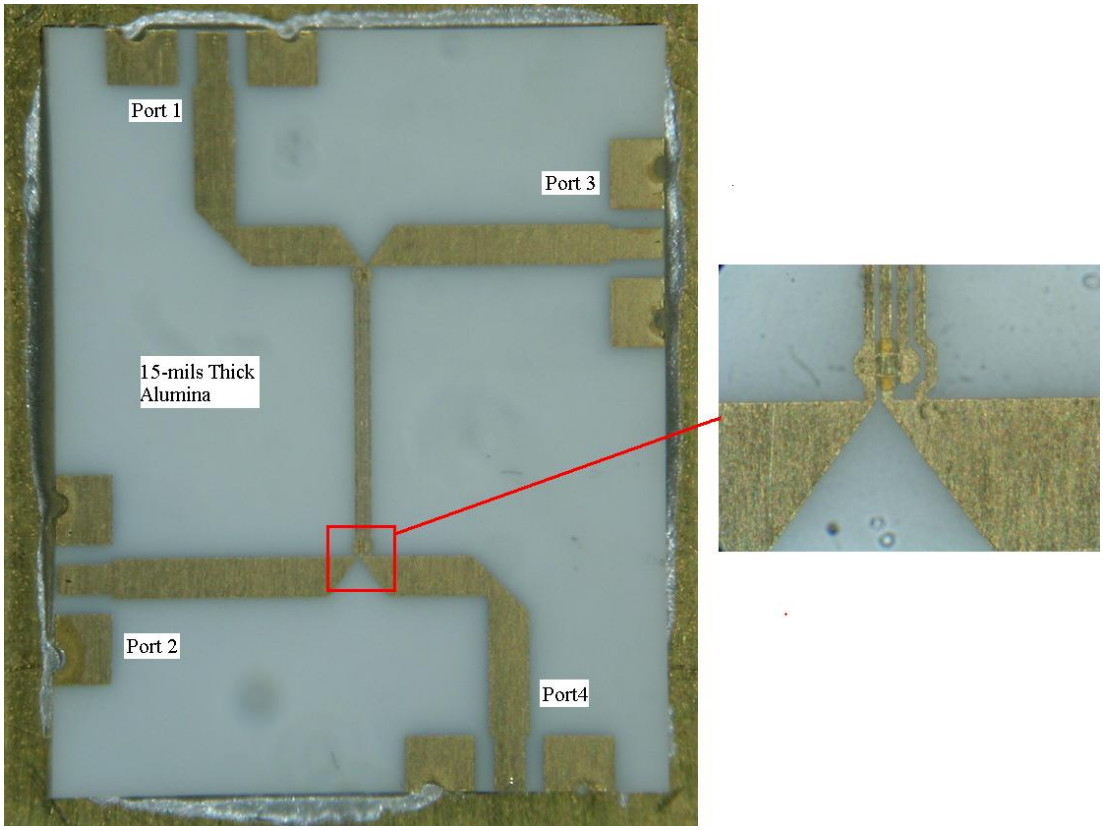

Figure 6.4 Fabricated Unfolded Lange Coupler and Close View of Air Bridge.

The measurement of unfolded Lange coupler is performed by using Cascade Microtech Microwave Probing Station and Agilent N5242A PNA-X 4 Port Network Analyzer operating between 10 MHz and 26.5 GHz. The measurement setup and probes that are approached to the coupler test points are illustrated in Figure 6.5 and Figure 6.6, respectively. The calibration of the four port network analyzer is done from the end points of the probes and Picoprobe calibration substrate CS-9 is used for the calibration process. Calibration is the most important part of measurements, since all results are dependent on the calibration done.

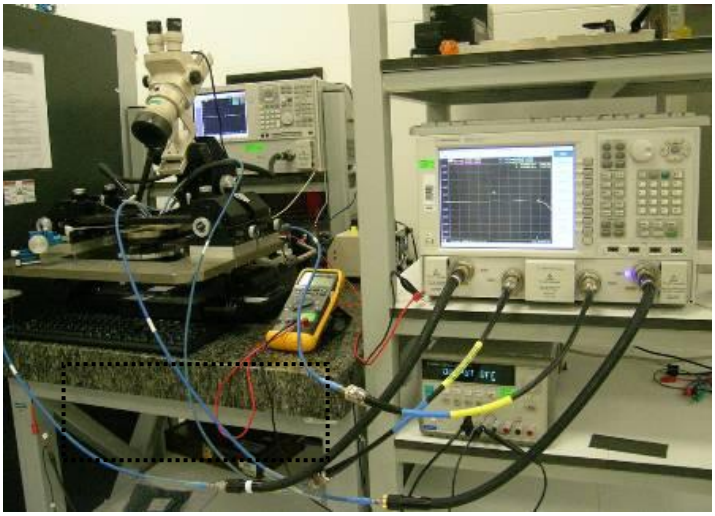

Figure 6.5 Measurement Setup of Lange Coupler.

The measurement results are shown in Figure 6.7. When the measurement result is compared with linear and EM simulation results, it is obvious that the coupling is increased. The reason of this increment comes from the production tolerance, because the spacing between the coupled lines decreased to almost 0.4 mils where it should have been 0.6 mils. The input return loss is lower than -17.5 dB up to 18 GHz where the isolation of the coupler is lower than -16.5 dB up to 18 GHz.

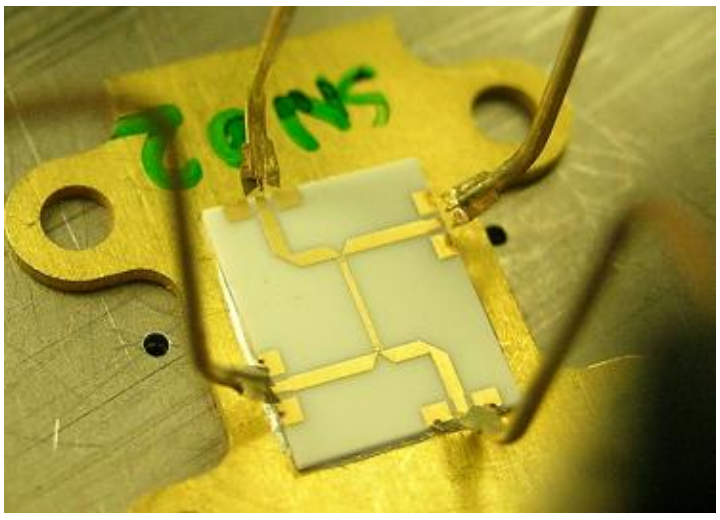

Figure 6.6 Close View of Lange Coupler Measurement.

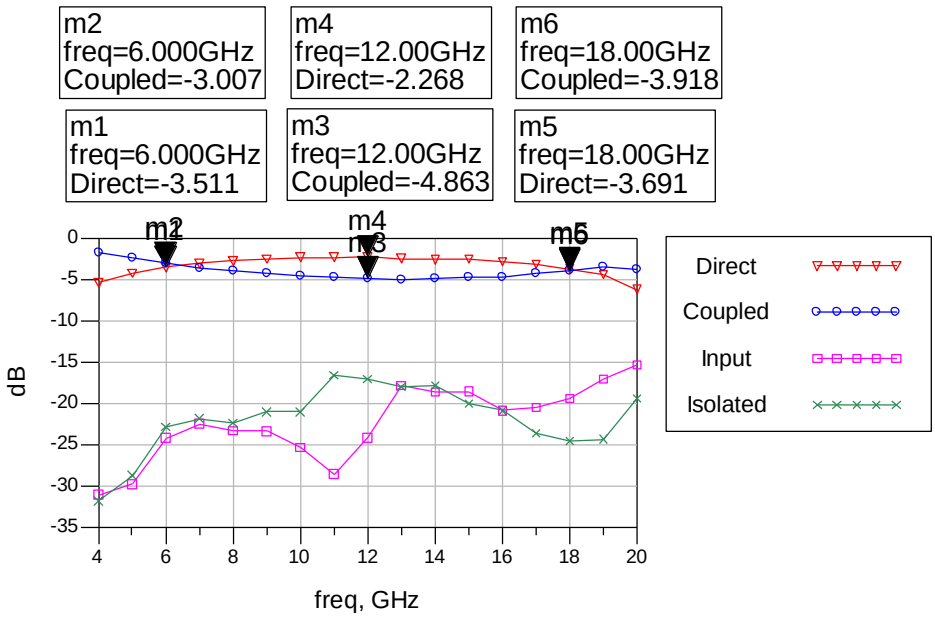

Figure 6.7 Measurement Result of Lange Coupler.

6.3 Design of Phase Shifter Bits

In the design of phase shifter bits, the circuit shown in Figure 3.17 is used as in the case of previous chapter. Since all designs including Lange coupler are fabricated simultaneously at abroad, the measured data file of Lange coupler could not be used in the designs of phase shifter circuits. Despite of it, the EM simulation of Lange coupler is used in the whole simulation with the S-parameter files of PIN diodes that are given in Appendix A. Using these files the radial stub sizes are determined according to the desired differential phase shift value The details of phase shifter designs for 11.25, 22.5, 45, and 90º are explained in this part.

6.3.1 11.25º Phase Shifter Bit

Figure 6.8 shows the circuit designed in ADS for 11.25º phase shifter bit where the Stub-1 is selected as the reflective load of the direct and coupled ports of unfolded Lange coupler. As explained previously, the EM simulation result of coupler and S-parameter data files are used in the circuit.

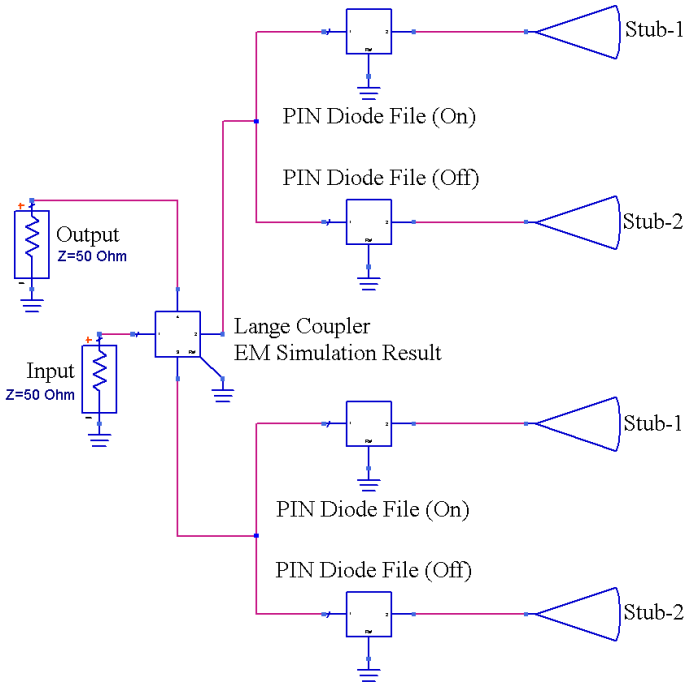

Figure 6.8 The Circuit Designed in ADS for 11.25º Phase Shifter Bit.

As explained previously, the EM simulation result of unfolded Lange coupler shown in Figure 6.3 and the S-parameter data file of the PIN diode for both forward biased (diode is On) and reverse biased (diode is Off) are used in ADS simulations. The biasing circuits are not included in the above circuit.

Similarly, the other circuit is designed where Stub-2 are selected as the reflective loads. In order to get the desired differential phase shift the insertion phases of each circuit are subtracted from each other as explained previously. So Stub-1 and Stub-2 sizes are determined for the desired differential phase shift. The input and output return losses of the circuit for both state are tried to be minimized while designing the stubs. Tuning and optimization properties of ADS are used in the design stages.

After obtaining the stub sizes for 11.25º differential phase shift value with minimum input and output return losses for both states, EM simulation of the whole circuit is performed by using Sonnet software. Unfolded Lange coupler and radial stubs are included in this simulation. The Sonnet layout of this circuit is given in Figure 6.9.

As in the design of Lange coupler, CPW transmission lines are used in the phase shifter circuit to go down probes into the circuit directly. So any extra component will not be placed into the input and output of the circuit such as test points and ribbon connections that affect the performance of the circuit. Circular vias between the top and bottom metal layer are used in order to provide ground planes for CPW lines. Internal ports also known auto-grounded ports are used at the end of direct and coupled ports of Lange coupler and inputs of the radial stubs. These ports are used to place the S-parameter file of the PIN diodes between Lange coupler ports and radial stubs. Hence, 8-port S-parameter data file is obtained at the end of EM simulation.

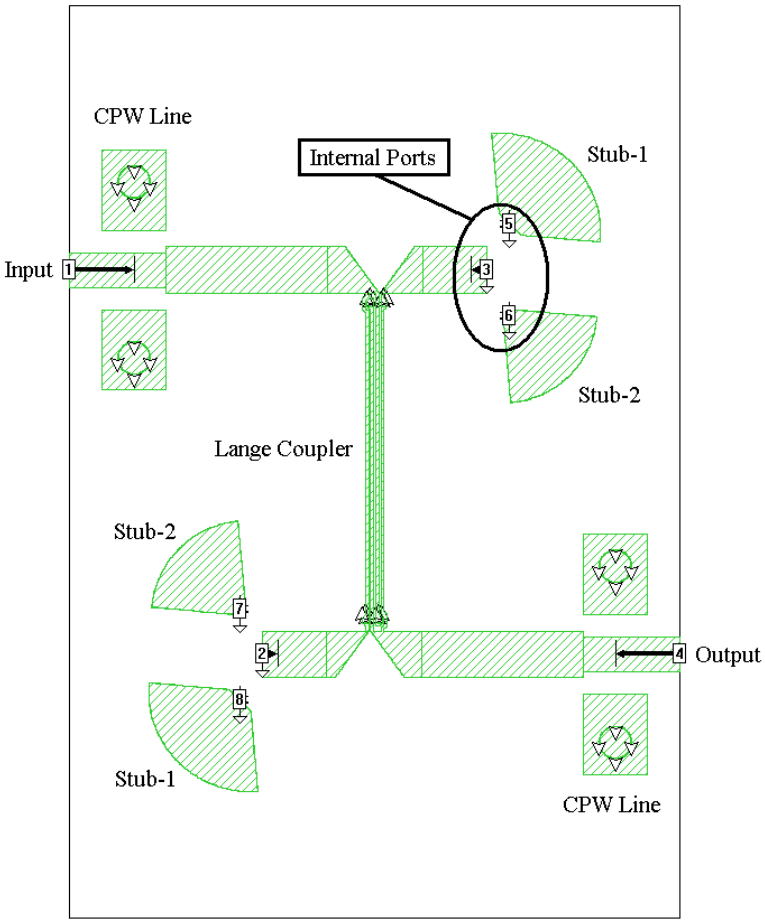

Figure 6.9 The Layout of 11.25º Phase shifter Bit.

Using ADS program the circuit shown in Figure 6.10 is formed. The circuit includes 8-port S-parameter file that contains the EM simulation result of Figure 6.9 and four

2-port S-parameter files that contain PIN diode On and Off data. According to simulation results of ADS the radial stubs, Stub-1 and Stub-2 are tuned in EM simulation. After some amount of iterations, the stub sizes are obtained as given in Table 6.1.

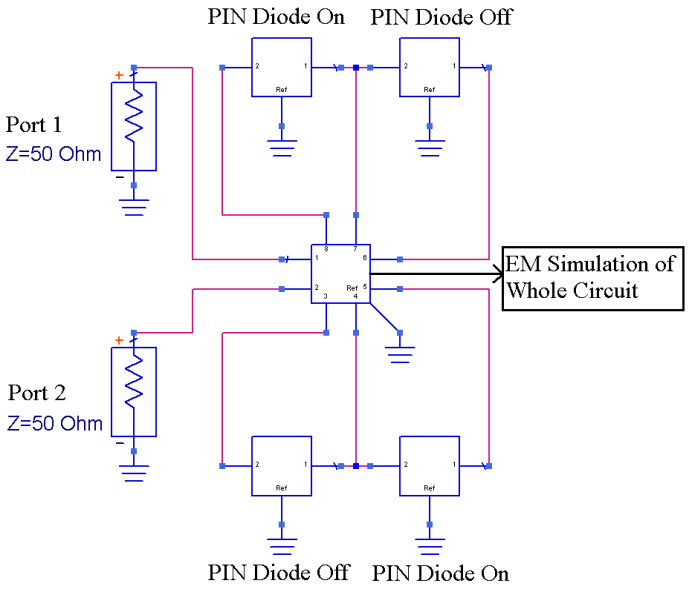

Figure 6.10 ADS Circuit Including PIN Diode Data Files.

Table 6.1 Radial Stub Parameters for 11.25º Phase Shifter Bit

Stub Parameters:	Stub-1	Stub-2
W (mils)	9.5	5
L (mils)	25	25.6
A (º)	100	81

The differential phase shift is obtained by changing the state of the diodes shown in Figure 6.9. Hence, the other radial stub pair is selected. The differential phase shift is given in Figure 6.11. The insertion loss, input and output return losses for both states of 11.25º phase shifter bit are shown in Figure 6.12 and Figure 6.13, respectively.

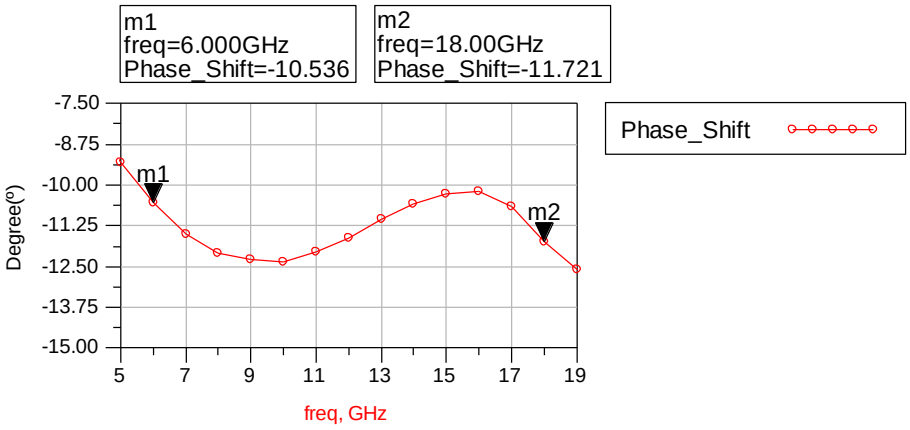

Figure 6.11 Differential Phase Shift for 11.25° Bit.

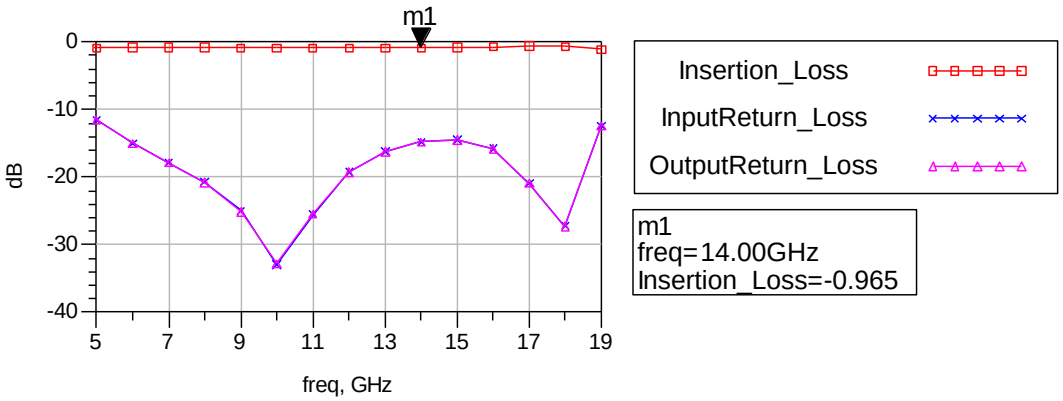

Figure 6.12 Insertion and Return Losses when Stub 1 is Selected.

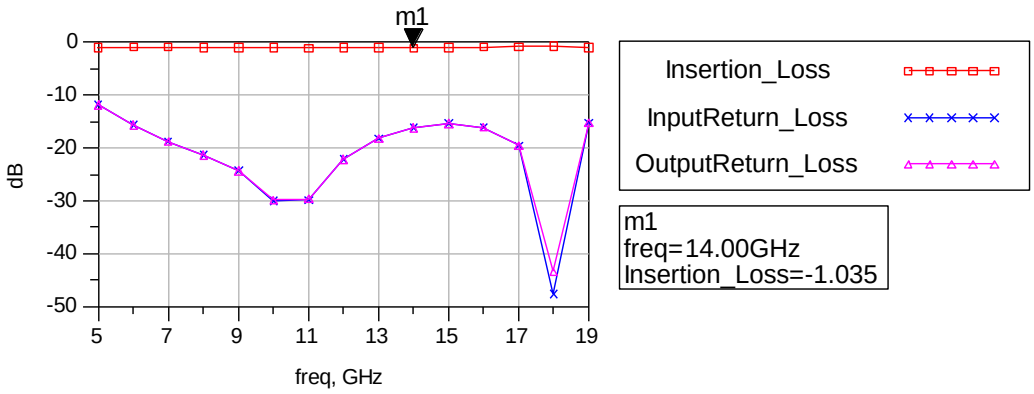

Figure 6.13 Insertion and Return Losses when Stub 2 is Selected.

As can be seen from the graphs above, 11.25º phase shift is satisfied for the frequency range 6-18 GHz with almost ±1.25º phase error. Also the input and output return losses for both states are lower than -15 dB for 6-18 GHz frequency range. Insertion losses for both states are higher than -1 dB approximately.

6.3.2 22.5º Phase Shifter Bit

The same design steps are followed for 22.5º phase shifter bit as in the case of 11.25º bit. Using the similar circuits shown in Figure 6.8, Figure 6.9, and Figure 6.10, the radial stub sizes are obtained as given in Table 6.2.

Table 6.2 Radial Stub Parameters for 22.5º Phase Shifter Bit

Stub Parameters:	Stub-1	Stub-2
W (mils)	13	4
L (mils)	24	23.5
A (º)	125	100

The differential phase shift is obtained by changing the state of the diodes shown in Figure 6.9. Hence, the other radial stub pair is selected. The differential phase shift is given in Figure 6.14. The insertion loss, input and output return losses for both states of 22.5º phase shifter bit are shown in Figure 6.15 and Figure 6.16, respectively.

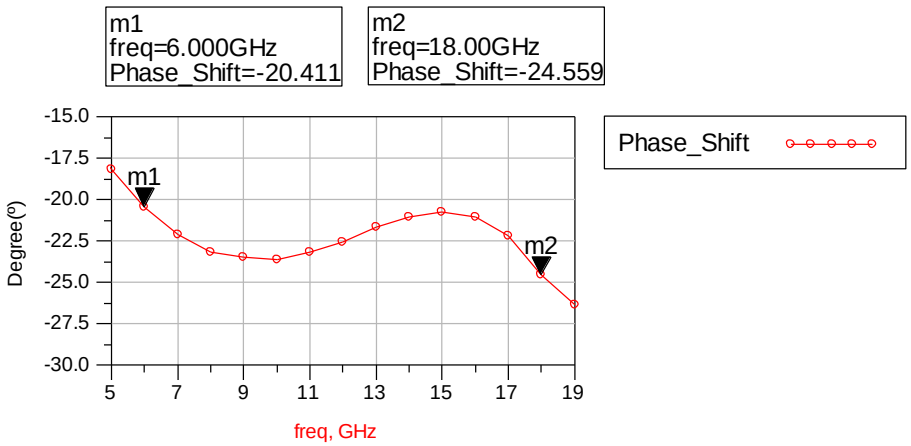

Figure 6.14 Differential Phase Shift for 22.5º Bit.

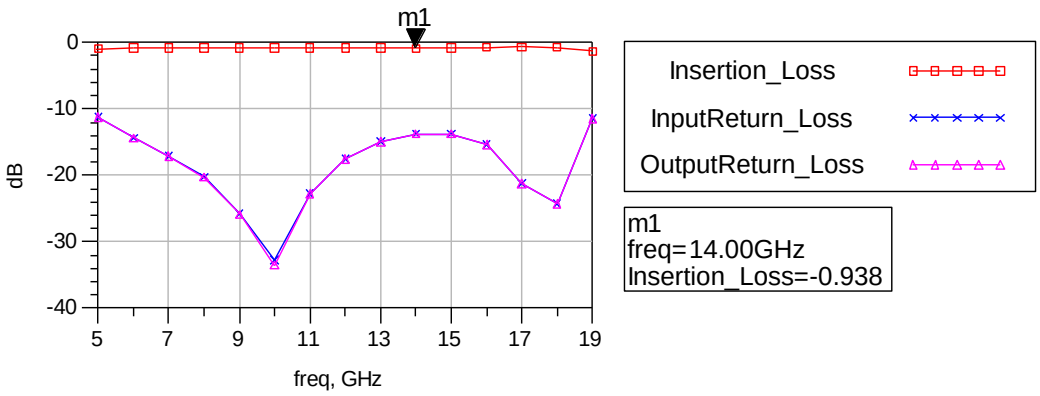

Figure 6.15 Insertion and Return Losses when Stub 1 is Selected.

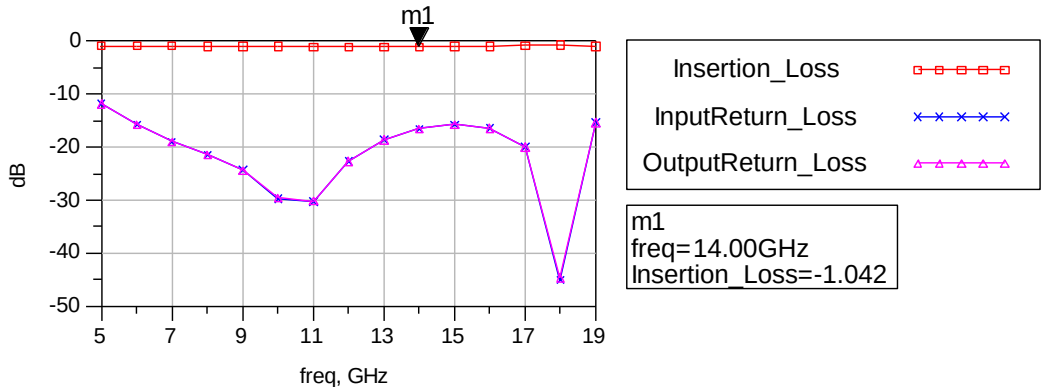

Figure 6.16 Insertion and Return Losses when Stub 2 is Selected.

As can be seen from the graphs above, 22.5º phase shift is satisfied for the frequency range 6-18 GHz with almost ±2º phase error. Also the input and output return losses for both states are lower than -14 dB for 6-18 GHz frequency range. Insertion losses for both states are higher than -1 dB approximately.

6.3.3 45º Phase Shifter Bit

The same design steps are followed for 45º phase shifter bit as in the case of 11.25º bit. Using the similar circuits shown in Figure 6.8, Figure 6.9, and Figure 6.10, the radial stub sizes are obtained as given in Table 6.3.

Table 6.3 Radial Stub Parameters for 45º Phase Shifter Bit

Stub Parameters:	Stub-1	Stub-2
W (mils)	12	4
L (mils)	32	28
A (º)	125	60

The differential phase shift is obtained by changing the state of the diodes shown in Figure 6.9. Hence, the other radial stub pair is selected. The differential phase shift for 45º phase shifter is given in Figure 6.17. The insertion loss, input and output return losses for both states of 45º phase shifter bit are shown in Figure 6.18 and Figure 6.19, respectively.

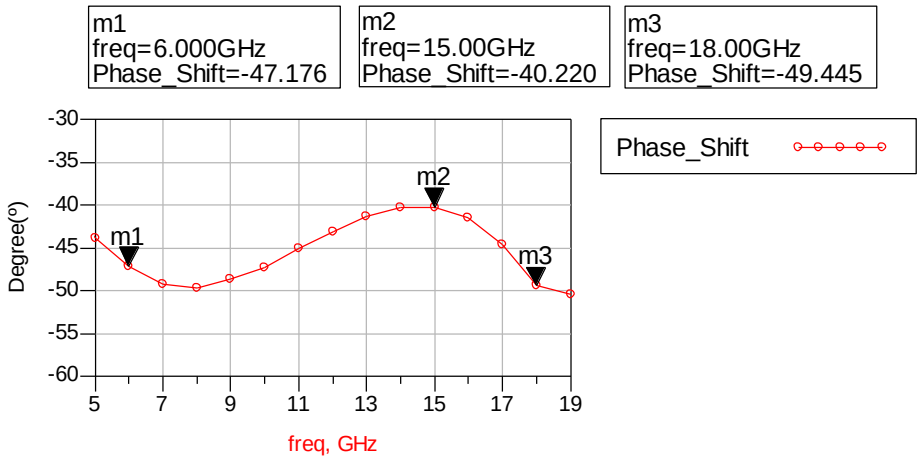

Figure 6.17 Differential Phase Shift for 45º Bit.

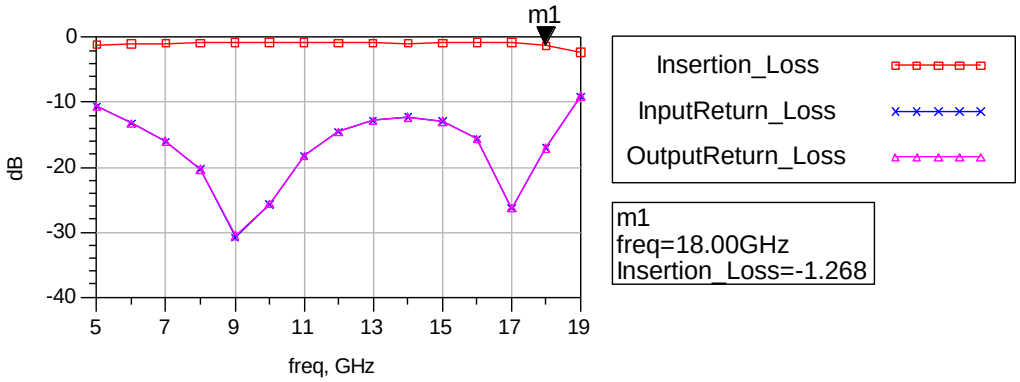

Figure 6.18 Insertion and Return Losses when Stub 1 is Selected.

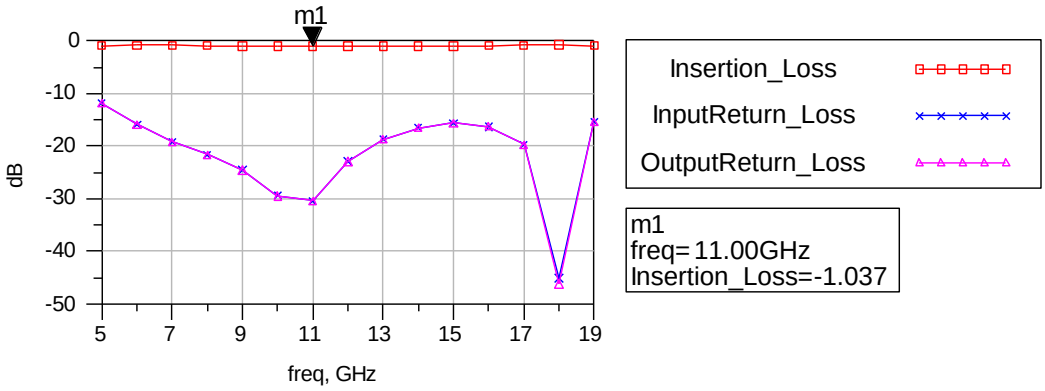

Figure 6.19 Insertion and Return Losses when Stub 2 is Selected.

As can be seen from the graphs above, 45º phase shift is satisfied for the frequency range 6-18 GHz with almost ±5º phase error. For 6-18 GHz frequency range, the input and output return losses are lower than -12 dB when Stub-1 is selected. Also they are lower than -16 dB when Stub-2 is selected. Maximum insertion losses for both states are higher than -1.3 dB approximately.

6.3.4 90º Phase Shifter Bit

The same design steps are followed for 90º phase shifter bit as in the case of 11.25º bit. Using the similar circuits shown in Figure 6.8, Figure 6.9, and Figure 6.10, the radial stub sizes are obtained as given in Table 6.4.

Table 6.4 Radial Stub Parameters for 90º Phase Shifter Bit

Stub Parameters:	Stub-1	Stub-2
W (mils)	16	4
L (mils)	39	18
A (º)	130	60

The differential phase shift is obtained by changing the state of the diodes shown in Figure 6.9. Hence, the other radial stub pair is selected. The differential phase shift for 90º phase shifter is given in Figure 6.20. The insertion loss, input and output

return losses for both states of 90º phase shifter bit are shown in Figure 6.21 and Figure 6.22, respectively.

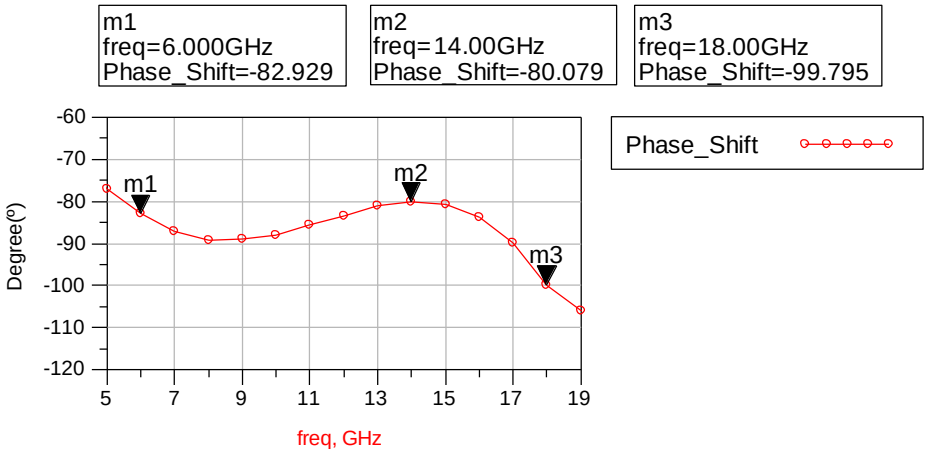

Figure 6.20 Differential Phase Shift for 90º Bit.

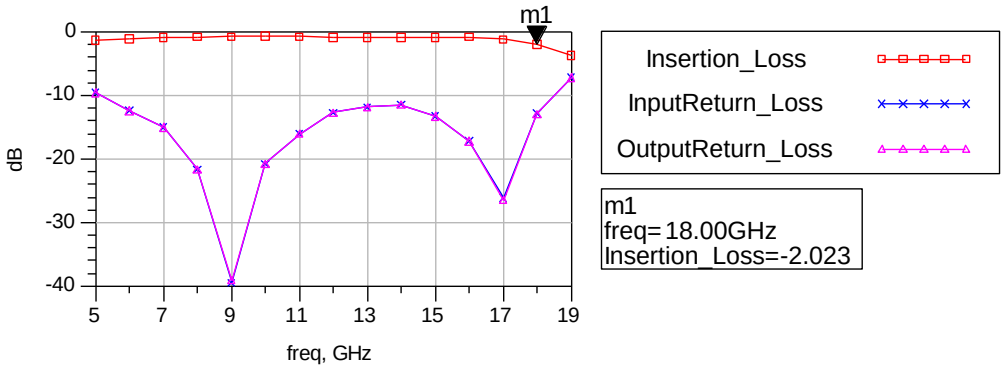

Figure 6.21 Insertion and Return Losses when Stub 1 is Selected.

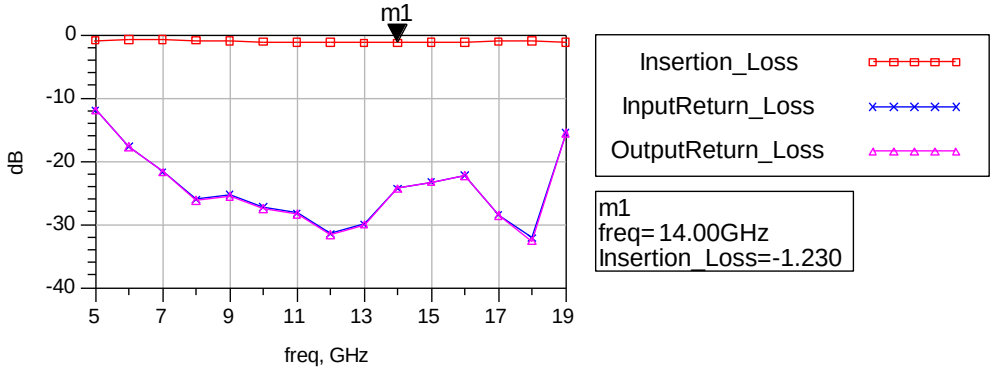

Figure 6.22 Insertion and Return Losses when Stub 2 is Selected.

As can be seen from the graphs above, 90º phase shift is satisfied for the frequency range 6-18 GHz with almost ±10º phase error. For 6-18 GHz frequency range, the input and output return losses are lower than -11 dB when Stub-1 is selected. Also they are lower than -18 dB when Stub-2 is selected. Maximum insertion losses for both states are higher than -2 dB approximately.

6.4 Fabrication and Measurement of Phase Shifter Bits

After designing the phase shifter bits for 11.25, 22.5, 45, and 90º differential phase shifting, the layouts of them are formed taking into account the design guidelines of ATC Thin Film division. The layout of the 11.25º is shown in Figure 6.23.

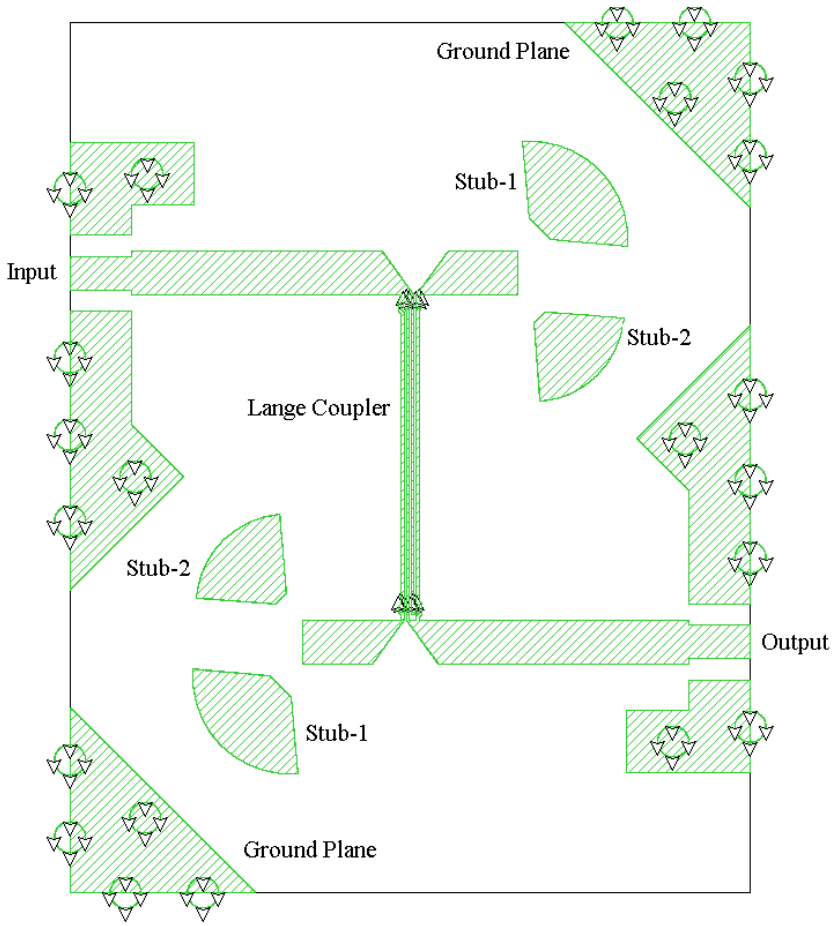

Figure 6.23 The Final Sonnet Layout of 11.25º Phase Shifter Bit.

CPW lines are used at the input and output of the phase shifter as explained previously. Plated vias are used in order to provide grounding. The vias at the edges

of the circuit are half vias and they are also plated with metal. There are also ground planes behind the radial stubs to provide grounding to the inductor that will be mounted for DC biasing of the PIN diode. The DC signal will be applied from the direct and coupled ports of the Lange coupler and the current will flow over the inductors to the ground while it will show high impedances to RF signals. The similar layouts are also formed for 22.5, 45, and 90º phase shifter bits. Fabrication, assembling and measurement results of each phase shifter is given in the next parts

6.4.1 11.25º Phase Shifter Bit

The layout given in Figure 6.23 is fabricated by ATC Thin Film Division. The dielectric substrate is 15-mil thick 99.5% alumina as explained previously. The top metal layer is 0.15 mil thick gold over 300 Å thick TiW. Unfolded Lange coupler sizes are same with the sizes given in EM simulation part. (Width=1 mil, Spacing= 0.6 mil, Length=102 and Air Bridge Height= 0.4 mil). The radial stub sizes are given in Table 6.1. The diameter of circular vias is 10 mils. The bottom side of the board is completely conductive and is plated with gold.

After the thin film processing, the circuit is mounted onto a gold plated carrier with conductive epoxy. The PIN diodes are mounted between the radial stubs and direct and coupled ports of unfolded Lange coupler. PIN diodes are attached to the circuit by using conductive epoxy. Since DC signal is applied from the direct and coupled ports of Lange coupler in common, PIN diodes are placed in reverse directions in order to select one of the radial stubs at the end of each port. Broadband conical inductor is placed between the radial stub and the ground planes that are shown in Figure 6.23. The inductance value of the inductor is 709nH and it is assembled to circuit using Kulicke Soffa AG 4124 Ball Bonder Machine shown in Figure 4.6. The close view of mounted PIN diodes and inductors are given in Figure 6.24

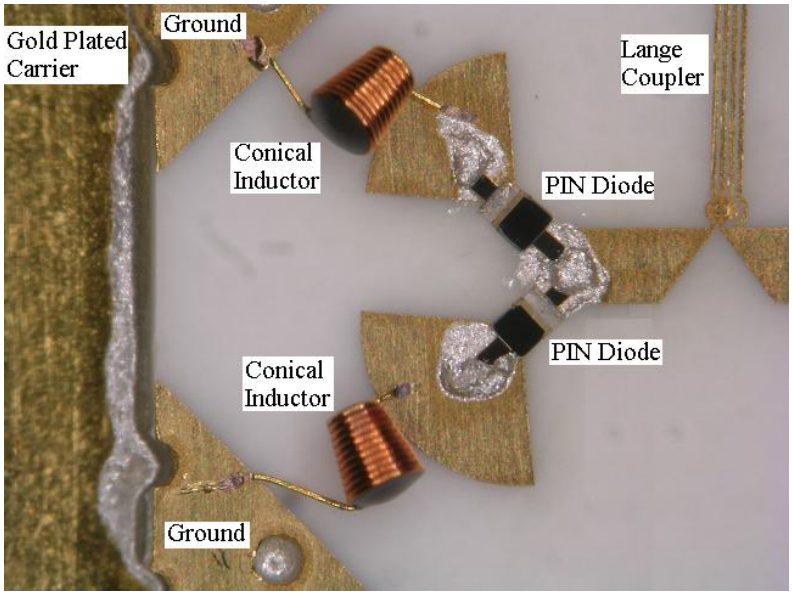

Figure 6.24 Close View of Mounted PIN Diodes and Conical Inductors.

To apply the DC signal from the power supply, a jumper that is placed into gold plated carrier is used. A 50 ohm series resistor is placed between the jumper and a 10nF capacitor to limit the DC current 10nF parallel capacitor is used to filter any possible RF signal in biasing. The jumpers, resistors and capacitors that are shown in Figure 6.25 are mounted onto gold plated carrier using conductive epoxy and they connected to each other with 1-mil diameter gold wire. Also 1-mil diameter gold wire is connected between the 10nF capacitor and direct and coupled port of Lange coupler. The length of the gold wire is approximately 280 mils length and provides almost 7nH that is required for filtering the RF signal.

All assembling processes that are explained above are performed in clean room facilities of ASELSAN Inc. Figure 6.25 shows fabricated 11.25º phase shifter bit.

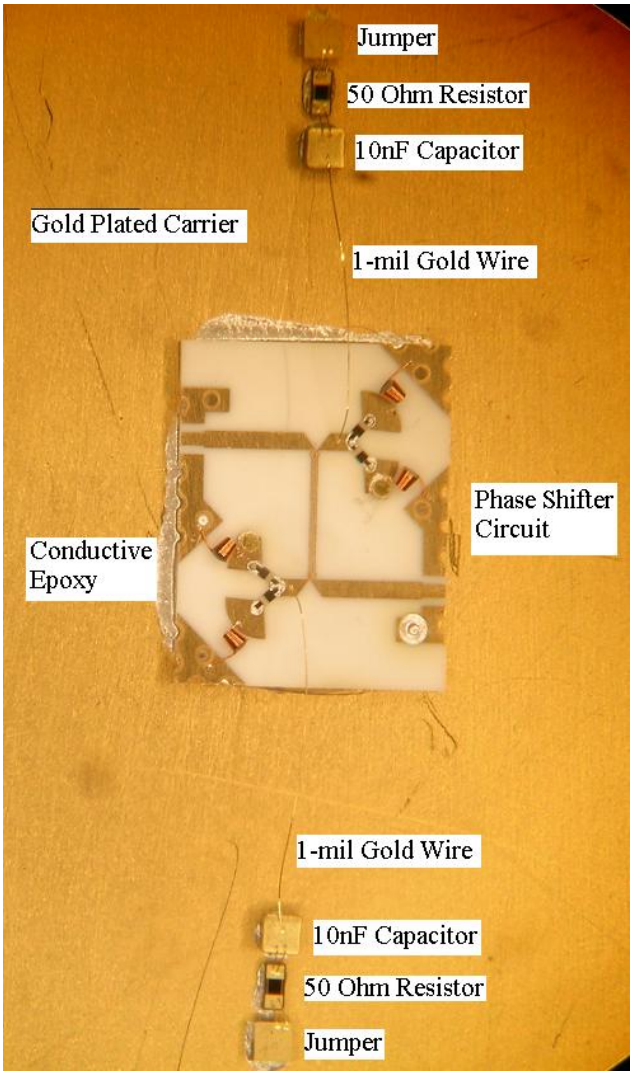

Figure 6.25 Fabricated 11.25º Phase Shifter Bit.

The measurement of 11.25º bit is performed by using Cascade Microtech Microwave Probing Station, Agilent E8346B PNA Network Analyzer operating between 10 MHz and 50 GHz, and Agilent E3631A Triple Output DC Power Supply. The DC blocking capacitors operating for DC-26.5 GHz are connected between the measurement cables and RF probes. The measurement setup is shown in Figure 6.26. The calibration of the network analyzer is done from the end points of the probes. Picoprobe calibration substrate CS-9 is used for the calibration process. The DC probes are used to apply the DC signal from power supply to the jumper. All measurements are performed in clean room facilities of ASELSAN Inc.

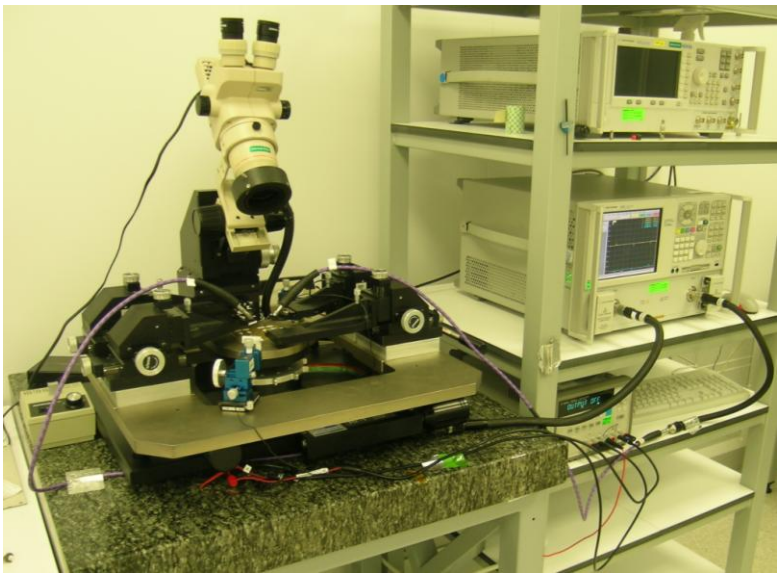

Figure 6.26 Measurement Setup.

When +1.5 V is applied from the power supply to the jumpers the PIN diodes that are connected to Stub 1 are forward biased. When -1.5 V is applied, the PIN diodes that are connected to Stub 2 are forward biased. Hence, the Stub-1 and Stub-2 are selected by applying +1.5 V or -1.5 V. The differential phase shift occurs between these two states.

In the design steps of the phase shifter, the biasing effects are not included to the ADS simulations. Also, the PIN diode S-parameter file that is provided by the producer is used instead of any measured data. Moreover, the fabrication and assembling processes have some errors on performance of phase shifter circuit. Because of these reasons, the tuning is performed on the sizes of radial stubs. Gold discs are used for tuning purposes. The diameter and the height of the gold discs are 16 and 10 mils, respectively.

The close view of fabricated and tuned 11.25º phase sifter is shown in Figure 6.27. The differential phase shift is obtained as shown in Figure 6.28. The insertion loss and input and output return losses for both states (when Stub-1 or Stub-2 is selected) are given in Figure 6.29 and Figure 6.30.

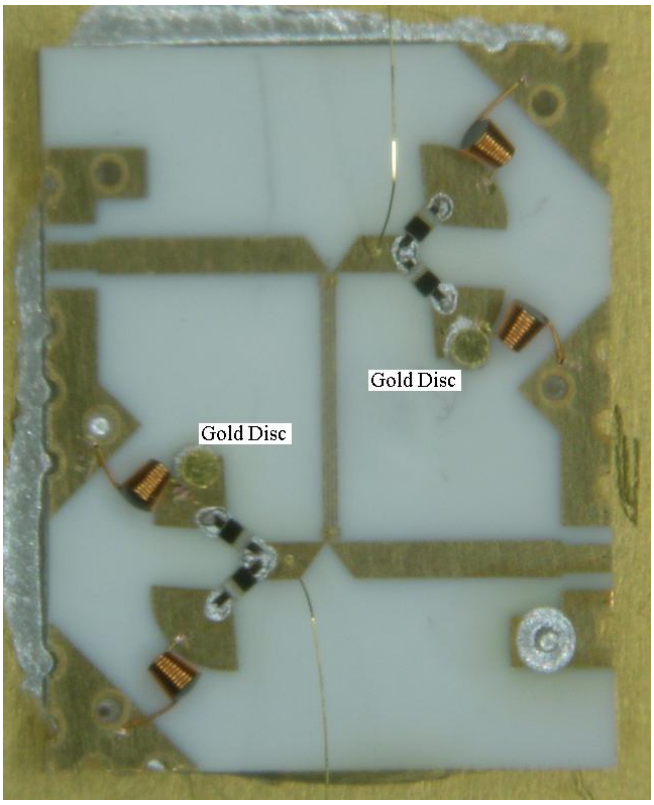

Figure 6.27 Tuned 11.25º Phase Shifter Bit.

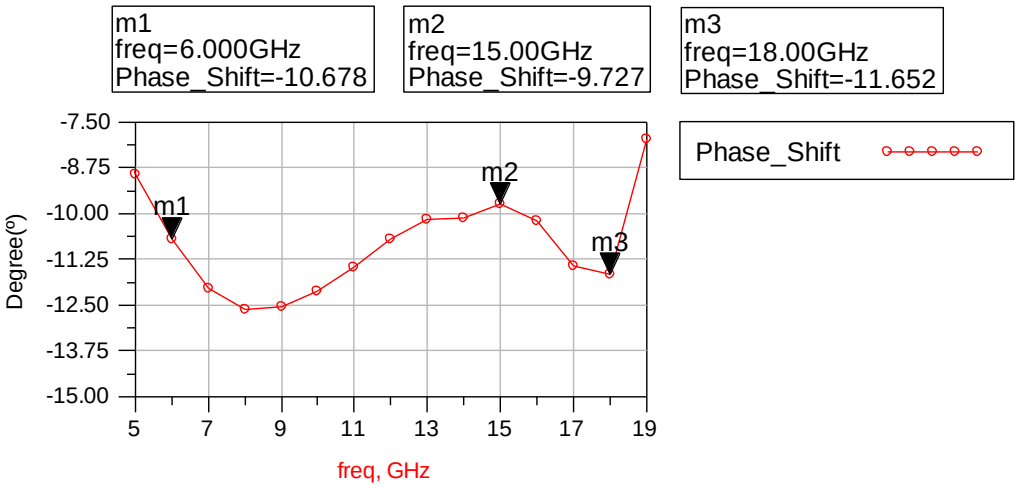

Figure 6.28 Differential Phase Shift for 11.25º Bit.

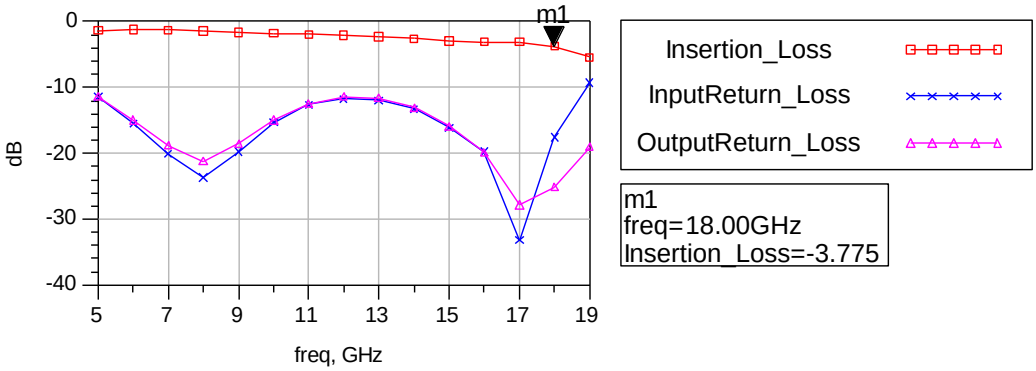

Figure 6.29 Insertion and Return Losses when Stub 1 is Selected.

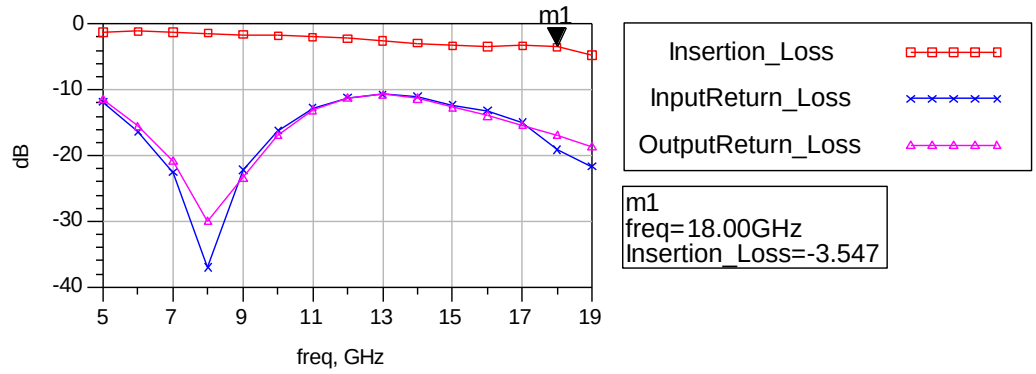

Figure 6.30 Insertion and Return Losses when Stub 2 is Selected.

As can be seen from the above graphs, 11.25º phase shift is satisfied for the frequency range 6-18 GHz with almost ±1.5º phase error. For 6-18 GHz frequency range, the input and output return losses are lower than -11 dB when Stub-1 is selected. Also they are lower than -10 dB when Stub-2 is selected. Maximum insertion losses for both states are higher than -3.8 dB approximately.

6.4.2 22.5º Phase Shifter Bit

The fabrication and assembling processes of 22.5º phase shifter are performed in the same way of 11.25º phase shifter bit. Same unfolded Lange coupler is used in the design. The only difference between them, of course, is the radial stub sizes which affect the differential phase shift. The radial stub sizes are given in Table 6.2.

The close view of fabricated and tuned 22.5º phase shifter bit is given in Figure 6.31. Figure 6.32 shows the differential phase shift of the circuit. The insertion loss and input and output return losses for both states (when Stub-1 or Stub-2 is selected) are given in Figure 6.33 and Figure 6.34.

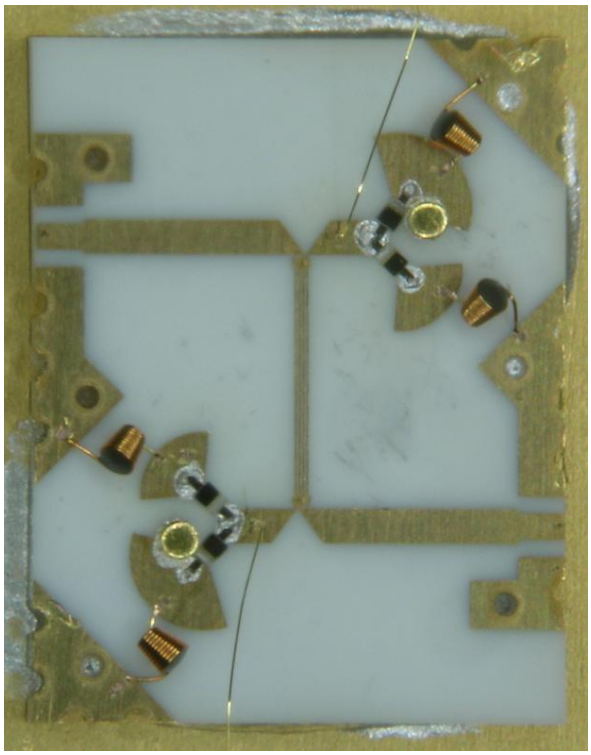

Figure 6.31 Tuned 22.5º Phase Shifter Bit.

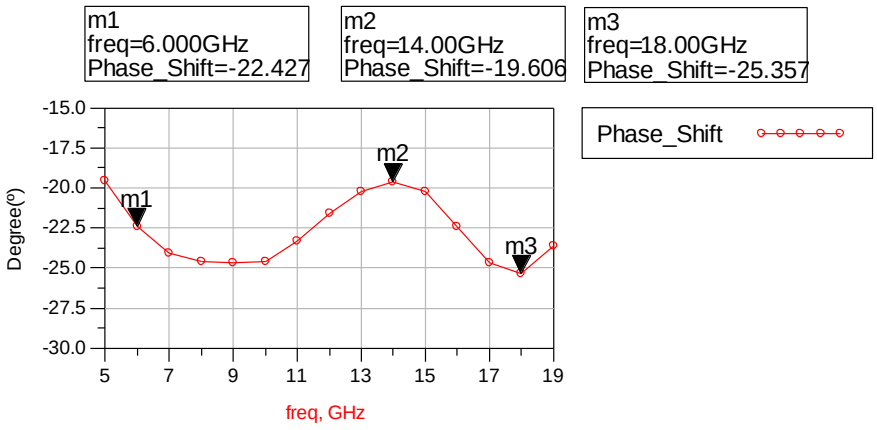

Figure 6.32 Differential Phase Shift for 22.5º Bit.

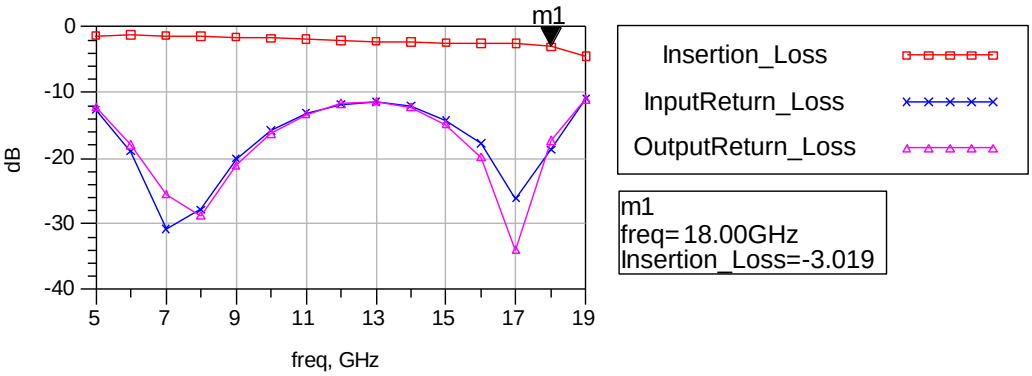

Figure 6.33 Insertion and Return Losses when Stub 1 is Selected.

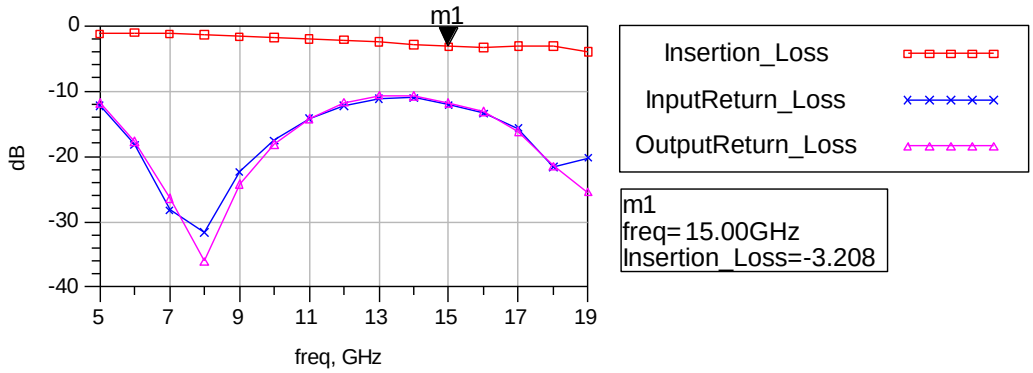

Figure 6.34 Insertion and Return Losses when Stub 2 is Selected.

Figure 6.31 shows that the 22.5º differential phase shift is satisfied for 6-18 GHz frequency band with ±2.9º phase error approximately. When the Stub-1 is selected the maximum insertion loss is almost -3.0 dB at 18 GHz, where the input and output return losses are lower than -11 dB for 6-18 GHz band. When the Stub-2 is selected the maximum insertion loss is almost -3.2 dB at 15 GHz, where the input and output return losses are lower than -10.5 dB for 6-18 GHz frequency band.

6.4.3 45º Phase Shifter Bit

The fabrication and assembling processes of 45º phase shifter are performed in the same way of 11.25º phase shifter bit. Same unfolded Lange coupler is used in the design. The only difference between them is the radial stub sizes which affect the differential phase shift. The radial stub sizes for 45º phase shifter are given in Table

6.3. The close view of fabricated and tuned 45º phase shifter bit is given in Figure 6.35. Figure 6.36 shows the differential phase shift of the circuit. The insertion loss and input and output return losses for both states (when Stub-1 or Stub-2 is selected) are given in Figure 6.37 and Figure 6.38.

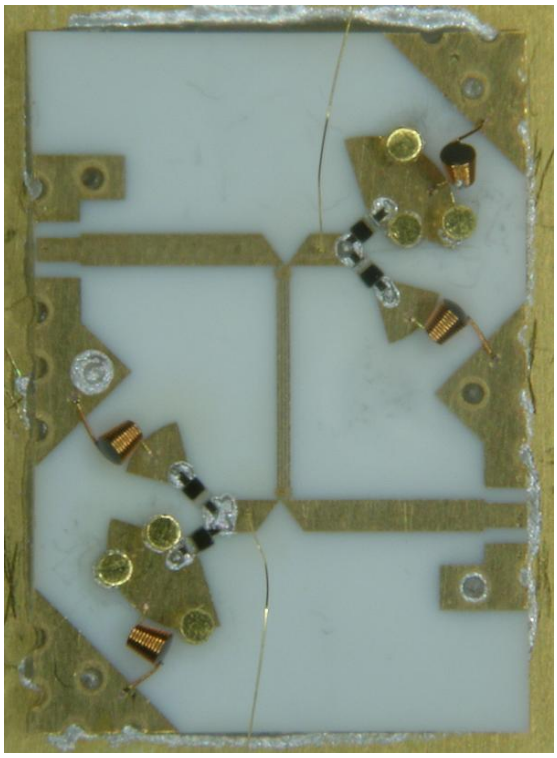

Figure 6.35 Tuned 45º Phase Shifter Bit.

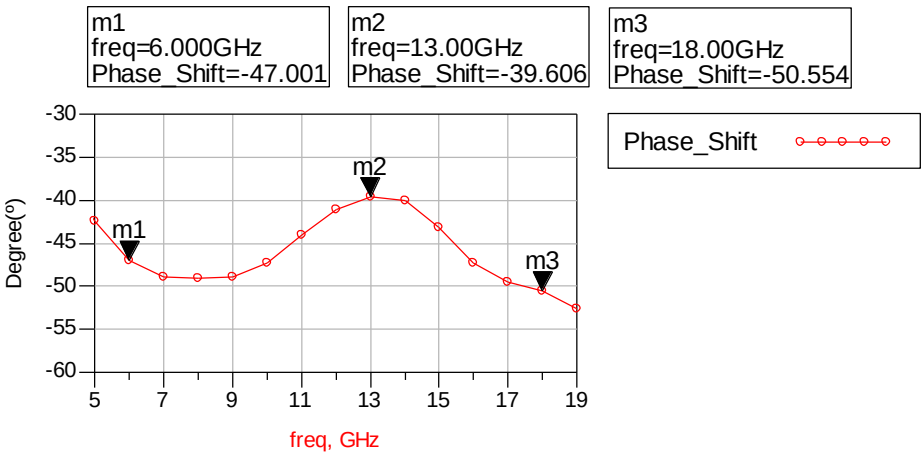

Figure 6.36 Differential Phase Shift for 45º Bit.

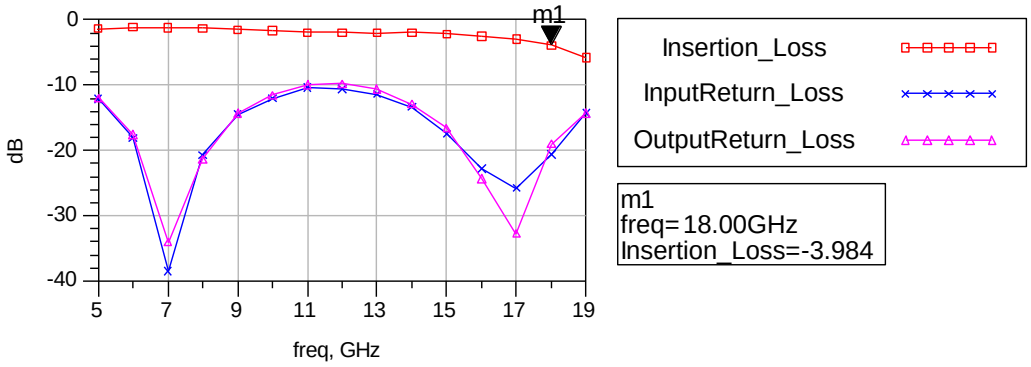

Figure 6.37 Insertion and Return Losses when Stub 1 is Selected.

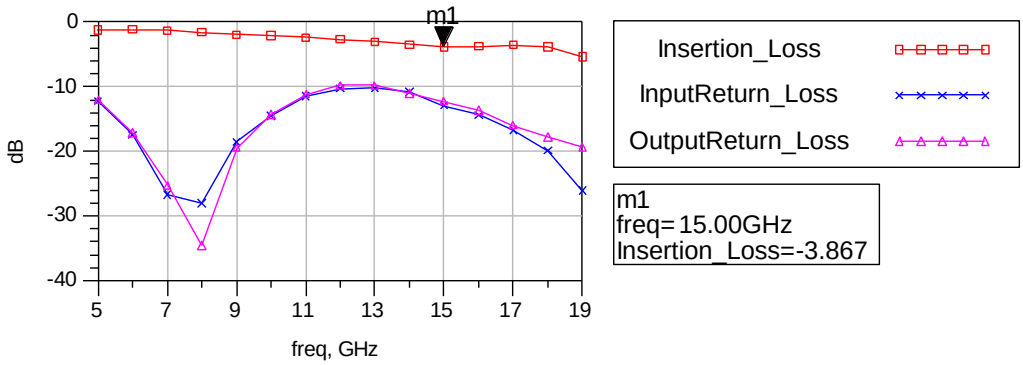

Figure 6.38 Insertion and Return Losses when Stub 2 is Selected.

Figure 6.36 shows that the 45º differential phase shift is satisfied for 6-18 GHz frequency band with ±5.5º phase error approximately. When the Stub-1 is selected the maximum insertion loss is lower than -4.0 dB at 18 GHz, where the input and output return losses are lower than -10 dB for 6-18 GHz band. When the Stub-2 is selected the maximum insertion loss is almost -3.9 dB at 15 GHz, where the input and output return losses are lower than -10 dB for 6-18 GHz frequency band.

6.4.4 90º Phase Shifter Bit

The fabrication and assembling processes of 90º phase shifter are performed in the same way of 11.25º phase shifter bit. Same unfolded Lange coupler is used in the design. The only difference between them is the radial stub sizes which affect the differential phase shift. The radial stub sizes are given in Table 6.4. The close view

of fabricated and tuned 90º phase shifter bit is given in Figure 6.39. Figure 6.40 shows the differential phase shift of the circuit. The insertion loss and input and output return losses for both states (when Stub-1 or Stub-2 is selected) are given in Figure 6.41 and Figure 6.42.

Figure 6.39 Tuned 90º Phase Shifter Bit.

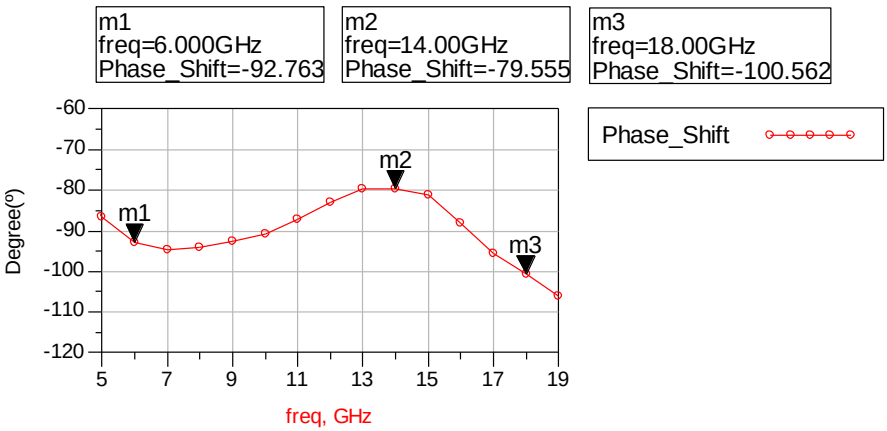

Figure 6.40 Differential Phase Shift for 90º Bit.

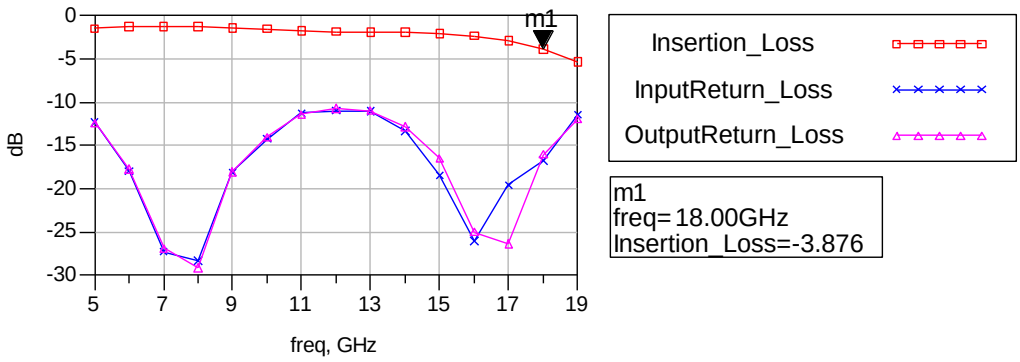

Figure 6.41 Insertion and Return Losses when Stub 1 is Selected.

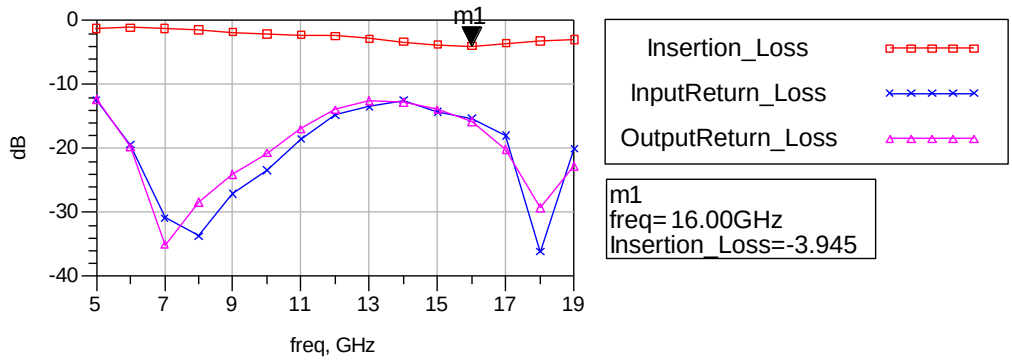

Figure 6.42 Insertion and Return Losses when Stub 2 is Selected.

Figure 6.40 shows that the 90º differential phase shift is satisfied for 6-18 GHz frequency band with ±10.5º phase error approximately. When the Stub-1 is selected the maximum insertion loss is lower than -3.9 dB at 18 GHz, where the input and output return losses are lower than -11 dB for 6-18 GHz band. When the Stub-2 is selected the maximum insertion loss is almost -4 dB at 15 GHz, where the input and output return losses are lower than -12 dB for 6-18 GHz frequency band.

6.5 Comparison of Simulation and Fabricated Results

The simulation results of phase shifter bits that are designed on alumina substrate are compared with the fabricated results in this part.

6.5.1 Comparison of 11.25º Phase Shifter Bit

Figure 6.43 shows the comparison of differential phase shifts between the simulation and fabricated results. The insertion loss and input return losses are also compared for both states in Figure 6.44 and Figure6.45.

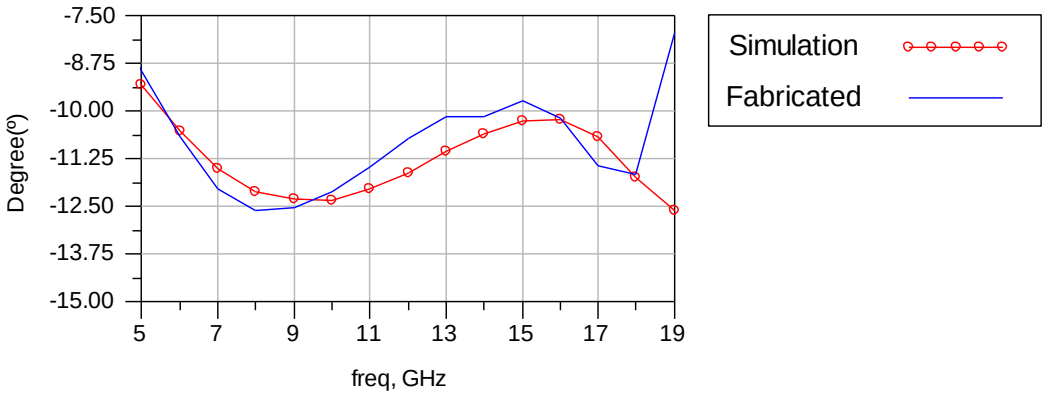

Figure 6.43 Comparison of Differential Phase Shift for 11.25º Bit.

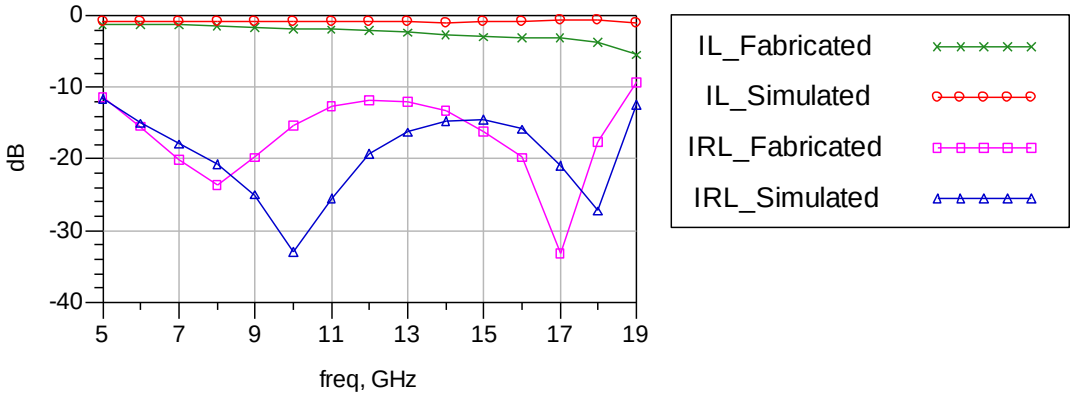

Figure 6.44 Comparison of Insertion and Input Return Losses for Stub 1.

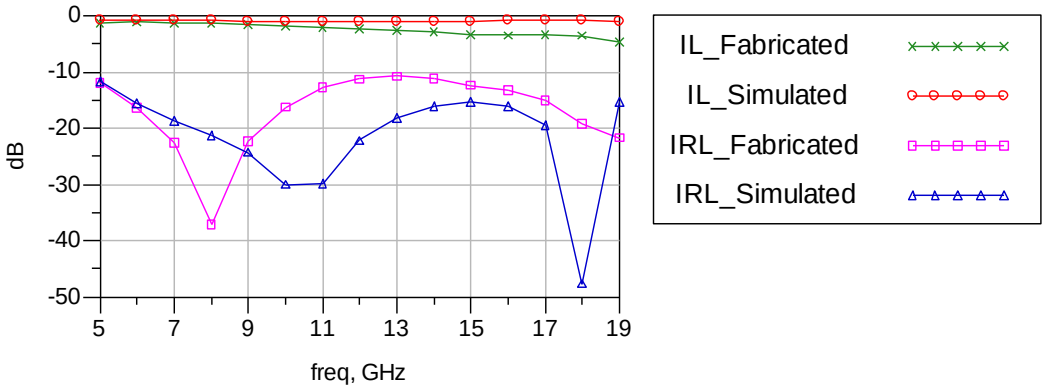

Figure 6.45 Comparison of Insertion and Input Return Losses for Stub 2.

6.5.2 Comparison of 22.5º Phase Shifter Bit

Figure 6.46 shows the comparison of differential phase shifts between the simulation and fabricated results for 22.5º phase shifter. The insertion loss and input return losses are also compared for both states in Figure 6.47 and Figure6.48.

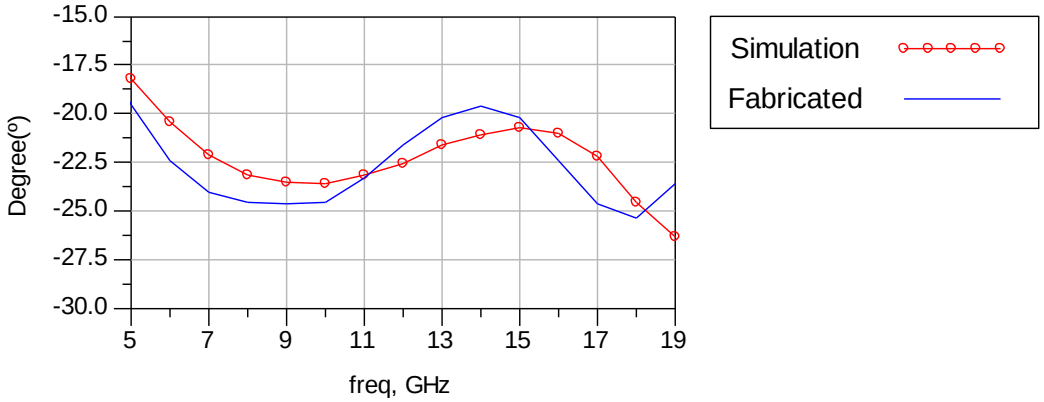

Figure 6.46 Comparison of Differential Phase Shift for 22.5º Bit.

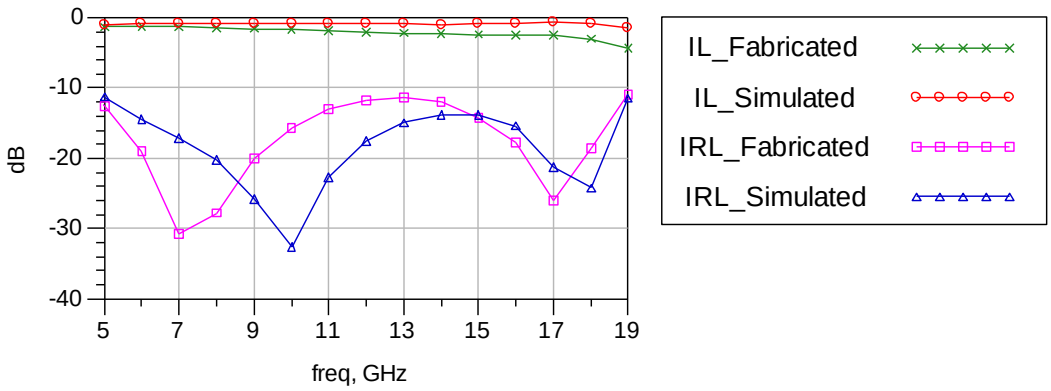

Figure 6.47 Comparison of Insertion and Input Return Losses for Stub 1.

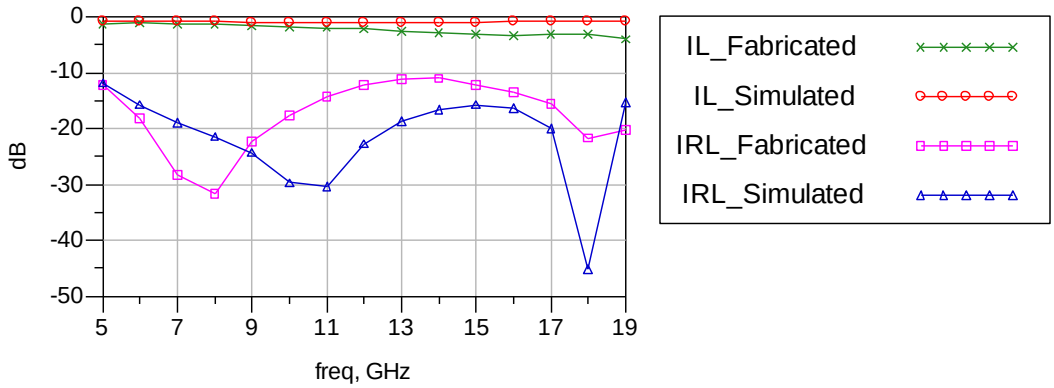

Figure 6.48 Comparison of Insertion and Input Return Losses for Stub 2.

6.5.3 Comparison of 45º Phase Shifter Bit

Figure 6.49 shows the comparison of differential phase shifts between the simulation and fabricated results for 45º phase shifter. The insertion loss and input return losses are also compared for both states in Figure 6.50 and Figure6.51.

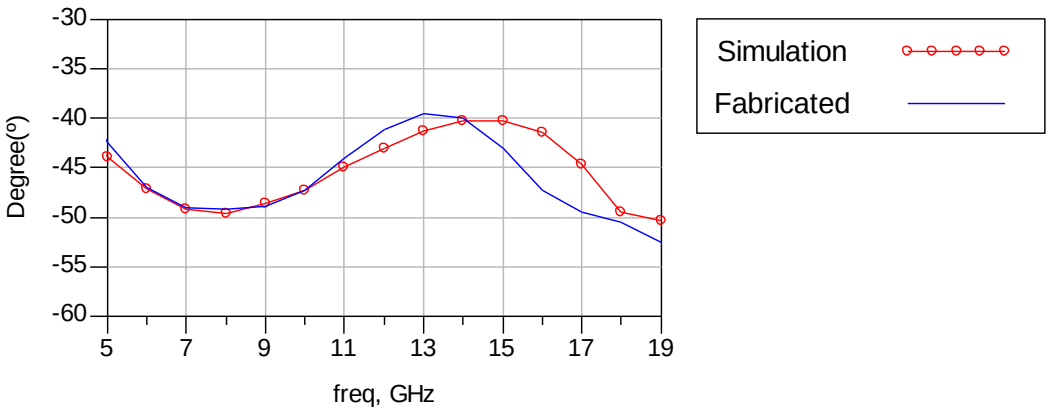

Figure 6.49 Comparison of Differential Phase Shift for 45º Bit.

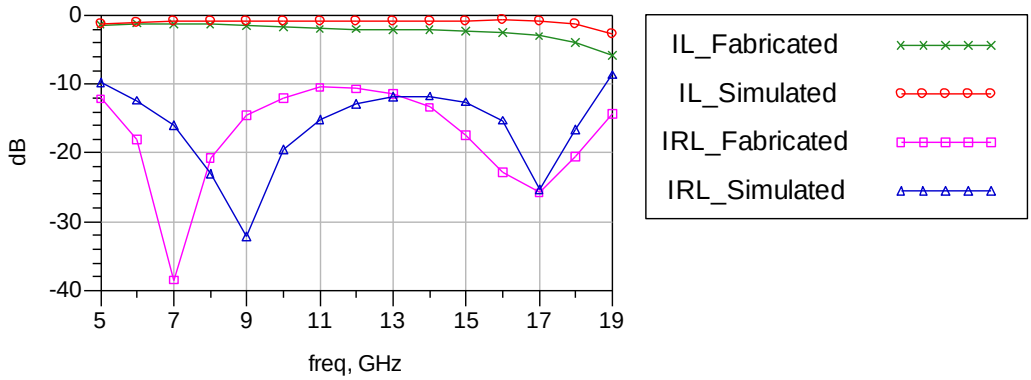

Figure 6.50 Comparison of Insertion and Input Return Losses for Stub 1.

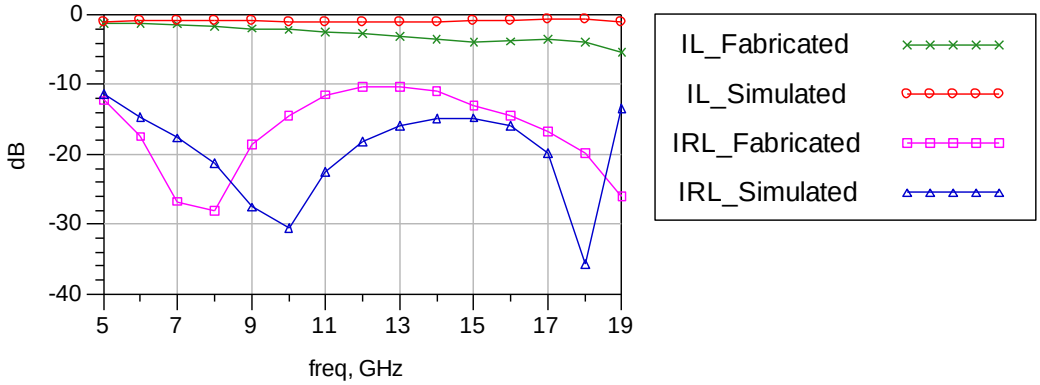

Figure 6.51 Comparison of Insertion and Input Return Losses for Stub 2.

6.5.4 Comparison of 90º Phase Shifter Bit

Figure 6.52 that the comparison of differential phase shifts between the simulation and fabricated results for 90º phase shifter. The insertion loss and input return losses are also compared for both states in Figure 6.53and Figure6.54.

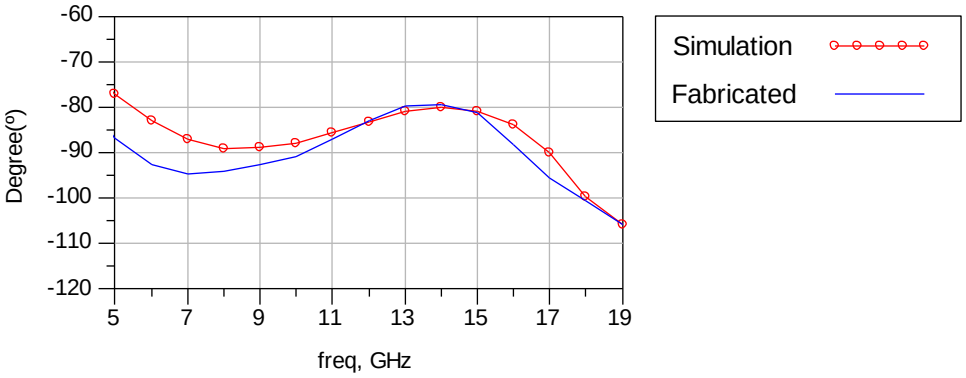

Figure 6.52 Comparison of Differential Phase Shift for 90º Bit.

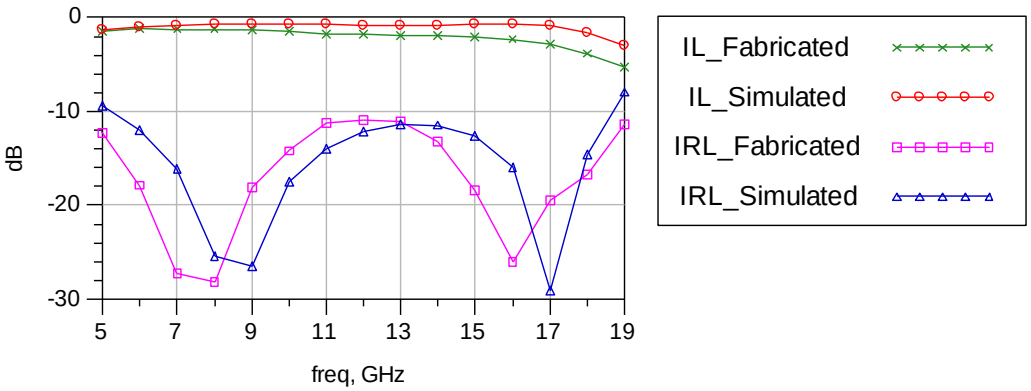

Figure 6.53 Comparison of Insertion and Input Return Losses for Stub 1.

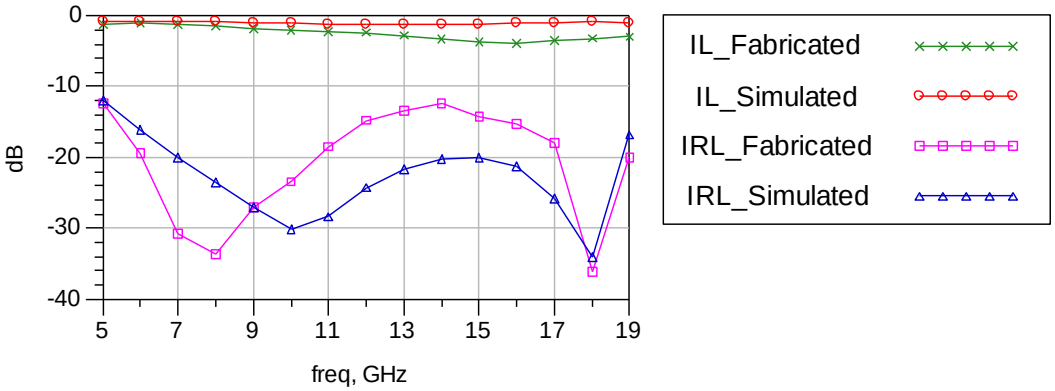

Figure 6.54 Comparison of Insertion and Input Return Losses for Stub 2.

CHAPTER 7

PHASE SHIFTER DESIGNS ON ALUMINA SUBSTRATE WITH SPIRAL INDUCTORS

Four wideband phase shifter bits are designed, simulated and fabricated onto TMM10i and alumina substrate in previous chapters. The inductors that are connected between the radial stub and ground plane in order to provide DC path for PIN diode biasing are realized using 1-mil gold wire and broadband conical inductors. However, these inductors have some parasitic effects on the RF signal. Hence, microstrip spiral inductors are designed in order to reduce these effects. Designing spiral inductors on the same substrate with unfolded Lange coupler and radial stubs makes the phase shifter circuits more compact. Since the spiral inductors are fabricated using thin film production, the assembling processes are reduced. However, the only handicap for spiral inductors that are designed in this study is the inductance value. The inductance values of 1-mil gold wire and conical inductors that are used in previous designs are 7nH and 709nH, respectively. On the other hand, the inductance of spiral inductors designed in this study is approximately 3.8nH without any resonances.

The design of microstrip spiral inductor and phase shifter circuits designed with spiral inductors are explained in this chapter. The fabricated phase shifter results are also given.

7.1 Microstrip Spiral Inductor Design and Simulation

Rectangular or spiral inductors are widely used as matching elements, impedance transformers, and reactive terminations in RF and microwave frequencies. The rectangular spiral inductors are designed and included into phase shifter circuits and they are used as RF chokes. A typical rectangular spiral inductor is illustrated in

Figure 7.1. The spiral inductor design parameters are width of the lines (W), spacing between the lines, vertical and horizontal lengths (L1, L2) and the number of turns (N). In the below inductor, the number of turns is 4.25.

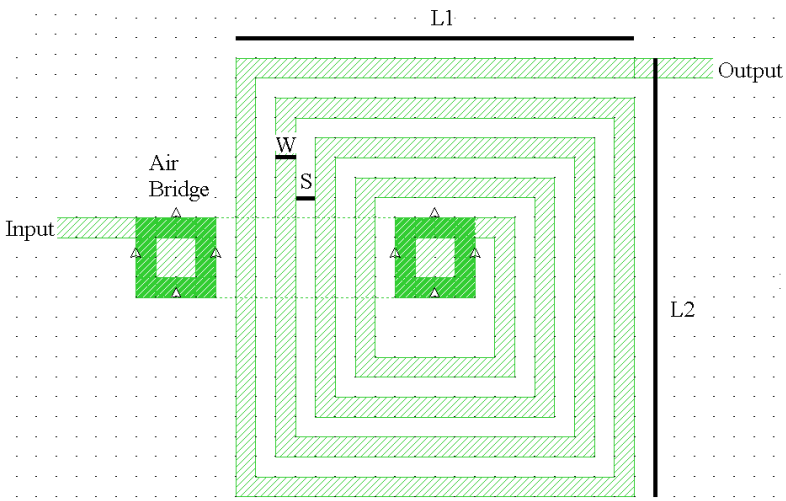

Figure 7.1 Layout of Spiral Inductor.

The input line of the inductor is connected to the inner side of the inductor via air bridge that is illustrated in Figure 7.2.

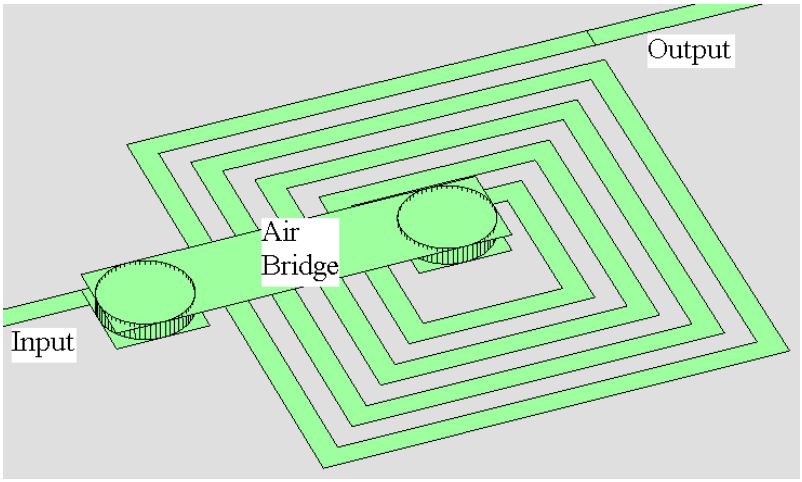

Figure 7.2 Layout of Spiral Inductor.

The circuit model of rectangular spiral inductor [30] is shown in Figure 7.3.

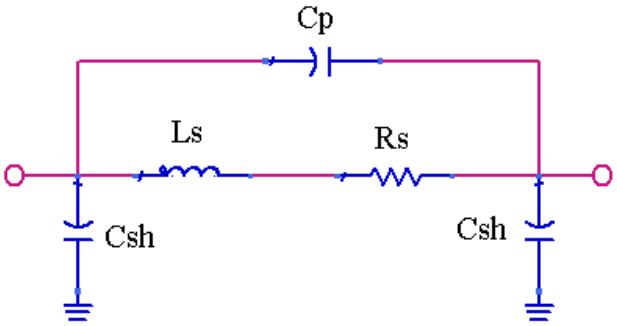

Figure 7.3 Circuit Model of Spiral Inductor.

The size information of the spiral inductor that is designed for phase shifter circuit is given in Table 7.1. Width, spacing and length sizes are given in mils.

Table 7.1 Size Information of Spiral Inductor

Design Parameters:	Value
W	0.5
S	0.5
L1	10
L2	11
N	4.25

The EM simulation of the rectangular spiral inductor with given sizes is performed using Sonnet software. Figure 7.4 shows the S-parameter comparison between the EM and circuit model (CM) simulation in ADS with the given circuit model parameters in Table 7.2.

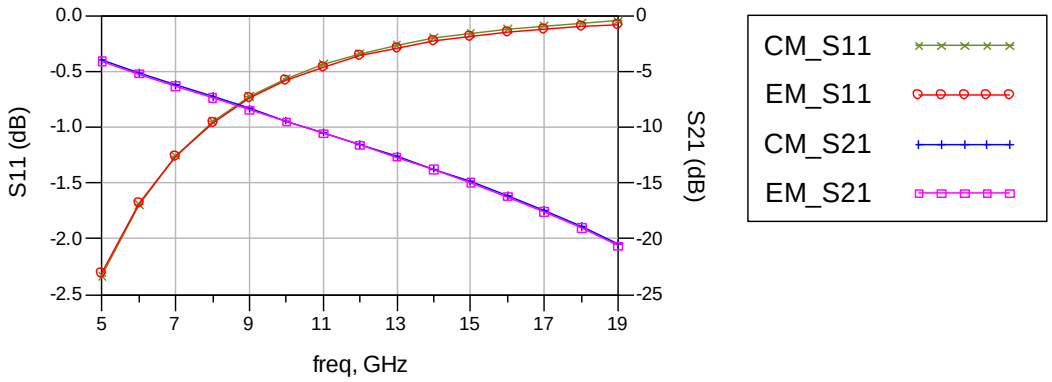

Figure 7.4 Comparison of EM and Circuit Model Simulations.

Table 7.2 Circuit Model Parameters of Spiral Inductor

Circuit Model Parameters:	Value
Cp (fF)	11
Ls (nH)	3.7
Rs (Ohm)	2
Csh (fF)	0.001

Hence, above results show that the inductance value of the spiral inductor with the given values in Table 7.1 is almost 3.7 nH. The inductance value can be increased by decreasing the spacing between the lines, however the spacing smaller than 0.5 mils can not be fabricated by the producer. Increasing the length of lines or number of turns will also increase the inductance value, but the resonance occurs less than 18 GHz which is the operating frequency. Hence, the spiral inductor designed above is used in the phase shifter circuits that are given in the next part.

7.2 Design of Phase Shifter Bits

After designing the microstrip spiral inductors, the phase shifter bits for 11.25, 22.5, 45, and 90º are designed. The design steps are same with the phase shifter bits designed in previous chapter. Same unfolded Lange coupler is used in the designs. Hence, the phase shifter circuits that are explained in part 6.3 are used in the beginning of the design. However, when the spiral inductors are added to the circuit

the memory required for the EM simulation exceeds the maximum memory limit. Because of this reason, the whole circuit could not be simulated. Instead of whole circuit EM simulation, the radial stubs are designed and simulated with spiral inductors given in previous part. In part 6.3 the radial stub sizes for each phase shifter bit are given in Table 6.1, 6.2, 6.3 and 6.4. Spiral inductors are connected between the outer edge of the radial stub and ground shown in Figure 7.5. In this example Stub-1 (in Table 6.1) of 11.25º phase shifter circuit is used.

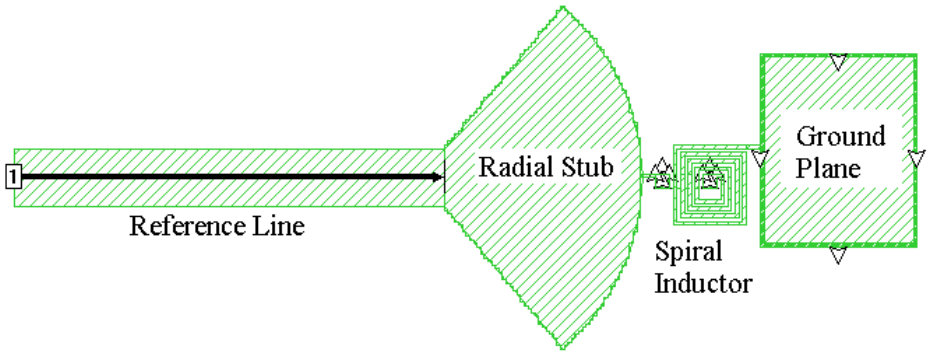

Figure 7.5 Spiral Inductor Connected Between Stub-1 and Ground.

When the EM simulation result of above structure is compared with the radial stub structure without spiral inductor given in Figure 7.6, a difference comes to existence especially in return losses. In fact it is expected since the spiral inductor value is not too high and can not show high impedance values for low frequencies. This situation is accepted because higher inductance values could not be obtained without any resonances and the design is continued.

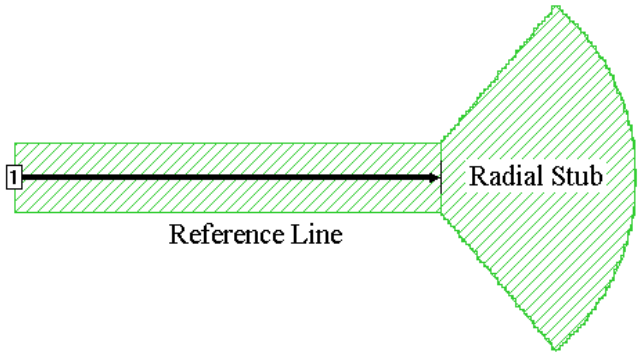

Figure 7.6 Stub-1 of 11.25º Phase Shifter Bit.

Afterwards, Stub-2 of 11.25º phase shifter bit is simulated in the circuits that are given in Figure 7.5 and 7.6. So, there are four circuits that are Stub-1 with spiral inductor, Stub-1 without spiral inductor, Stub-2 with spiral inductor, and Stub-2 without spiral inductor. Then, the phase responses of Stub-1 with spiral inductor and Stub-2 with spiral inductor are subtracted from each other, called phase difference with spiral inductor. Similarly, the phase responses of Stub-1 without spiral inductor and Stub-2 without spiral inductor are subtracted from each other, called phase difference without spiral inductor. In the design these differences are compared and tried to be get same results by tuning the radial stub sizes of with spiral inductors. After some amount of iterations, the new radial stub sizes given in Table 7.3 are obtained for 11.25º phase shifter bit where spiral inductors are added to the circuit.

Table 7.3 Radial Stub Sizes for 11.25º Phase Shifter Bit with Spiral Inductor

Stub Parameters:	Stub-1	Stub-2
W (mils)	8	7
L (mils)	25.4	24.8
A (º)	100	80

The comparison of phase differences of with and without spiral inductors are given in Figure 7.7.

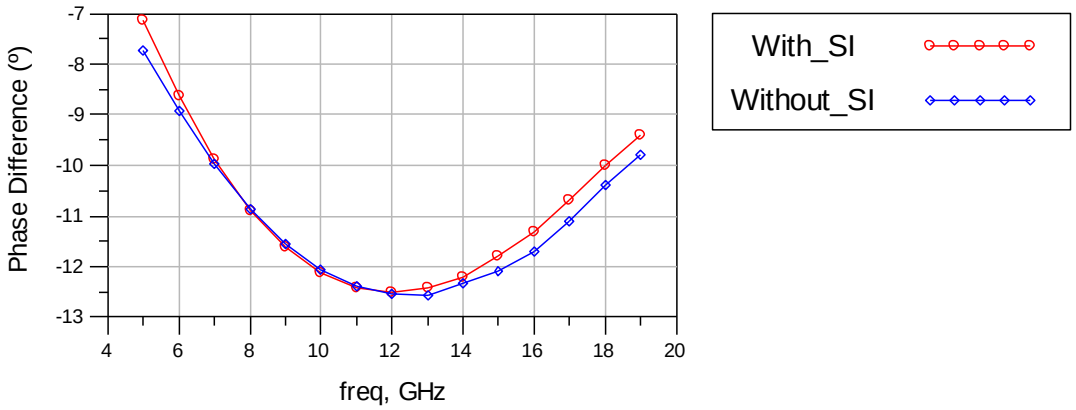

Figure 7.7 Stub-1 of 11.25° Phase Shifter Bit.

Using this approach the close responses for phase shifter circuits are expected, since same unfolded Lange coupler is used. Also, the effect of spiral inductor addition to the circuits that are given in part 6.3 is compensated by changing the radial stub sizes given in Table 6.1, 6.2, 6.3, and 6.4 as explained above. The new radial stub sizes of 11.25° phase shifter circuit are given in Table 7.3. Table 7.4, 7.5, and 7.6 give the new radial stub sizes for 22.5, 45, and 90° phase shifter circuits with spiral inductor version, respectively.

Table 7.4 Radial Stub Sizes for 22.5° Phase Shifter Bit with Spiral Inductor

Stub Parameters:	Stub-1	Stub-2
W (mils)	8	7
L (mils)	25.7	22.4
A (°)	125	100

Table 7.5 Radial Stub Sizes for 45° Phase Shifter Bit with Spiral Inductor

Stub Parameters:	Stub-1	Stub-2
W (mils)	8	7
L (mils)	33.1	24.8
A (°)	115	70

Table 7.6 Radial Stub Sizes for 90º Phase Shifter Bit with Spiral Inductor

Stub Parameters:	Stub-1	Stub-2
W (mils)	8	5
L (mils)	42	21
A (º)	100	70

The layout for 11.25º phase shifter bit with spiral inductors is formed as shown in Figure 7.8.

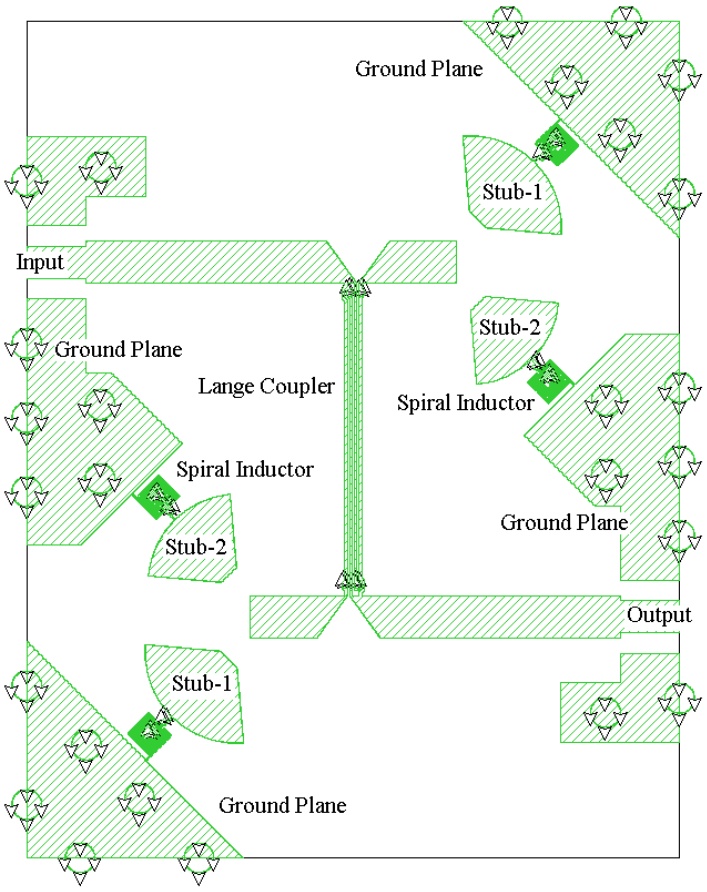

Figure 7.8 The Layout of 11.25º Phase Shifter Bit with Spiral Inductors.

To sum up, the same phase shifter circuits are designed as given in part 6.3. There are two differences between them. One of them is the addition of spiral inductors to

the circuit and the other is the modification of radial stub sizes because of the effect of spiral inductors.

Similarly, the layouts for the other bits are formed and fabricated by American Technical Ceramics by using thin film production. After fabrication of the phase shifter bits with spiral inductors, the assembling processes are performed in clean room facilities of ASELSAN Inc. The assembling of the PIN diodes and the biasing circuit components are same as explained in part 6.4. There is only one difference that conical inductors are not used in here since they are realized as spiral inductors. Also the measurement setup is the same and the same biasing conditions are used while measuring the circuits.

7.3 Fabricated Phase Shifter Bits

The phase shifter bits with spiral inductors for 11.25, 22.5, 45, and 90º are fabricated and the measurement results are given in this part. As explained previously, the assembling and measurement processes are performed in the same way as told in part 6.4. As an example, 11.25º phase shifter bit with spiral inductors and biasing components is given in Figure 7.9.

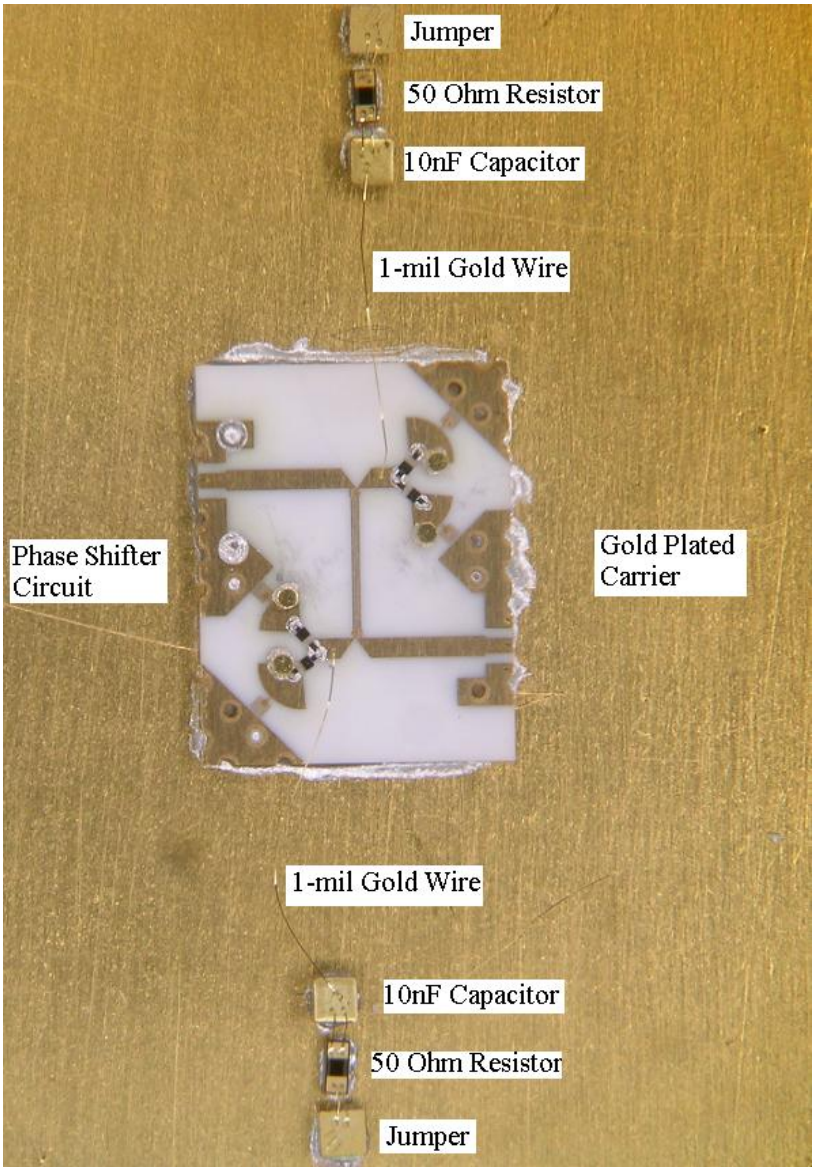

Figure 7.9 The Fabricated 11.25º Phase Shifter Bit with Spiral Inductors.

7.3.1 11.25º Phase Shifter Bit

The close view of fabricated 11.25º phase shifter bit with spiral inductors is given in Figure 7.10. The tuning is applied to the radial stubs with gold discs as in the case of phase shifter bits with conical inductors in part 6.4.

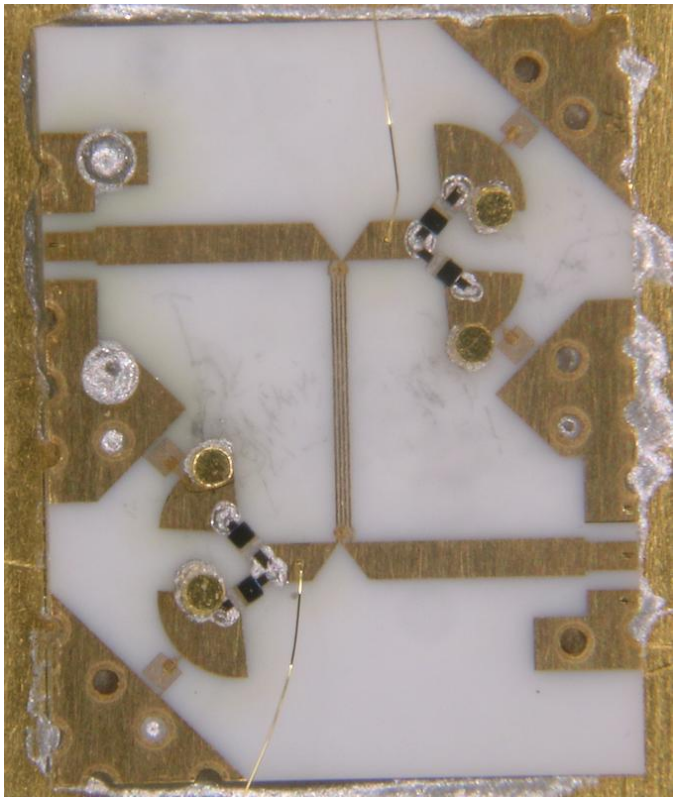

Figure 7.10 Close View of Fabricated 11.25° Phase Shifter with Spiral Inductors.

The differential phase shift of the circuit is given in Figure 7.11. The insertion loss, input and output return losses when Stub-1 and Stub-2 is selected are given in Figure 7.12 and 7.13, respectively.

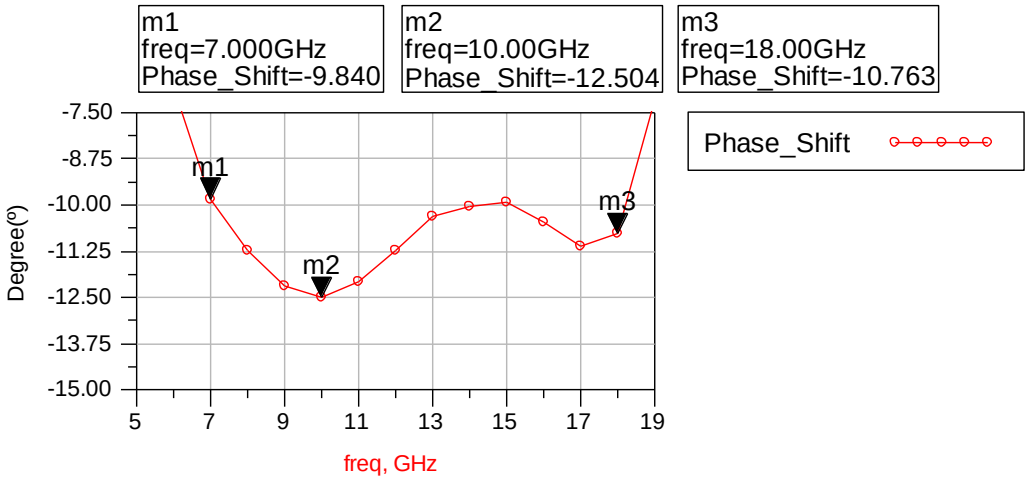

Figure 7.11 Differential Phase Shift for 11.25° Bit.

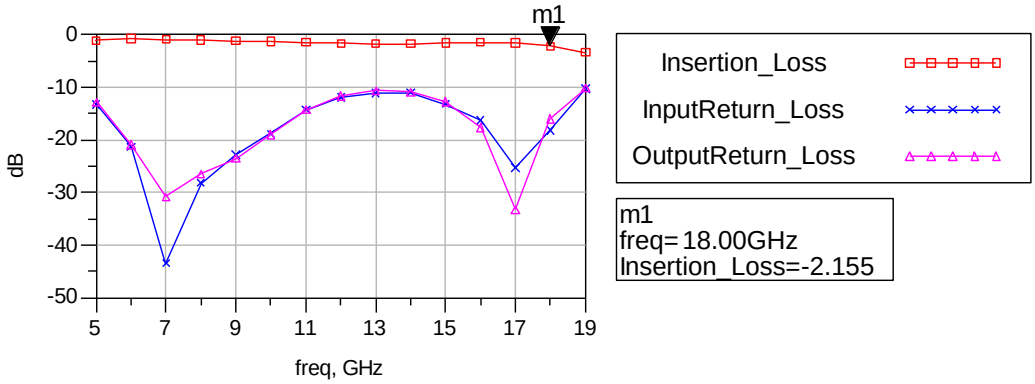

Figure 7.12 Insertion and Return Losses when Stub 1 is Selected.

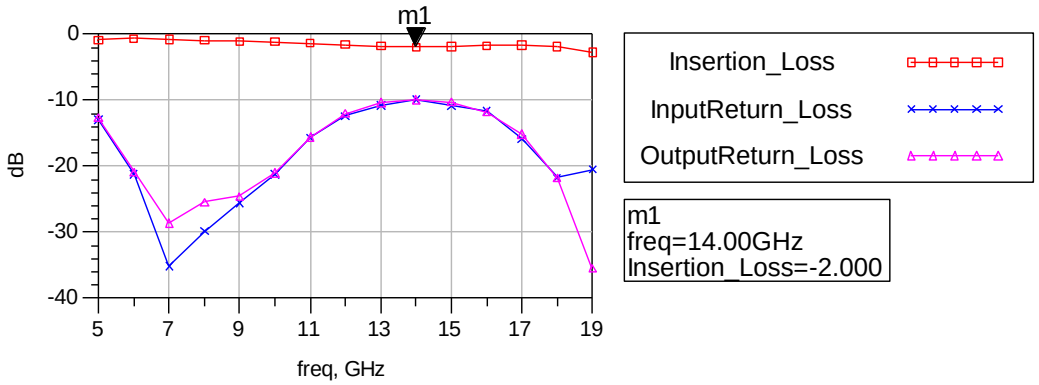

Figure 7.13 Insertion and Return Losses when Stub 2 is Selected.

When the above graphs are examined, the differential phase shift for 11.25º is satisfied for 7-18 GHz frequency band with maximum 1.4º phase error. This is an expected result, because the inductance value of the designed spiral inductors are low and this affects the performance of the phase shifter. When the Stub-1 is selected, the maximum insertion loss is -2.2 dB approximately at 18 GHz, where the input and output return losses are lower than-10 dB. When the Stub-2 is selected, the maximum insertion loss is -2 dB at 14 GHz. The input and output return losses are below -10 dB.

7.3.2 22.5º Phase Shifter Bit

The close view of fabricated 22.5º phase shifter bit with spiral inductors is given in Figure 7.14. The tuning is applied to the radial stubs by using gold discs with 16 mils diameter and 10 mils height.

Figure 7.14 Close View of Fabricated 22.5º Phase Shifter with Spiral Inductors.

The differential phase shift of the circuit is given in Figure 7.15. The insertion loss, input and output return losses when Stub-1 and Stub-2 is selected are given in Figure 7.16 and 7.17, respectively.

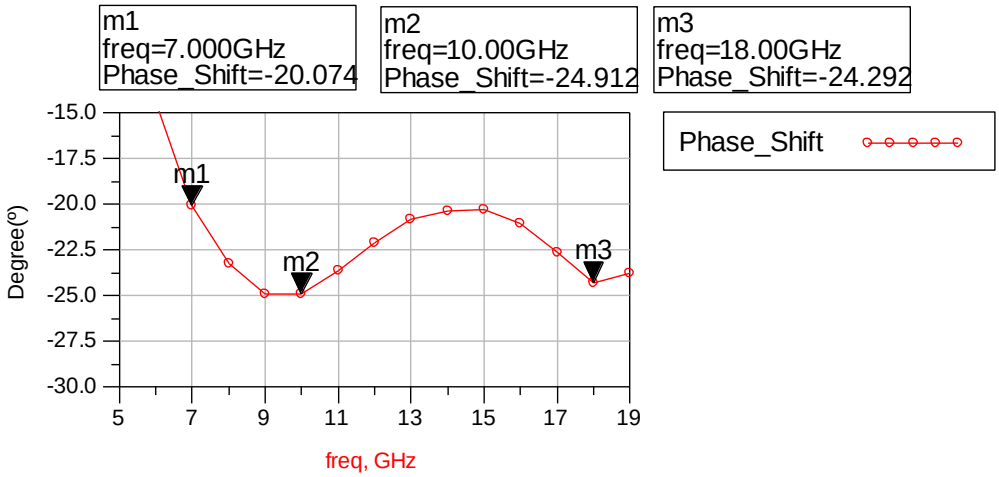

Figure 7.15 Differential Phase Shift for 22.5° Bit.

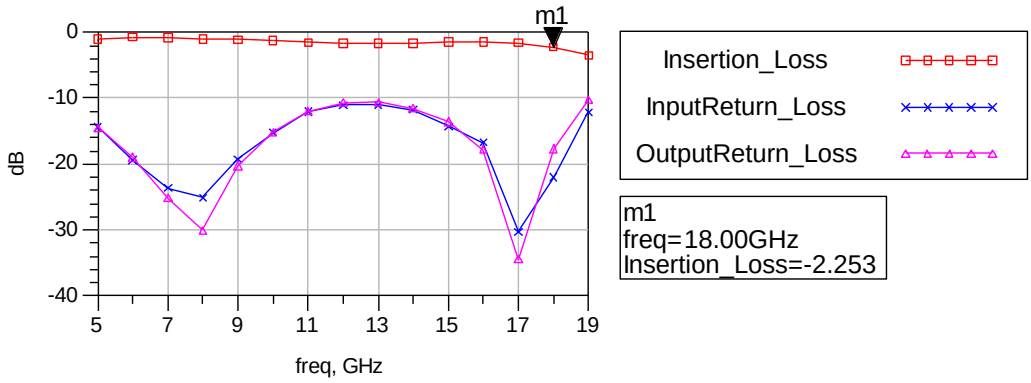

Figure 7.16 Insertion and Return Losses when Stub 1 is Selected.

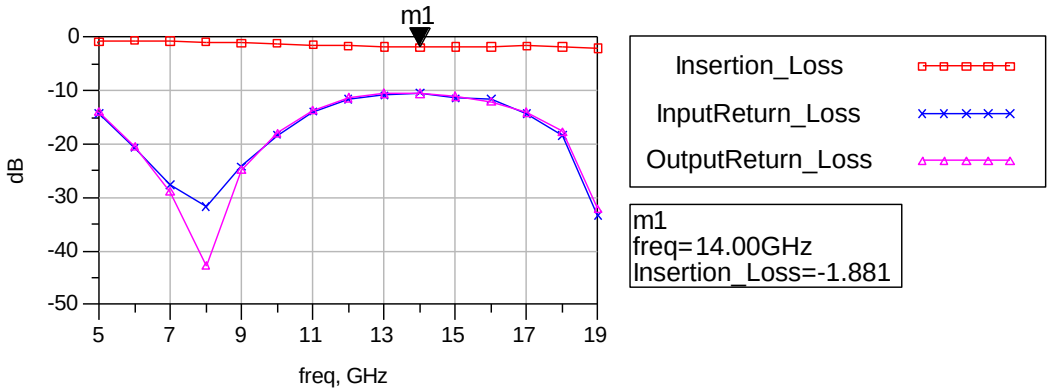

Figure 7.17 Insertion and Return Losses when Stub 2 is Selected.

According to the above graphs, the differential phase shift for 22.5º is satisfied for 7-18 GHz frequency band with maximum ±2.5º phase error. When the Stub-1 is selected, the maximum insertion loss is -2.2 dB approximately at 18 GHz, where the input and output return losses are lower than-10 dB. When the Stub-2 is selected, the maximum insertion loss is almost -1.9 dB at 14 GHz. The input and output return losses are below -10 dB.

7.3.3 45º Phase Shifter Bit

The close view of fabricated and tuned 45º phase shifter bit with spiral inductors is given in Figure 7.18.

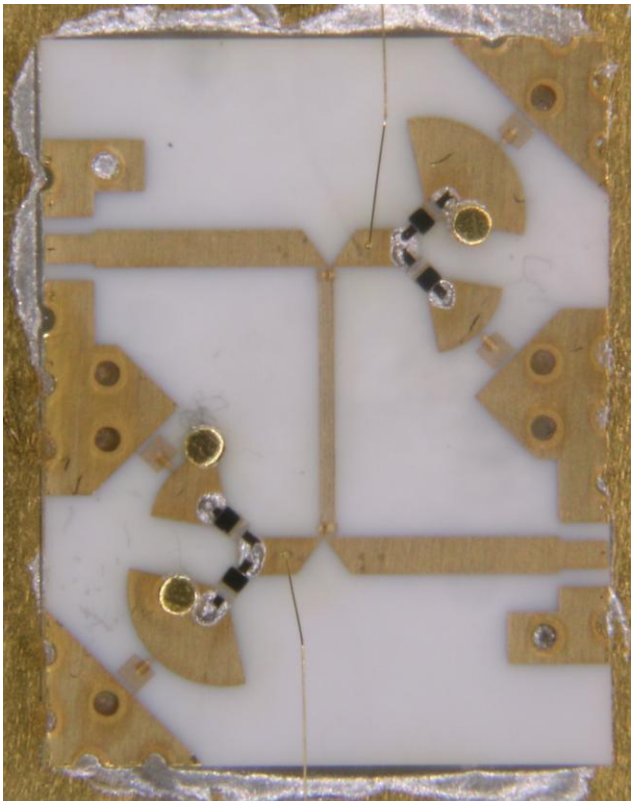

Figure 7.18 Close View of Fabricated 45º Phase Shifter with Spiral Inductors.

The differential phase shift of 45º phase shifter bit is given in Figure 7.19. The insertion loss, input and output return losses when Stub-1 and Stub-2 is selected are given in Figure 7.20 and 7.21, respectively.

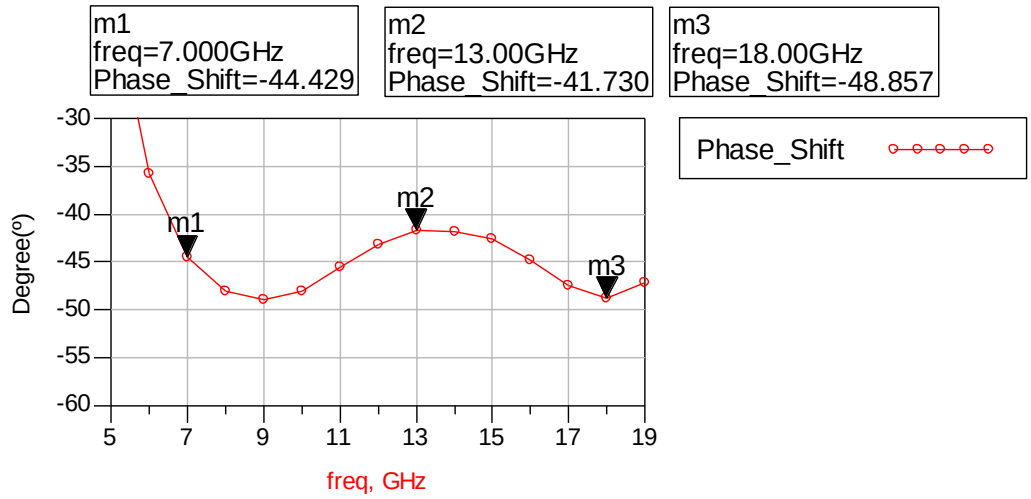

Figure 7.19 Differential Phase Shift for 45° Bit.

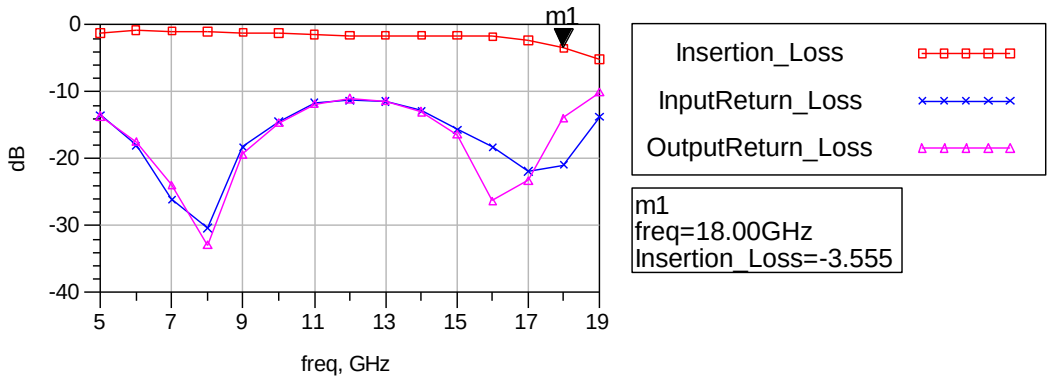

Figure 7.20 Insertion and Return Losses when Stub 1 is Selected.

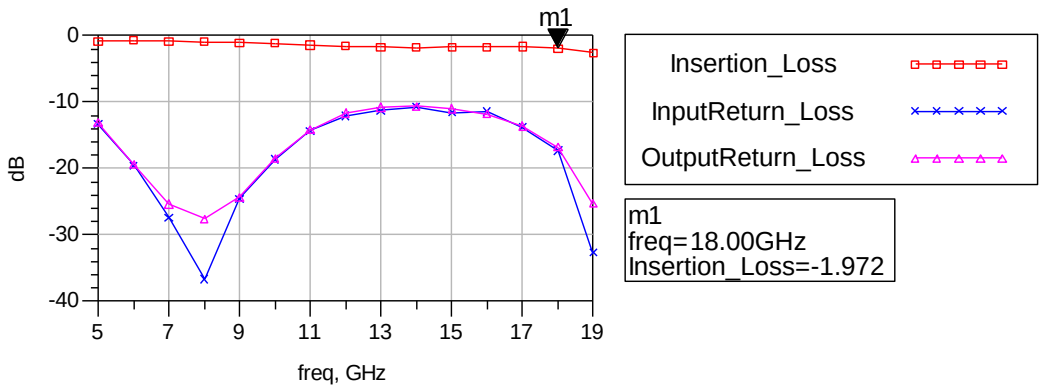

Figure 7.21 Insertion and Return Losses when Stub 2 is Selected.

When the graphs given above are examined, the differential phase shift for 45º is satisfied for 7-18 GHz frequency band with maximum ±4º phase error. When the Stub-1 is selected, the maximum insertion loss is -3.5 dB approximately at 18 GHz, where the input and output return losses are lower than-11 dB. When the Stub-2 is selected, the maximum insertion loss is almost -2 dB at 14 GHz. The input and output return losses are lower than -10 dB.

7.3.4 90º Phase Shifter Bit

The close view of fabricated and tuned 90º phase shifter bit with spiral inductors is given in Figure 7.22.

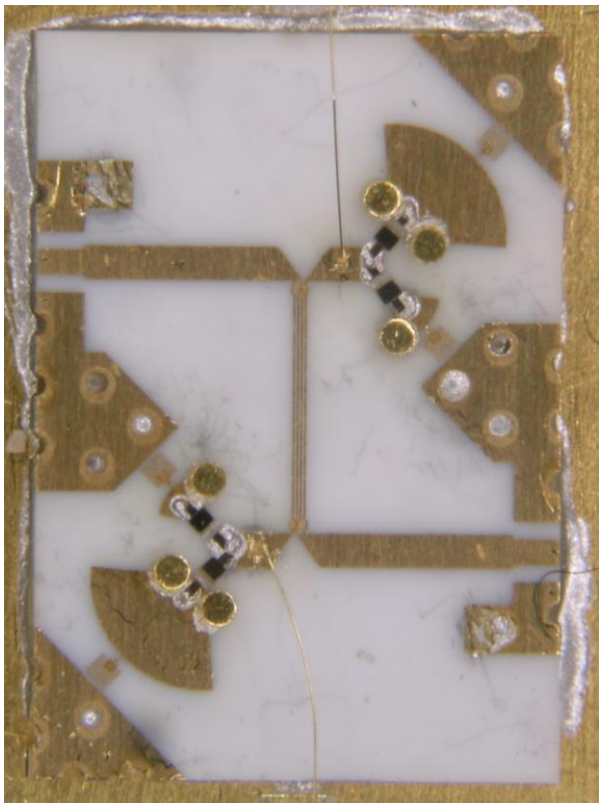

Figure 7.22 Close View of Fabricated 90º Phase Shifter with Spiral Inductors.

The differential phase shift of 90º phase shifter bit is given in Figure 7.23. The insertion loss, input and output return losses when Stub-1 and Stub-2 is selected are given in Figure 7.24 and 7.25, respectively.

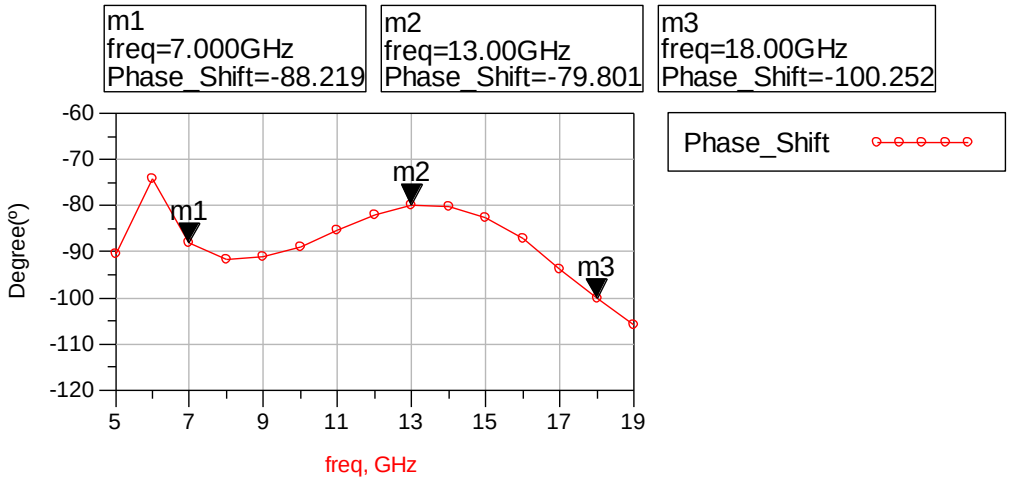

Figure 7.23 Differential Phase Shift for 90° Bit.

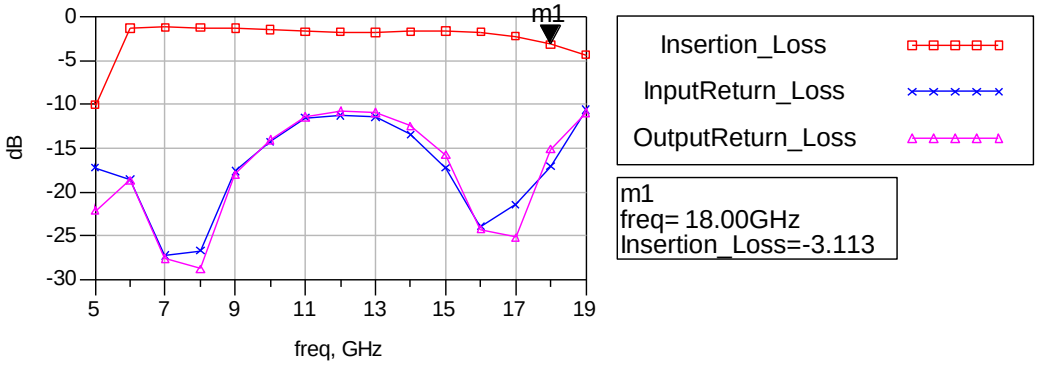

Figure 7.24 Insertion and Return Losses when Stub 1 is Selected.

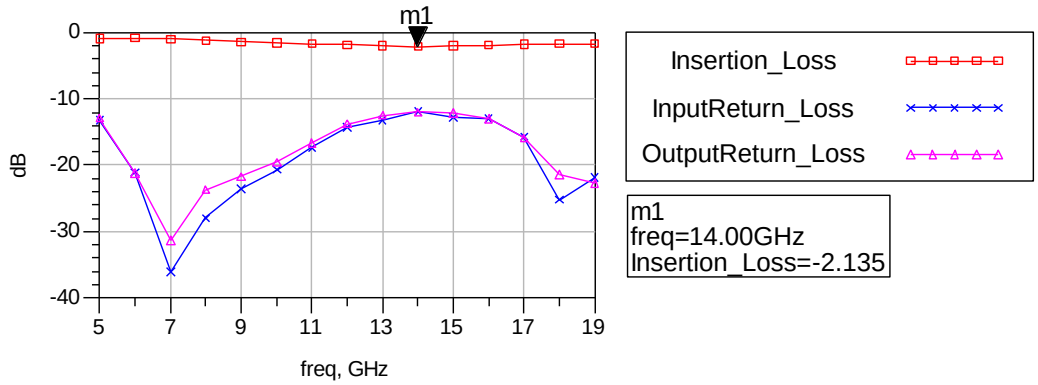

Figure 7.25 Insertion and Return Losses when Stub 2 is Selected.

When the graphs given above are examined, the differential phase shift for 90° is satisfied for 7-18 GHz frequency band with ±10.2° phase error. When the Stub-1 is

selected, the maximum insertion loss is -3.1 dB approximately at 18 GHz, where the input and output return losses are lower than-10 dB. When the Stub-2 is selected, the maximum insertion loss is almost -2.1 dB at 14 GHz. The input and output return losses are lower than -11 dB.

CHAPTER 8

CONCLUSION

Phase shifters operating in microwave frequencies are one of the most important components that are widely used in radar and telecommunication applications. Since the wideband operating frequency range is considerable in most of the systems, the circuit components that have broadband characteristics are preferred by the system designers. This situation is also valid for the microwave phase shifters that are key components of electronic warfare systems.

In this thesis, wideband digital phase shifters operating in 6-18 GHz frequency band are considered. Phase shifter circuits that provide 11.25, 22.5, 45, and 90º differential phase shifting are designed, simulated and fabricated individually. In the design steps, the minimum phase errors and low return losses are taken into account. Hybrid coupled phase shifter topology is used in the scope of this study. The phase shifter circuits are designed onto two different dielectric substrates as Rogers TMM10i and Alumina.

One of the most popular implementation of a wideband phase shifter is using a 3 dB, 90º coupler where its direct and coupled ports are terminated with two identical capacitive loads. Unfolded Lange coupler is used as a hybrid coupler in the designs. Radial stubs are selected as reflective capacitive loads, since their reflection coefficient is much higher than conventional stubs. Beam lead PIN diodes with low insertion loss are selected as switching components that are required for selecting relevant radial stub pairs.

For 6-18 GHz frequency band, 11.25, 22.5, 45, and 90º phase shifter circuits are designed on 25 mils thick Rogers TMM10i substrate. The design and fabrication details are given in Chapter 4 and Chapter 5. The whole fabrication processes are

performed in ASELSAN Inc using PCB manufacturing. Although, the aimed frequency band is 6-18 GHz, the phase shifter circuits are fabricated that operate in 7-14 GHz frequency range. The main reason that narrows the bandwidth comes from the production errors on Lange coupler and the thickness of the substrate that increase the loss at high frequencies. In order to produce the coupler in laser machine, the spacing between the lines increased that decreases the coupling and bandwidth of the coupler. The fabricated Lange coupler is measured and the designs are performed according to this measurement. Also the circuit model of PIN diode for forward and reversed biasing is obtained. Finally, for 7-14 GHz frequency band, 11.25, 22.5, 45, and 90º phase shifter circuits are fabricated and tuned. For the whole frequency band, the measured maximum phase errors were ±2.1, 3.2, 5.5, and 13º for the 11.25, 22.5, 45, and 90 phase shifters, respectively. The maximum insertion losses were 2.2, 2.1, 2.1, and 2.3 dB in whole frequency band for the 11.25, 22.5, 45, and 90 phase shifters, respectively. The fabricated results are consistent with the simulated ones.

The design and fabrication details of phase shifters that are designed onto 15 mil thick Alumina substrate are given in Chapter 6. The phase shifter circuits are fabricated using thin film production technology by American Technical Ceramics. The same phase shifter topology and same beam lead PIN diodes are used as in TMM10i designs. The phase shifter circuits are designed to operate in 6-18 GHz frequency range. The broadband conical inductors are used for biasing the PIN diodes. All assembling processes are performed in ASELSAN Inc. To sum up, 11.25, 22.5, 45, and 90º phase shifter circuits are fabricated and tuned for 6-18 GHz frequency band. For the whole frequency band, the measured maximum phase errors were ±1.5, 2.9, 5.5, and 10.5º for the 11.25, 22.5, 45, and 90 phase shifters, respectively. The maximum insertion losses were 3.8, 3.2, 4.0, and 4.0 dB in whole frequency band for the 11.25, 22.5, 45, and 90 phase shifters, respectively. The fabricated results agree with the simulation results.

The phase shifter bits are also fabricated including spiral inductors for the biasing of PIN diodes to the circuits. The details of the design steps and fabrication of the phase shifters are given in Chapter 7. Phase shifter bits are fabricated onto 15 mils thick

alumina substrate as the phase shifter bits explained in Chapter 6. The microstrip spiral inductors are designed with inductance value 3.8 nH approximately. The radial stubs are tuned in order to compensate of effects coming from the addition of spiral inductors. With the new values of radial stubs that are designed in Chapter 6, the phase shifter circuits are fabricated using thin film production. The PIN diodes and the remaining biasing circuits are assembled in ASELSAN Inc. The operating frequency range is obtained as 7-18 GHz, since the inductance value of the spiral inductors are low. 11.25, 22.5, 45, and 90º phase shifters are tuned in order to compensate the uncalculated parasitic effects come from biasing circuits and measurement setup. In conclusion, for 7-18 GHz frequency band, the measured maximum phase errors were ±1.4, 2.5, 4.0, and 10.2º for the 11.25, 22.5, 45, and 90 phase shifters, respectively. The maximum insertion losses were 2.2, 2.2, 3.5, and 3.1 dB in whole frequency band for the 11.25, 22.5, 45, and 90 phase shifters, respectively.

REFERENCES

[1] Marc A. Antoniades, "Compact Linear Metamaterial Phase Shifters for Broadband Applications", A master thesis submitted to Department of Electrical and Computer Engineering of University of Toronto, 2004.

[2] A.G. Fox, "An Adjustable Waveguide Phase Changer," Proc. IRE, Vol. 35, pp. 1489-1498, December 1947.

[3] F. Reggia and E.G. Spencer, "A New Technique in Ferrite Phase Shifting for Beam Scanning of Microwave Antennas," Proc. IRE, Vol. 45, pp. 1510-1517, November 1957.

[4] B. Schiffman, "A New Class of Broadband Microwave 90-degree Phase Shifter," IRE Trans. Microw. Theory Tech., Vol. MTT-6, No. 4, pp. 232-237, Apr. 1958.

[5] Ramos Quirarte, J.L. and J.P. Starski, "Synthesis of Schiffman Phase Shifters," IEEE Transactions on Microwave Theory and Techniques, Vol. 39, No. 11, pp. 1885-1889, November 1991.

[6] Amin M. Abbosh, "Ultra-Wideband Phase Shifters," IEEE Trans. Microw. Theory Tech., Vol. 55, No. 9, pp. 1935-1941, Sep. 2007.

[7] J.F. White, "High Power, p-i-n Diode Controlled, Microwave Transmission Phase Shifters," IEEE Trans. Microwave Theory Tech., Vol. MTT-13, pp. 233-242, Mar. 1965

[8] W. A. Little, J. Yuan, and C.C. Snellings, "Hybrid Integrated Circuit Digital Phase Shifters," in 1967 IEEE Int. Solid-State Circuits Conf. Dig., pp. 58-59.

[9] Garver R., V., "Broad-Band Diode Phase Shifters," IEEE Transactions on Microwave Theory and Techniques, Vol. MTT-20, No. 5, pp. 314-323, May 1972.

[10] Hyukjin Kwon, Hongwook Lim, and Bongkoo Kang, "Design of 6-18 GHz Wideband Phase Shifters Using Radial Stubs," IEEE Microwave and Wireless Components Letters, Vol. 17, No. 3, pp. 205-207, March 2007.

[11] D. Adler and R. Popovich, "Broadband Switched-Bit Phase Shifter Using All-Pass Networks," 1991 IEEE MTT-S Int. Microwave Symp. Dig., Vol. 1, pp. 265-268, July 1991.

[12] S. Koul and B. Bhat, "Microwave and Millimeter Wave Phase Shifters," Volume I, Boston, MA: Artech House, 1991.

[13] G. M. Rebeiz, G. L. Tan, J. S. Hayden, "RF MEMS Phase Shifters: Design and Applications," IEEE Microwave Magazine, Vol. 3, pp. 72-81, June, 2002.

[14] Jung-Mu Kim, Sanghyo Lee, Jae-Hyoung Park, Chang-Wook Back, Youngwoo Kwon, and Yong-Kweon Kim, "A 5-17 GHz Wideband Reflection-Type Phase Shifter Using Digitally Operated Capacitive MEMS Switches," The 12th International Conference on Solid State Sensors, Actuators and Microsystems, pp. 907-910, Boston, June 8-12, 2003.

[15] Young J. KO, Jae Y. Park, and Jong U. Bu, "Integrated RF MEMS Phase Shifters with Constant Phase Shift," IEEE MTT-S International Microwave Symposium Digest, Vol. 3, pp. 1489-1492, 2003.

[16] S. Koul and B. Bhat, "Microwave and Millimeter Wave Phase Shifters," Volume II, Boston, MA: Artech House, 1991.

[17] D. C. Boire, G. St. Onge, C. Barratt, G. B. Norris, and A. Moysenko, "4: 1 Bandwidth Digital Five-Bit MMIC Phase Shifters," in IEEE Microwave and MMWave Monolithic Circuits Symposium, pp. 69-73, 1989.

[18] Kenichi Miyaguchi, Morishige Hieda, Yukinobu Tarui, Mikio Hatamoto, Koh Kanaya, Michiaki Kasahara and Tadashi Takagi, "A 6-18 GHz 5-Bit Phase Shifter MMIC Using Series/Parallel LC Circuit," 32nd European Microwave Conference, Milan, Italy, 2002.

[19] Mary Teshiba, Robert Van Leeuwen, Glenn Sakamoto, and Terry Cisco, "A SiGe MMIC 6-Bit PIN Diode Phase Shifter," IEEE Microwave and Wireless Components Letters, Vol. 12, No. 12, December 2002.

[20] Yong-Sheng Dai, Da-Gang Fang, and Yong-Xin Guo, "A Novel Miniature 1–22 GHz 90 MMIC Phase Shifter with Microstrip Radial Stubs," IEEE Microwave and Wireless Components Letters, Vol. 18, No. 2, February 2008.

[21] Dmitry Kholodnyak, Elena Serebraykova, Irina Vendik, and Orest Vendik, "Broadband Digital Phase Shifter Based on Switchable Right- and Left-Handed Transmission Line Sections," IEEE Microwave and Wireless Components Letters, Vol. 16, No. 5, May 2006.

[22] I.D. Robertson and S. Lucyszyn, "RFIC and MMIC Design and Technology," London, Institution of Electrical Engineers, 2001.

[23] D. Parker and D.C. Zimmerman, "Phased Arrays – Part II: Implementations, Applications, and Future Trends", IEEE Transactions on Microwave Theory Techniques, Vol.50, No.3, pp. 688–698, March 2002.

[24] Arun K. Bhattacharyya, "Phased Array Antennas: Floquet Analysis, Synthesis, BFNs and Active Array Systems, " John Wiley, 2006.

[25] I.J. Bahl and P. Bhartia, "Microwave Solid State Circuit Design," John Wiley and Sons, May 2003.

[26] David M. Pozar, "Microwave Engineering," John Wiley and Sons, 1998.

[27] E.H. Fooks and R.A. Zakarevicius, “Microwave Engineering Using Microstrip Circuits,” Prentice Hall, 1990.

[28] R. Waugh and D. LaCombe, “Unfolding the Lange Coupler,” IEEE Transactions on Microwave Theory and Techniques, Vol. MTT-20, pp. 777-779, November 1972.

[29] S.L. March, “Analyzig Lossy Radial-Line Stubs,” IEEE Transactions on Microwave Theory and Techniques, Vol. MTT-33, No. 3, pp. 269-271, March 1985.

[30] I.Bahl, “Lumped Elements for RF and Microwave Circuits,” Artech House, 1985.

APPENDIX A

DATASHEET OF HPND-4038 BEAM LEAD PIN DIODE

HPND-4028, HPND-4038

Beam Lead PIN Diodes for Phased Arrays and Switches

AVAGO TECHNOLOGIES

Data Sheet

Description

The HPND-4028 and 4038 beam lead PIN diodes are designed for low capacitance, low resistance, and fast switching at microwave frequencies. These characteristics are achieved at low bias levels for minimal power consumption. Advanced processing techniques ensure uniform and consistent electrical performance, allowing guaranteed capacitance windows. This translates to improved performance in phased array applications.

Rugged construction and strong beams ensure high assembly yields while nitride passivation and polyimide coating ensure reliability.

Applications

These beam lead PIN diodes are designed for use in stripline, coplanar waveguide, or microstrip circuits. Applications include phase shifting and switching. The guaranteed capacitance windows ensure uniform performance in phased array radar. The low capacitance makes them ideal for circuits requiring high isolation in the series configuration. These devices have been fully characterized and S-parameters have been provided.

Maximum Ratings

Operating Temperature	-65°C to +150°C
Storage Temperature	-65°C to +200°C
Power Dissipation at T_{CASE} = 25°C (Derate linearly to zero at 150°C.)	250 mW
Minimum Lead Strength	4 grams pull on either lead per MIL-S-19500, LTPD = 20

Features

- Low Capacitance
  0.025 pF Maximum at 1 MHz Guaranteed Min./Max.
- Fast Switching
  2.0 nsec
- Low Resistance at Low Bias
  1.5 Ω at IF = 10 mA (Typical)
- Rugged Construction
  Typical 10 Gram Lead Pull
- Silicon Nitride Passivation

Outline 83

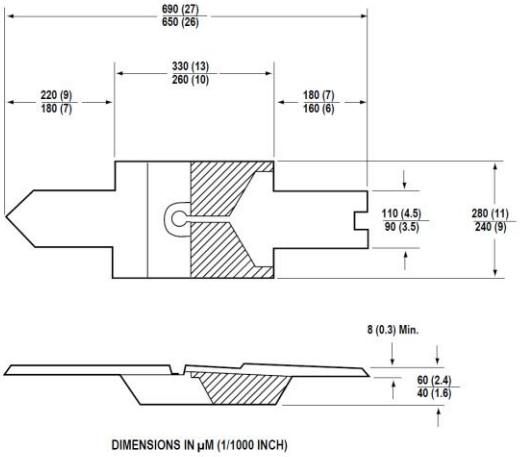

DIMENSIONS IN µM (1/1000 INCH)

Electrical Specifications at TA = 25°C

Part Number	Capacitance (pF)		Series Resistance R_S (Ω)		Break-down Voltage V_{BR} (V)	Reverse Current I_R (nA)	Forward Voltage V_F (V)	Carrier Lifetime τ (ns)	Reverse Recovery trr (ns)	Series Resistance R_S (Ω)
HPND-	Min.	Max.	Typ.	Max.	Min.	Max.	Max.	Typ.	Typ.	Typ.
4028	0.025	0.045	2.3	3.0	60	100	1.1	36	2.6	2.0
4038	0.045	0.065	1.5	2.0	60	100	1.1	45	2.4	1.0
Test Conditions	$V_R = 30$ V f = 1 MHz		$I_F = 10$ mA f = 100 MHz		$V_R = V_{BR}$ Measure $I_R \leq 10$ mA	$V_R = 50$ V	$I_F = 20$ mA	$I_F = 10$ mA $I_R = 6$ mA	*$I_F = 10$ mA $I_F = 5$ mA $V_R = 10$ V	$I_F = 50$ mA f = 100 MHz 90% recovery

Typical Parameters

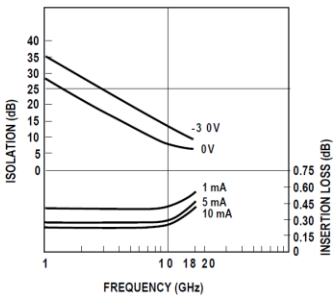

Figure 1. Typical Isolation and Insertion Loss, HPND-4028.

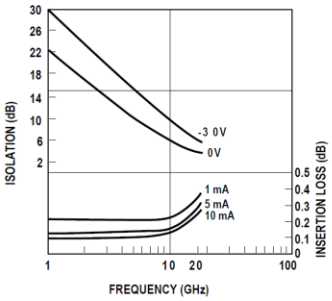

Figure 2. Typical Isolation and Insertion Loss, HPND-4038.

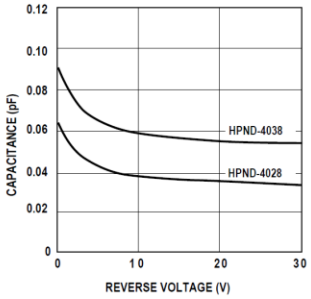

Figure 3. Typical Capacitance vs. Reverse Voltage (at 1 MHz).

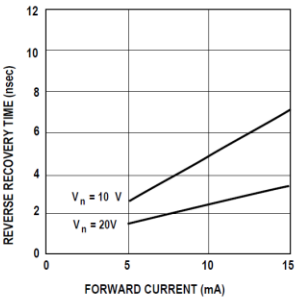

Figure 4. Typical Reverse Recovery Time vs. Forward Current (Series Configuration). HPND-4028, HPND-4038.

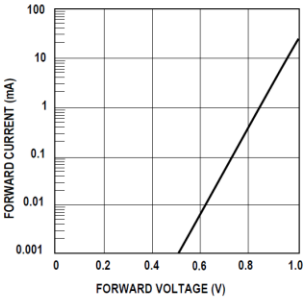

Figure 5. Typical Forward Characteristics.

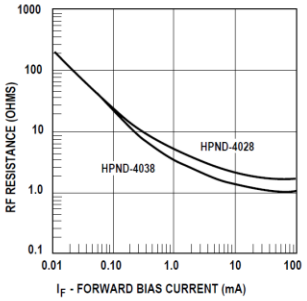

Figure 6. Typical RF Resistance vs. Forward Bias Current (at 100 MHz).

Typical S-Parameters (in series configuration) at $Z_0 = 50\ \Omega$, 25°C (cont.)

HPND-4038

Freq.	$I_F = 1$ mA					$I_F = 5$ mA					$I_F = 10$ mA				
	S_{11}/S_{22}		S_{21}/S_{12}			S_{11}/S_{22}		S_{21}/S_{12}			S_{11}/S_{22}		S_{21}/S_{12}		
(MHz)	Mag.	Ang.	dB	Mag.	Ang.	Mag.	Ang.	dB	Mag.	Ang.	Mag.	Ang.	dB	Mag.	Ang.
1000	0.028	15	-0.22	0.976	-1	0.019	28	-0.12	0.987	-1	0.017	35	-0.10	0.989	-1
2000	0.032	34	-0.24	0.974	-2	0.026	50	-0.16	0.984	-2	0.024	56	-0.14	0.986	-2
3000	0.037	47	-0.22	0.975	-3	0.034	61	-0.14	0.985	-3	0.033	66	-0.12	0.988	-4
4000	0.045	55	-0.22	0.975	-5	0.042	67	-0.14	0.985	-5	0.042	70	-0.12	0.987	-5
5000	0.052	61	-0.24	0.974	-6	0.051	72	-0.16	0.984	-6	0.051	75	-0.14	0.986	-6
6000	0.060	65	-0.24	0.974	-7	0.059	74	-0.16	0.984	-7	0.059	77	-0.14	0.986	-7
7000	0.067	67	-0.24	0.974	-8	0.067	76	-0.16	0.984	-8	0.067	78	-0.12	0.987	-8
8000	0.073	69	-0.24	0.974	-9	0.074	76	-0.16	0.983	-9	0.073	78	-0.14	0.986	-9
9000	0.081	70	-0.24	0.973	-10	0.081	77	-0.16	0.984	-10	0.081	78	-0.14	0.986	-10
10000	0.087	71	-0.24	0.974	-11	0.088	77	-0.16	0.982	-11	0.089	79	-0.14	0.986	-11
11000	0.092	71	-0.22	0.975	-12	0.094	77	-0.16	0.984	-12	0.094	79	-0.14	0.986	-12
12000	0.099	70	-0.24	0.974	-14	0.100	76	-0.16	0.984	-14	0.101	77	-0.14	0.986	-14
13000	0.104	70	-0.22	0.975	-15	0.106	75	-0.14	0.985	-15	0.107	76	-0.12	0.987	-15
14000	0.110	69	-0.26	0.972	-16	0.112	74	-0.16	0.982	-16	0.113	75	-0.16	0.984	-16
15000	0.118	67	-0.24	0.973	-17	0.119	72	-0.16	0.983	-17	0.120	73	-0.14	0.985	-17
16000	0.123	66	-0.24	0.973	-18	0.125	71	-0.16	0.982	-18	0.126	72	-0.16	0.984	-18
17000	0.132	64	-0.26	0.972	-19	0.133	68	-0.16	0.982	-19	0.133	69	-0.16	0.984	-19
18000	0.141	62	-0.26	0.972	-20	0.143	66	-0.18	0.980	-20	0.143	67	-0.16	0.983	-20

HPND-4038

Freq.	$V_R = 0$ V					$V_R = 10$ V					$V_R = 30$ V				
	S_{11}/S_{22}		S_{21}/S_{12}			S_{11}/S_{22}		S_{21}/S_{12}			S_{11}/S_{22}		S_{21}/S_{12}		
(MHz)	Mag.	Ang.	dB	Mag.	Ang.	Mag.	Ang.	dB	Mag.	Ang.	Mag.	Ang.	dB	Mag.	Ang.
1000	0.993	-5	-23.10	0.070	83	0.998	-3	-28.88	0.036	89	0.999	-3	-29.90	0.032	90
2000	0.976	-10	-17.28	0.137	76	0.995	-7	-22.86	0.072	84	0.996	-6	-23.76	0.065	85
3000	0.953	-15	-14.04	0.199	70	0.990	-10	-19.26	0.109	81	0.992	-9	-20.18	0.098	82
4000	0.923	-19	-11.88	0.255	64	0.982	-13	-16.78	0.145	78	0.986	-12	-17.74	0.130	79
5000	0.890	-23	-10.36	0.304	58	0.973	-16	-14.90	0.180	74	0.977	-15	-15.88	0.161	75
6000	0.857	-27	-9.20	0.347	53	0.962	-20	-13.40	0.214	71	0.968	-19	-14.30	0.193	73
7000	0.822	-31	-8.28	0.386	49	0.947	-23	-12.08	0.249	68	0.956	-22	-12.96	0.225	69
8000	0.790	-34	-7.58	0.418	45	0.933	-27	-11.06	0.280	65	0.945	-25	-11.92	0.254	66
9000	0.757	-38	-7.00	0.447	41	0.915	-30	-10.12	0.312	61	0.928	-29	-10.94	0.284	63
10000	0.727	-41	-6.54	0.471	38	0.897	-34	-9.40	0.339	58	0.912	-32	-10.22	0.309	61
11000	0.697	-44	-6.10	0.496	34	0.877	-37	-8.62	0.371	54	0.892	-35	-9.44	0.338	57
12000	0.668	-46	-5.74	0.517	32	0.854	-41	-8.00	0.399	52	0.874	-38	-8.76	0.365	54
13000	0.643	-49	-5.56	0.528	29	0.834	-44	-7.60	0.417	49	0.854	-42	-8.34	0.383	51
14000	0.620	-51	-5.22	0.549	26	0.813	-47	-7.04	0.445	45	0.839	-45	-7.76	0.410	48
15000	0.599	-53	-5.16	0.553	24	0.793	-50	-6.82	0.457	43	0.818	-48	-7.50	0.422	45
16000	0.584	-55	-4.90	0.569	21	0.778	-53	-6.42	0.478	39	0.805	-50	-7.10	0.442	42
17000	0.570	-57	-4.80	0.576	19	0.762	-55	-6.22	0.489	37	0.790	-53	-6.88	0.453	40
18000	0.556	-59	-4.84	0.574	17	0.747	-58	-6.18	0.491	35	0.776	-55	-6.86	0.454	37